ABSTRACT

Title of Document: INVESTIGATIONS IN INTERKINGDOM SIGNALING AND CONTROL OF QUORUM SENSING DEPENDENT PHENOTYPES

Amin Zargar, Doctor of Philosophy, 2015

Directed By: Professor William E. Bentley
Fischell Department of Bioengineering

Bacteria secrete and recognize communication molecules to coordinate gene expression in a process known as quorum sensing (QS). Through coordinated expression, bacteria are able to influence phenotypic changes on a larger population scale, such as biofilm formation. Recent studies into interkingdom communication have found cross-talk communication among bacteria and eukarya as well, which has been shown to influence actions pathogenicity and inflammation, among others. In this work, we developed *E. coli* 'controller cells' that guide and attenuate harmful bacterial QS phenotypes coordinated by the QS molecule autoinducer-2 (AI-2), as well as further the understanding of the interkingdom effects of these bacterial secretions (secretome) on human cells, particularly intestinal epithelial cells (IECs) that line the GI tract. Extending beyond natural networks, these 'controller cells' provide a useful tool in metabolic engineering, as synthetic biologists have incorporated QS networks to create sophisticated genetic circuits.

Through next generation RNA sequencing, we found that *E. coli* secretomes activate a number of defense-related signaling pathways in epithelial cells, including the cytokine-cytokine receptor pathway, the chemokine signaling pathway, and the NF-κB signaling pathways. Further, we found the inflammatory cytokine interleukin-8 (IL-8) responded to AI-2 with a time-course pattern of initial upregulation followed by subsequent downregulation. We propose this pattern

fits the paradigm where bacterial metabolites cause changes in the host cell which are returned to homeostasis through negative feedback regulators.

To develop ‘controller cells’, we characterized the kinetics of the *lsr* operon in *E. coli* through the generation of a suite of bacterial strains that overexpress the components of AI-2 processing: uptake (LsrACDB), phosphorylation (LsrK) and degradation (LsrFG). These engineered ‘controller cells’ can regulate the extracellular AI-2 environment, silence bacterial communication, and modulate biofilm formation. Using the insight gained from our mathematical model of the AI-2 processing mechanisms, we developed a high-efficiency (HE) controller cell that could guide QS-dependent behaviors while being sequestered from the target population inside an alginate-chitosan capsule. This work has helped clarify the interkingdom interaction between IECs and commensal bacteria, and created a novel method to control bacterial communication.

INVESTIGATIONS IN INTERKINGDOM SIGNALING AND CONTROL OF QUORUM SENSING DEPENDENT PHENOTYPES

By

Amin Zargar

Dissertation submitted to the Faculty of the Graduate School of the
University of Maryland, College Park, in partial fulfillment
of the requirements for the degree of
Doctor of Philosophy
2015

Advisory Committee:
Professor William E. Bentley, Chair
Assistant Professor Rohan Fernandes
Associate Professor Herman Sintim
Assistant Professor Kimberly Stroka
Associate Professor Ian White

© Copyright by
Amin Zargar
2015

Dedication

I dedicate this work to my parents, Sharif and Mahin, my older brothers, Arsalan and Ehsan, and my little sister Anita.

Acknowledgements

I would like to acknowledge the members of my committee for their time, advice and mentorship. In particular, I would like to thank my adviser, Dr. William Bentley. As a mentor, he has guided my research over the past four years, and as a role model, he has helped clarify the career path I wish to pursue for my future. I also wish to acknowledge my fellow lab members, past and present, for their contributions to this work. I especially would like to thank the senior members of the laboratory when I joined: Dr. David Quan, Dr. Chen Yu Tsao, Dr. Karen Carter and Dr. Hsuan-Chen Wu. They patiently trained and guided me at a time when I would have been completely lost without them, and I am indebted to their kindness and goodwill. I also thank all of my co-authors, collaborators, and undergraduate research assistants who helped shape this work. On a personal level, I would like to thank all of my friends who have supported me throughout my time at Maryland.

Contents

List of Tables

List of Figures

Chapter 1: Introduction

The goal of this work was to determine the interkingdom effects of bacterial secretions, including autoinducer-2 (AI-2), on colonic epithelial cells of the GI tract, and then develop engineered microbes that could regulate AI-2 and effect prokaryotic quorum sensing (QS) dependent phenotypes. To better explore the concepts discussed, this chapter will first provide a brief background into the fields of quorum sensing, synthetic biology, quorum quenching, interkingdom signaling, and next-generation RNA sequencing. We will then explore the motivation for this work and provide a brief summary of the work and the upcoming chapters. Subsequent chapters are designed to be self-contained, and have been adapted from manuscripts (accepted, submitted, or in preparation) to peer-reviewed journals.

1.1 Background

1.1.1 Quorum Sensing

QS bacteria produce and respond to their own signaling molecules for induction of gene expression, hence classes of QS molecules are denoted as autoinducers. Quorum sensing is involved in biofilm formation, bioluminescence, virulence factor secretion, sporulation and other critical bacterial functions (reviewed by [1-4]). The first class of QS molecules described were acyl homoserine lactones (AHLs), termed autoinducer-1 (AI-1) and is depicted in **Scheme1A**. This QS system was first discovered with *Vibrio fischeri* [5], a bacterium that provided bioluminescent light in a symbiotic process with its marine, eukaryotic host. Investigations revealed that this process was performed through luxI synthesized the AHL, which once it reach a concentration threshold, bound the luxR protein, and activated the luciferase promoter. This luxI/luxR was later revealed to be a QS paradigm[6,7], with the generation and response to these QS molecules considered species-specific.

A second class of autoinducers, AI-2, were found to consist as two classes (with or without boron), and in equilibrium in a mixture of isomers of 4,5-dihydroxy-2,3-pentadione (DPD) that rapidly interconvert (reviewed by [8]). Depicted in **Scheme 1B,** AI-2 is synthesized by LuxS from the precursor SAH, where it is secreted by TqsA into the extracellular space. AI-2 is imported into the cell primarily through the LsrACDB complex, where it is subsequently phosphorylate din the intracellular space by the kinase LsrK. Phosphorylated AI-2 derepresses LsrR, the master regulator of the *lsr*-system, which allows genomic transcription of the *lsr*-operon. Phosphorylated AI-2 is degraded through a two-step process through enzymes LsrG and LsrF. Unlike AHLs, AI-2 is considered as a 'universal' QS molecule, as the *lsr*-system is widespread among prokaryotes[9].

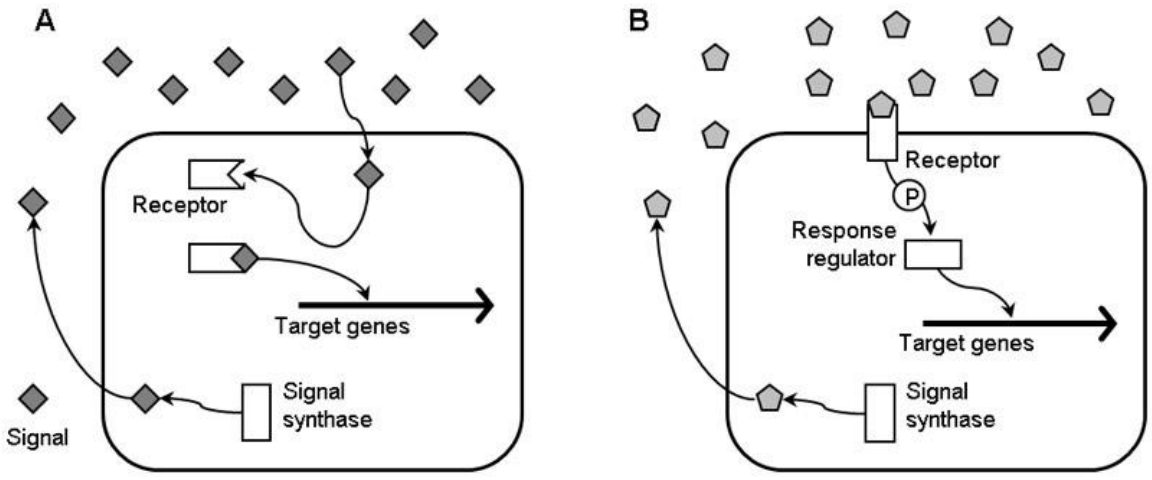

Scheme 1: Quorum sensing paradigms. A) AHL dependent quorum sensing is illustrated where a signal synthase produces the AHL signal that is exported out of the cell. The signal diffuses back into the cell and binds to a QS receptor that activates gene expression. **B)** AI-2 dependent quorum sensing is illustrated where the signal is imported into the cell by an ABC type transporter, and then binds to a response regulator that activates gene expression.

1.1.2 Synthetic Biology

The concept of biological parts that could process logical operations was first envisioned over 50 years ago[10], and the beginning of the 20th century coincided with the rapid emergence of the synthetic biology field as a simple toggle switch [11] was used to create the first of many

increasingly sophisticated gene circuits (reviewed by [12,13]). Most of our knowledge of endogenous genetic circuits (interacting gene networks that guide cellular functions) has consisted of top-down genetic perturbations that have proved to be challenging to develop reliable outcomes. Synthetic biology provides a bottom-up approach to rationally design genetic circuits and test them in living cells.

Synthetic genetic circuits allow the programming of complex, large scale cellular behavior and phenotypes. A common method to connect synthetic circuits has been to leverage the process of quorum sensing (QS), a natural cell-cell process that bacteria use to coordinate action. For example, QS synthetic networks have been used to autonomously produce proteins[14], detect arsenic[15], and produce a synthetic E. coli predator-prey system[16]. QS synthetic networks have also been used to develop bacterial-directed therapies such as cancer-fighting bacteria [17] and probiotic bacteria that can prevent cholera infections[18]. As more complex circuits are being built, dynamic control over these signal molecules will be needed. Through rational design and directed evolution [19], synthetic biology is developing tools that influence the fields of metabolic engineering, biomedicine, and related biological processes.

1.1.3 Interkingdom Communication

The co-evolution of prokaryotes and eukaryotes over millions of years has resulted in symbiotic, commensal, and parasitic interactions, and it is well-established that different bacterial species modulate the host physiological system. Recently, a field has emerged from quorum sensing involving interkingdom communication, specifically the communication between prokaryotes and eukaryotes. The first observation of interkingdom signaling was made by Telford et al., who discovered that an AI-1 molecule, OdDHL, N-(3-*oxo*-dodecanoyl)-l-homoserine lactone, had immunomodulatory effects on murine and human leukocytes[20]. Since then, OdDHL has been found to have many different effects on different tissues by entering and

functioning inside mammalian cells, but the mechanism of entry and OdDHL receptor remains unknown[21,22].

Exploitation of interkingdom signaling networks could result in novel methods to combat infections and develop therapeutics. As an example, while EHEC (enterohemorrhagic *E. coli*) can hijack the hormones epinephrine and norepinephrine to activate pathogenicity [23], this activation can be blocked through the use of α and β adrenergic antagonists[24]. Another example is the QS signal produced from *Pseudomonas aeruginosa*, a common cause of infection in the lungs of cystic fibrosis patients. *P. aeruginosa*-infected lungs secrete OdDHL, which in turn causes the release of large quantities of IL-8, signaling high migration of neutrophils and resulting in extensive tissue damage[25]. With this knowledge, therapeutics could be designed to not only to attack *P. aeruginosa*, but to attenuate these pro-inflammatory signals. Almost all studies on interkingdom communication have concerned AHLs and AI-2, while the interkingdom effects of AI-2 has consisted of a single microarray study at 50 μM of AI-2 with alveoli cells, which found only 4 genes differentially expressed [22]. As a 'universal' signal, the understanding of AI-2 is important not only in polymicrobial networks but also in regards to interkingdom communication.

1.1.4 Quorum quenching

The emergence of multi-drug resistant antibiotic strains has ushered in an era where there is no "magic bullet" to deal with patients with antibiotic-resistant infections [26]. The selective pressure from these bacteriostatic or bacteriocidal agents exert help drive these microbes to develop antibiotic resistance through genotypic or phenotypic agents [27]. While new research suggests that quorum quenching should not be considered impervious to the development of resistance [28], it is nonetheless a promising approach as quorum quenching studies have targeted AHLs using lactonases, acylases and analogues, and AHL-consuming bacteria. Successful applications include the use of AHL-consuming bacteria to reduce virulence of *V. cholera* in

mice[18,29] , the application of synthetic autoinducer peptides to reduce Staphylococcal lesion formation in mice [30], among several others (reviewed [31]).

While most quorum quenching studies have targeted AHLs, there have also been studies targeting AI-2. These AI-2 strategies have used compounds and enzymes to target the extracellular signal, and the intracellular signal generator [27]. In our lab and with our collaborators, we have developed both enzymes that target the extracellular AI-2 signal as well as synthetic analogues to interfere with AI-2 mediated quorum sensing[32,33]. Additionally, an *E. coli* double knockout mutant strain (*ΔluxS ΔlsrR*) has been shown to interfere with bioluminescence and alter the gut microbiome [34,35].

1.1.5 RNA Sequencing

RNA-seq has distinct advantages over microarrays. These include low background noise, absolute transcript count, higher resolution, larger dynamic range, and increased accuracy [36]. The general outlines of upstream RNA-sequencing are shown in **Scheme 2**. The sequenced reads from RNA-seq are mapped to the genome to quantify gene expression, and statistical software is used to determine significantly differentially expressed genes and pathways. A brief overview of the purification, analysis pipeline, and statistical software used is described below.

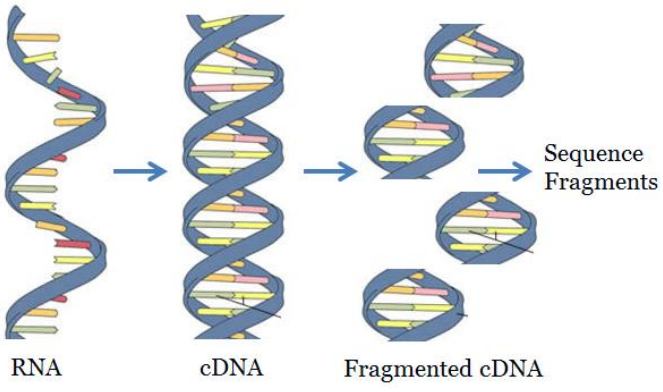

Scheme 2: General outline of RNA- sequencing. RNA is isolated from cells, synthesized to a cDNA library, fragmented to smaller pieces and sequenced from either end.

Samples are sequenced with an Illumina HiSeq1000 at a sequencing facility. A TruSeq RNA Sample Prep Kit (Illumina) is used to purify for polyadenylated mRNA, synthensize a cDNA library from the RNA, and then shear the cDNA into an average library size of 200 base pairs. The RNA is sequenced from both ends in 100 bp lengths with the HiSeq1000 (Illumina). The raw reads obtained from the Illumina HiSeq1000 are first run on the FastQC software to measure quality of the RNA reads based on Phred scores, which calculates a probability of the accuracy of a base call based on peak resolution and peak shape [37]. All reads with an average quality score over 20, which is the most commonly accepted cutoff for reliable RNA reads, will be kept[38].

The sequencing results are analyzed with open-source software to determine biological meaning. Each sample's reads will be aligned to the latest annotated human genome, hg19, using the open-source software Tophat [39]. The output of Tophat are raw read abundances mapping each transcript to its alignment on the human genome. Tophat uses a built-in program Bowtie[40] to first align the cDNA reads to the genome, then uses Tophat to align reads that did not align because of a splicing event and discards reads that cannot be aligned. Using the Integrative Genome Viewer (IGV), the transcript abundances can be viewed at the genome level, the chromosome level, the gene level, down to individual base pairs [41]. While lacking the statistical power to analyze and group sample conditions, IGV provides useful graphical illustrations of the data.

For determination of differential expression, raw read abundances from Tophat are outputted into DESeq[42], an open-source program in R that analyzes the statistical significance of differential expression. This software uses variance, transcript abundance, and fold-change to determine differential expression, normalized by the size of each sample's cDNA library. High abundance of transcripts and low variance in each gene transcript will result in a lower fold change required for significant differential expression. DESeq outputs a significance value for

each gene and a multiple hypothesis tested adjusted p value for each gene. With the thousands of simulataneous inferences being made, multiple hypothesis testing is needed to account for the false discovery rate.

The significanlty differentially expressed genes ($p_{adj}<0.1$) output of DESeq are outputted into the open-source software Signaling Pathway Impact Analysis, SPIA[43]. These differentially expressed genes are then fed into the software SPIA, signaling pathway impact analysis, to determine the biologically relevent pathways that were activated or inhibited. SPIA uses over-representation analysis (the prevalence of differential genes compared to all background genes), functional class scoring (the similarity of functions in genes differentially expressed) and pathway topology (a priori knowledge of signaling pathways).

1.2 Motivation

The symbioses of prokaryotes and eukaryotes in the GI tract leads to the question of what is the role that bacterially produced secretions (secretome), including QS molecules, have on eukaryotes. Interkingdom signaling is an emerging field of research that explores the 'cross-talk' between prokaryotes and eukaryotes. This relationship is of particular importance considering there are over 400 indigenous species of bacteria that comprise the gut and oral cavity, and these bacteria play an important role in proliferation and differentiation of epithelial cells, providing nutrients, influencing and maintaining immune responses. While the mechanisms behind AI-2 quorum sensing networks have been well-studied, the interkingdom signaling relationship between quorum signaling molecules and human cells is not yet understood. Therefore, before we engineer a commensal microbe to remove AI-2, we sought to determine the impact bacterial secretions have on epithelial cells, including in the presence or absence of AI-2.

The motivation behind engineering microbes to rapidly consume the QS molecule AI-2 extends to both natural and synthetic networks. As bacteria are developing resistance to antibiotics at a faster rate than the development of new therapies [44], which is a worldwide

crisis, interfering with quorum sensing as a stand-alone or adjuvant therapy is looked as a promising alternative. Quorum sensing inhibitors using synthetic, plant, or bacterial compounds has shown promising results in attenuating QS-dependent phenotypes, but some of these compounds have stability and toxicity issues, and all of these compounds have localized site of delivery issues. Engineering commensal bacteria that can remove the QS molecule at the site of infection could provide a promising alternative to antibiotics in human and health and disease. Extending beyond natural networks, many synthetic biology applications have incorporated QS networks, which lead to the need for developing tools to control these communication molecules.

1.3 Dissertation Outline

Chapter 2 describes the *in vitro* investigation into the interkingdom effects of the bacterial "secretome", particularly AI-2, on epithelial cells. Two different strains of *E. coli*, BL21 and W3110, and a negative control of growth media only are co-cultured with HCT-8 epithelial cells. To ensure that interaction is only between soluble factors, a transwell was placed between the epithelial cell culture and the bacterial cell culture (the negative control also uses a transwell). After 6 hours, the effects of the secretomes on epithelial cells are determined by extracting the colonic epithelial cell RNA and determining the transcriptome. We found that BL21 and W3110 *E. coli*, which exhibit phenotypic differences including production of flagella, acetate, and AI-2, caused a similar reaction in epithelial cells, with the activation of cytokine-cytokine receptor pathways and the upregulation of negative feedback components of these pathways.

Chapter 3 describes the development of a suite of QS consumers, 'controller cells', which can be deployed to regulate the 'universal' QS molecule autoinducer-2 (AI-2) in a predictable fashion using the well-characterized QS mechanisms of *E. coli*. In this design, we separately overexpressed the three main components responsible for the uptake and degradation of AI-2 from the environment: AI-2 transport into the cell through the protein complex LsrACDB, phosphorylation of AI-2 to AI-2P (a form of AI-2 that cannot cross the cell membrane) by the

kinase LsrK, and degradation of AI-2P by the two-step process of isomerase LsrG and cleavage by LsrF. This study revealed that overexpression of the *lsr*-transporter, LsrACDB, causes the greatest increase in AI-uptake rate, and that overexpression of the kinase, LsrK, results in increased AI-2 uptake by limiting secretion of AI-2 back into the extracellular environment. Further, we developed a simple mathematical model that recapitulates experimental data and characterizes the dynamic balance among the various uptake mechanisms. We show that these 'controller cells' modulate phenotypic outcomes such as biofilm formation and chemotaxis and provide an orthogonal means of manipulation of natural and synthetic gene networks and phenotypes (in press *Metabolic Engineering*). However, these controller cells needed large numbers directly interacting with the QS-dependent bacteria to block communication, required the addition of an exogenous inducing agent, functioned only in the absence of glucose—a common nutrient in a variety of environments—and quenched, but did not tune QS-mediated gene expression.

Chapter 4 describes an extension of this work to encapsulate a controller cell inside a multifunctional polysaccharide capsule to tune protein expression of QS-dependent protein expression systems, without direct interaction with the QS culture, the need for an inducing agent, or the exclusion of glucose. Our previous work revealed that the separate overexpression of LsrK and LsrACDB both resulted in increased uptake, and we hypothesized that the overexpression of both mechanisms would result in greater uptake than each individual overexpression. Therefore, we rationally designed a high-efficiency (HE) 'controller cell' through a two promoter constitutive system on a single plasmid to overexpress all aspects of the *lsr*-system, save the *lsr* repressor. Further, since the metabolic controls prevent AI-2 uptake and phosphorylation when glucose is present, our previously engineered 'controller cells' could not be applied in glucose-rich environments. The HE 'controller cell' constitutively expresses the *lsr*-system on the plasmid independently of genomic transcription, which removes this constraint.

We show that the HE ‘controller cell’ provides the most rapid uptake of AI-2 compared to all previously engineered cells, and that it is able to effectively remove all AI-2 from the extracellular environment in the presence of glucose. Further, the HE cells can silence QS-dependent protein expression at very low HE to target cell ratios, and also when encapsulated inside a biocompatible capsule. We show that these encapsulated HE controller cells can quench QS signaling, which can be envisioned to be used as a quorum quenching treatment to reduce the expression of harmful phenotypes while sequestering the encapsulated bacteria. Our overarching goal was to not only quench protein expression, but to guide a QS-dependent system that would minimally interact with the controller cell populations. We show here that we can tune protein expression by adjusting the quorum activated population through capsule dosage. We envision that by enabling controlled manipulation of quorums, this tool could be used to assay threshold responses, manipulate complex genetic circuits, and develop and interrogate spatially-patterned cell populations.

Chapter 5 discusses the development of an autonomous system that only turns ‘on’ and removes when AI-2 is present. This system not only uptakes and removes AI-2, but reports its presence by fluorescing. The system is well characterized with growth rates, AI-2 uptake kinetics, transcription and protein expression illustrated. We envision these cells could be used in in vivo applications to report and function in a programmable fashion.

Chapter 6 provides a summary of the work, as well as discusses the contributions to science and future work.

Chapter 2: Bacterial secretions of nonpathogenic *E. coli* elicit inflammatory pathways: a closer investigation of interkingdom signaling

This chapter was primarily reproduced directly or adapted from Zargar, Amin, et al. "Bacterial Secretions of Nonpathogenic Escherichia coli Elicit Inflammatory Pathways: a Closer Investigation of Interkingdom Signaling." *mBio* 6.2 (2015) with permission [45]

2.1 Abstract

There have been many studies on the relationship between nonpathogenic bacteria and human epithelial cells; however, the bidirectional effects of the secretomes (secreted substances, where there is no direct bacteria-cell contact) have yet to be fully investigated. In this study, we use a transwell model to explore the transcriptomic effects of bacterial secretions from two different non-pathogenic *Escherichia coli* strains on the human colonic cell line HCT-8 using next-generation RNA-seq transcriptional profiling. BL21 and W3110 *E. coli*, while genetically very similar (99.1% homology), exhibit key phenotypic differences including their production of macromolecular structures (e.g., flagella, lipopolysaccharide), and secretion of metabolic byproducts (e.g., acetate) and signaling molecules (e.g., quorum sensing autoinducer, AI-2). After analysis of differential epithelial responses to the respective secretomes, this study shows for the first time that a non-pathogenic bacterial secretome activates the NF$\kappa\beta$-mediated cytokine-cytokine receptor pathways while also upregulating negative feedback components including the NOD-like signaling pathway. Because of its relevance as a bacteria-bacteria signaling molecule and the differences in its secretion rate between these strains, we investigated the role of autoinducer-2 (AI-2) on the HCT-8 cells. We found that the expression of inflammatory cytokine IL-8 responded to AI-2 with a pattern of rapid upregulation before subsequent downregulation after 24 hrs. Collectively, these data demonstrate that secreted products from non-pathogenic

bacteria stimulate transcription of immune related-biological pathways followed by the upregulation of negative feedback elements that may serve to temper the inflammatory response.

2.2 Importance

The symbiotic relationship between the microbiome and the host plays an important role in the maintenance of human health. There is a growing need to further understand the nature of these relationships to aid in the development of homeostatic probiotics and also in the design of novel antimicrobial therapeutics. To our knowledge, this is the first global transcriptome study of bacteria co-cultured with human epithelial cells in a model to determine transcriptional effects of epithelial cells, while allowing epithelial and bacterial cells to "communicate" to each other only through diffusible small molecules and proteins. By beginning to demarcate the direct and indirect effects of bacteria on the GI tract, two-way interkingdom communication can potentially be mediated between host and microbe.

2.3 Introduction

With approximately 10^{14} bacterial cells [46] populating the human GI tract, scientific investigations have uncovered that interkingdom interactions play an important role in maintaining homeostasis [47-49]. However, the normal microbiome can also elicit a dysregulated immune response that can be a source of pathogenicity in inflammatory bowel diseases, most commonly Crohn's disease and ulcerative colitis. In the GI tract, intestinal epithelial cells (IECs), which are an important part of the innate immune system, act as a bridge to the adaptive immune system through their expression and secretion of inflammatory cytokines. IECs initiate this mechanism through pathogen associated molecular pattern (PAMP) receptors, such as toll-like receptors (TLRs) and nucleotide-binding oligomerization domain (NOD) receptors, which recognize bacterial products such as lipopolysaccharides, flagella, and peptidoglycan. These receptors activate signaling pathways, mainly through the transcription factor NF$\kappa\beta$, that culminate in the production of cytokines [50-52]. As the first point of contact, IECs are

continuously exposed to huge numbers of Eubacteria (10^{10}-10^{12} cells per gram) in the colon [53] and therefore play an important role in bacterial-host communication [54-56].

An understanding of the mechanisms of response and communication between the secretomes of epithelial cells and bacteria can aid in the understanding of the evolutionary biology of signal development as well as interventional design strategies for maintaining homeostasis (**Figure 2.1**) [56,57]. Moreover, signals that coordinate phenomena among bacteria (e.g., quorum sensing) and signals that mediate bacterial – IEC interactions are of particular interest as these communication networks are involved in pathogenesis and the progression of disease [55,58,59]. Commensurate with the need to understand this interkingdom communication, there have been many studies exploring the effects of non-pathogenic, commensal strains of bacteria on human cells [60-64]. However, most of these involved direct bacterial – IEC interaction, and those that investigated the secretome did not determine a global transcriptomic or proteomic response, leaving the effects of bacterial secretions to be largely unexplored. We have characterized the effects of the *E. coli* secretome, which is well-represented in the colon [65], through the use of a transwell that separates bacteria from epithelial cells while allowing small molecules and proteins to pass, and we have employed RNA-Seq because it provides several advantages over DNA microarrays including lower background noise, an absolute transcript count, and higher resolution [36]. By determining the global transcriptomic response of IECs to bacterial incubations in a system that allows only indirect contact, we can then more closely investigate the commonalities of interkingdom communication.

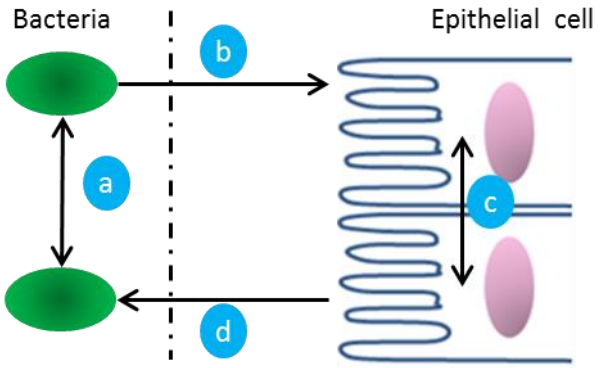

Figure 2.1: Interkingdom communication between microbiome and host in the GI tract. a) Quorum sensing (QS) molecules coordinate action among bacteria. b) Secretome of bacteria, including QS molecules, affect the host's cellular machinery c) Epithelial cells secrete signals to neighboring and distant cells through signaling molecules d) Soluble factors secreted by the host affect bacteria

In this work, we exposed nonpathogenic strains of two Gram-negative, Group A *E. coli*, BL21 and W3110, grown in the upper chamber of a transwell to the IEC line, HCT-8, cultured in a monolayer beneath the transwell. BL21, B strain derivative, and W3110, a K-12 strain derivative, have significantly different transcriptomes and proteomes leading to important phenotypic differences[66,67]. Our investigations show that the secretomes of either BL21 or W3110 activated the cytokine-cytokine receptor pathway (e.g. IL-8, TNF), while also upregulating the negative feedback regulators in NF$\kappa\beta$ and NOD-like signaling pathways, NF$\kappa\beta$ – α and TNFAIP3, respectively. The upregulation of cytokines that activate the immune system as well as negative feedback regulators that reduce the transcription of these cytokines, could be part of the normal physiological response using a negative feedback loop [68] without which uncontrolled stimulation of inflammatory cytokines would lead to damaging inflammation to the host [47,68].

The role of AI-2 was investigated further by incubating the *in vitro* synthesized signal molecule at varied concentrations and time periods with IECs in follow on studies. The inflammatory cytokine, IL8, which plays an important role in attracting neutrophils, was found to be initially upregulated at all concentration levels of AI-2 tested (50, 150 and 400 µM) at 6 and

12 hours post-addition. It was subsequently significantly reduced at all concentrations relative to the control after 24 hours. These data support a hypothesis that AI-2 is an IEC signaling molecule and that bacterial secretions, including AI-2, may have an initial transcriptional inflammatory response that is downregulated through alternative mechanisms, possibly including negative regulators NF$\kappa\beta$ –α and TNFAIP3.

2.4 Materials and Methods

2.4.1 HCT-8 incubations with bacteria.

HCT-8 cells were plated in 6 well culture plates (Fisher Scientific) at a seeding density of 750,000 cells per well (375,000 cells/mL) in 10% Horse Serum (vol/vol) RPMI 1640 media (ATCC). The culture was grown to confluence for 48 hours at 37°C in the presence of 5% CO_2 humidified air. A 0.4 μm transwell (Becton Dickinson) was placed in each culture plate and BL21 (2.6% overnight culture), W3110 (2.6% overnight culture) in 1.5 mL of RPMI media was added. RPMI media alone was added as a negative control. The co-culture was then incubated for 6 hours at 37°C in the presence of 5% CO_2 humidified air. After incubation, the transwell and enclosed media in the upper chamber were discarded, and the media of the lower chamber was removed and harvested for the *Vibrio harveyi* BB170 AI-2 activity assay and ELISA assays. The RPMI media is supplemented with phenol red, and there was no change in color in the lower chamber, indicating that there were no significant pH changes during incubation. RNA was extracted with the RNAqueous kit (Invitrogen) and eluted RNA was stored at -80°C until thawed for sequencing and qPCR.

2.4.2 HCT-8 incubations with AI-2.

HCT-8 cells were plated and cultured in a similar manner as above. Synthetic AI-2 (10 mM) in water was generously provided by the Sintim research group. AI-2 at 50, 150 and 400 μM in 2 mL of fresh RPMI media and incubated with HCT-8 cells for 6, 12 and 24 hours.

2.4.3 AI-2 activity assay.

After incubation for 6 hours with the respective conditions, the media of the HCT-8 cells were harvested and tested for the presence of AI-2 by inducing luminescence in *Vibrio harveyi* reporter strain BB170, which was outlined Bassler and coworkers[69]. Briefly, BB170 was grown for 16 hours with shaking at 30°C in AB medium and kanamycin, diluted 1:5,000 in fresh AB medium and kanamycin, and aliquoted to sterile 12- by 75-mm tubes (Fisher Scientific). The media of each condition was added to a final concentration of 10% (vol/vol) to these tubes. Luminescence was measured by quantifying light production with a luminometer and obtained values were in the linear range. Values represent fold change compared to negative control. All conditions were taken in triplicate.

2.4.4 RNA Downstream Analysis.

Each sample's reads were aligned to the RefSeq annotated human genome, hg19, using the software Tophat [39]. These read abundances were then outputted into DESeq [42], an open-source program in R that analyzes the statistical significance of differential expression. The abundance of sequenced reads, 'counts', of each gene were input into DESeq, a software that uses variance, transcript abundance, and fold-change to determine differential expression, normalized by the size of each sample's cDNA library. A modified Fisher's exact test with data fit to a negative binomial distribution of the DESeq package was used to identify the differentially expressed (DE) genes. Differentially expressed genes were outputted to SPIA [43] to evaluate pathway activation.

2.4.5 Quantitative reverse transcription polymerase chain reaction (qPCR).

RNA was synthesized to cDNA using the BIO-73005 SensiFast SYBR Hi-Rox One Step Kit. For the selected candidate genes, primers were taken from the literature or designed using PrimerQuest. β-2-microglobulin, β2M, was used as a housekeeping gene, and qPCR was

performed on the 7900HT real time PCR System (Applied Biosystems) and thermal conditions of 10 min at 45°, 2 min at 95°, and 40 cycles of 5 s at 95°and 20 s at 60°. The relative gene expression level of each target gene was then normalized to the mean of β2M in each group. The control for each gene expression sample set data was selected to be 0 μM AI-2 samples at each time point. Fold change was calculated using the ΔΔCT relative comparative method. Data from all the studies were analyzed using analysis of variance. Samples were completed in triplicate and standard deviations are reported (n=3).

2.4.6 Enzyme-linked immunosorbent assay (ELISA)

Cell culture supernatants of HCT-8 cells in transwell incubations with BL21, W3110, and media alone were harvested and subsequently assayed with the Human Inflammatory Cytokines Multi-Analyte ELISArray Kit MEH-004A (Qiagen)

2.5 Results

2.5.1 The secretome of BL21 and W3110 causes differential gene expression in HCT-8 cells.

In this study, we explored the transcriptomic changes of co-incubations of BL21 and W3110 in a transwell model with the IEC cell line, HCT-8. We chose a coincubation model, instead of using conditioned medium because bacteria themselves are affected by secretable molecules from mammalian cells, and we chose to include any such crosstalk [70,71]. Toward this end, overnight cultures of BL21 and W3110 were re-inoculated in fresh media in the upper chamber of the transwell, and blank media alone was used as a negative control (**Figure 2.2A**). The 0.4 μM transwell does not allow measureable amounts of bacteria to pass through the upper chamber (verified through optical density measurements of the lower chamber), but is large enough to allow metabolites and signaling molecules to pass. After 6 hours of coincubation, both bacterial strains reached similar cell densities (OD_{600} ~ 1, data not shown), and IECs appeared visibly intact with a cell viability assay showing less than 5% cell death [data not shown]. The

RNA of the HCT-8 cells was extracted, and cDNA libraries were created from polyadenylated RNA.

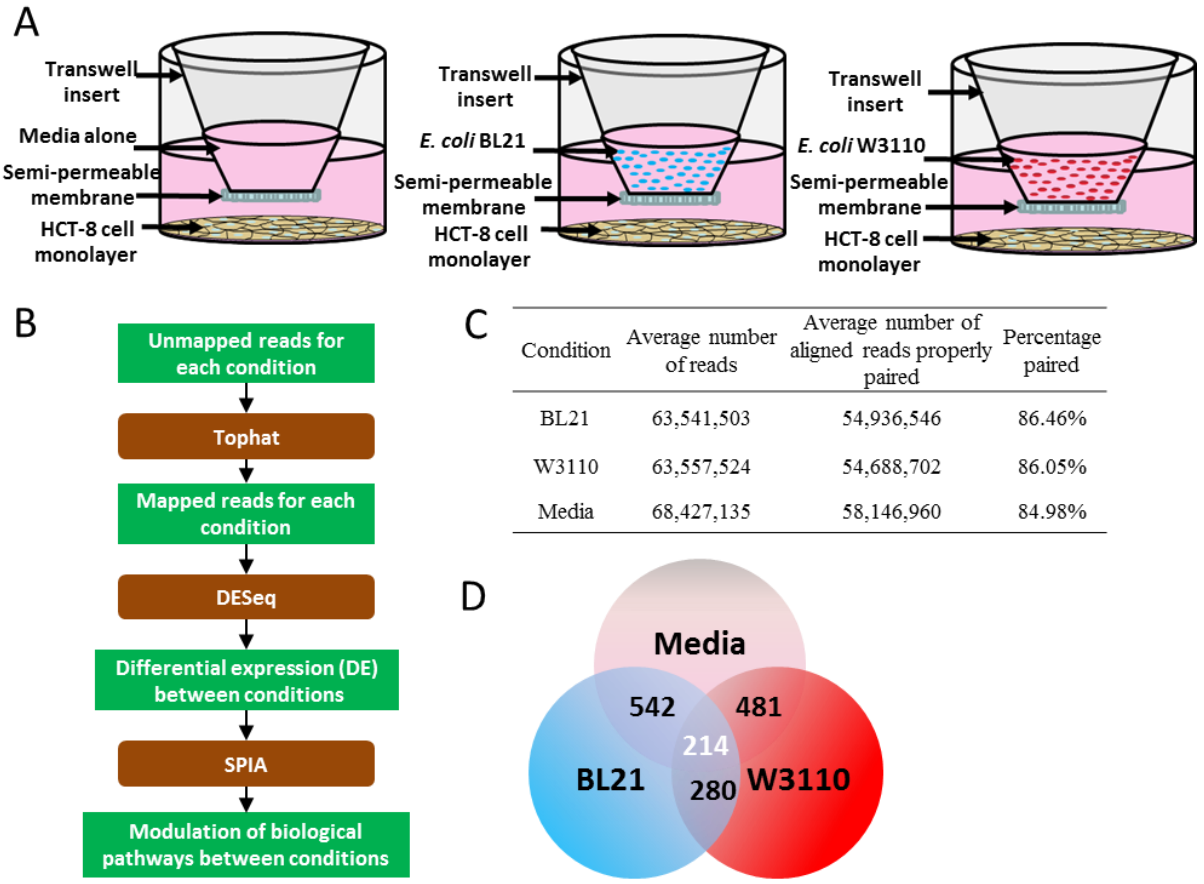

Condition	Average number of reads	Average number of aligned reads properly paired	Percentage paired
BL21	63,541,503	54,936,546	86.46%
W3110	63,557,524	54,688,702	86.05%
Media	68,427,135	58,146,960	84.98%

Figure 2.2: Schematic of experimental setup. A) HCT-8 epithelial cells were grown to confluency, and then incubated with BL21, W3110 or media alone in the upper chamber of a transwell. After 6 hours of incubation, the RNA of the epithelial cells were extracted and sequenced. **B)** Downstream RNA-Seq pipeline for analysis of sequencing data (red boxes indicate open-source program). **C)** Mapping results of HCT-8 NGS transcripts to Refseq annotated human genome, hg19, with 5 biological replicates using the software Tophat **D)** Differentially expressed genes using the software DESeq. 542 differentially expressed genes between HCT-8 cells incubated with BL21 or blank media, 481 genes between HCT-8 cells incubated with W3110 or blank media, 280 genes between HCT-8 cells incubated with BL21 or W3110. We found 214 DE genes in common in incubations of BL21 or W3110 compared to blank media.

The cDNA libraries of each condition were sequenced via NGS (see Methods) and then analyzed with downstream statistical software (**Figure 2.2B**). We performed five biological replicates, each constituting an average of over 60 million 100 bp paired-end reads mapping to

hg19, a RefSeq annotated human genome (**Figure 2.2C**). Mapping sequenced reads to the genome was performed using Tophat [39] (which uses a built-in alignment tool) and Bowtie [40] (which maps the cDNA reads to the reference genome). Tophat then aligns reads that did not initally align because of a splicing event and discards reads that cannot be aligned. The aligned reads were inputted into the open-source software DESeq [42], which was used to determine significantly differentially expressed genes (Benjamini-Hochberg-adjusted p values below 0.05).

DESeq results indicated that BL21 and W3110 caused 542 and 481 differentially expressed genes to be up or down-regulated when compared to blank media and 280 were differentially expressed between BL21 and W3110 bacterial incubations. BL21 and W3110 affected 214 genes in common when compared to blank media (**Figure 2.2D**). A closer examination of differentially expressed transcriptional levels between the three comparisons illustrate that the majority of differentially expressed fold changes were small magnitude differences that were less than two-fold **(Table 2.1).** With five biological replicates, we were able to determine significant differential gene expression between conditions that displayed these small differences. Additionally, we selected 8 genes for qPCR verification that spanned a wide range of expression, and measured transcriptional levels with qPCR, which showed a high degree of correlation, as expected **(Supplementary Figure 2.1)**.

DE gene category		BL21 / Media	W3110 / Media	BL21 / W3110
Upregulated genes				
	1 < FC[b] < 1.5	154	154	66
	1.5 < FC < 2	45	28	33
	FC > 2	42	21	126
	Total no. upregulated	241	203	225
Downregulated genes				
	1 < FC < 1.5	262	166	39
	1.5 < FC < 2	26	26	14
	FC > 2	13	86	2
	Total no. downregulated	301	278	55
Total number of DE genes[a]		542	481	280

[a] DE is determined using open-source software DESeq. All genes listed have Benjamini-Hochberg-adjusted $p < 0.05$

[b] FC is fold change

Table 2.1: Differentially expressed (DE) genes. DE genes in HCT-8 cells in incubations with BL21, W3110, or media alone.

2.5.2. BL21 and W3110 activate the cytokine-cytokine receptor pathway.

The biological implications of these differentially expressed genes were determined using Signaling Impact Pathway Analysis [43]. SPIA uses over-representation analysis (the prevalence of differential genes compared to all background genes), functional class scoring (the similarity of functions in genes differentially expressed) and pathway topology (*a priori* knowledge of signaling pathways) to identify activated or inhibited pathways **(Supplementary Figure 2.2)**.

Since epithelial cells are often damaged through extracellular stimuli, they often initiate inflammation through the release of cytokines [72]. The cytokine-cytokine interaction pathway is regulated through the chemokine and NF$\kappa\beta$ pathways, and as expected, these pathways were activated in both bacterial incubations **(Table 2.2)**. The toll-like receptor (TLR) pathway is not listed in **Table 2.2** as the pathway was not activated. It has been shown that TLR receptors in

444 colonic IECs, unlike other types of epithelial cells, develop tolerance after exposure to PAMPs
445 such as LPS and lipotechnoic acid (LTA) [73,74], and only activate the TLR pathway after being
446 primed with interferon-gamma (IFNγ) [75].

447

BL21 / Media			W3110 / Media		
KEGG Pathway	p-value[a]	Status	KEGG Pathway	p-value[a]	Status
Cytokine-cytokine receptor interaction	9.27E-06	Activated	Cytokine-cytokine receptor interaction	4.26E-05	Activated
Chemokine signaling pathway	4.06E-04	Activated	Chemokine signaling pathway	1.81E-04	Activated
Osteoclast differentiation	3.58E-03	Activated	NOD-like receptor signaling pathway	1.93E-04	Inhibited
NFκβ signaling pathway	1.10E-02	Activated	HTLV-I infection	2.67E-04	Activated
HTLV-I infection	1.18E-02	Activated	Epstein-Barr virus infection	4.10E-04	Activated
Chagas disease	4.10E-02	Activated	NFκβ signaling pathway	7.94E-04	Activated
NOD-like receptor signaling pathway	5.48E-02	Inhibited	Osteoclast differentiation	5.47E-02	Activated

[a] pGFWER is Bonferroni adjusted global p-values

Table 2.2 SPIA significance. DE genes were inputted into SPIA (Signaling Pathway Impact Analysis) software to determine activated or inactivated pathways. Incubations of BL21 compared to media alone resulted in the modulation of seven annotated KEGG pathways, and incubations of W3110 compared to media alone also resulted in the modulation of seven annotated KEGG pathways. Common to both sets were the activation of the cytokine-cytokine receptor interaction, chemokine signaling pathway, osteoclast differentiation, NFκβ signaling pathway, human T-lymphotropic virus-1 (HTLV-I) infection, and the inactivation of the NOD-like receptor signaling pathway.

A closer investigation of the cytokine network found that 10 cytokines were significantly differentially expressed in one sample or the other (**Figure 2.3A**). All of these cytokines were upregulated, except BMP4, which is reponsible for the regeneration of epithelial cells. The upregulation of granulocyte macrophate colony-stimulating factor (CSF2) stimulates stem cells to produce granulocytes (neutrophils, eosinophils, and basophils) and monocytes. The CXC cytokines that were upregulated, (CXCL1, CXCL2, CXCL3, IL8) are chemotactic for neutrophils, and all of the CXC chemokines upregulated act as agonists for the same receptor. TNF, TNFSF9, and TNFRSF9 were upregulated and act as pro-apoptotic signals or receptors, as well as promoting leukocyte chemotaxis through the induction of proinflammatory cytokines [76]. CCL20, a CC motif cytokine, is weakly chemotactic for neutrophils, and strongly attractive for lymphocytes. Taken together, the cytokines act collectively to induce activation and long-term

survival of neutrophils. This upregulation indicates that bacterial secretions have caused the IEC to signal the adaptive immune response due to the secretome of these nonpathogenic bacteria.

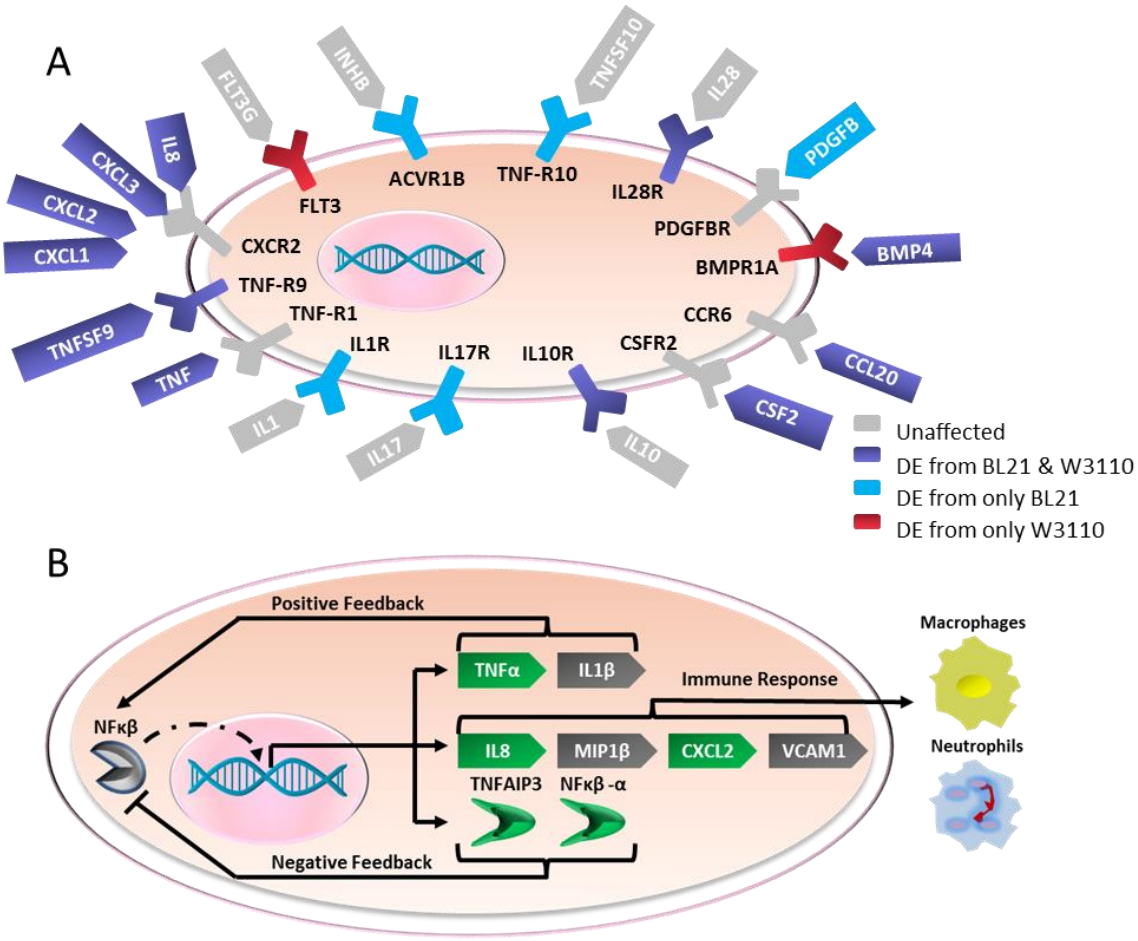

Figure 2.3: Signaling pathway analysis. A) Activation of cytokine-cytokine receptor interaction pathway in incubations with BL21 or W3110. Schematic shows cytokines (ovals) and cytokine receptors (rectangles) upregulated only by incubation with BL21 (blue), only by incubation with W3110 (red). Incubations with either *E. coli* strain (purple), or with no change in regulation by either *E. coli* strain is also shown (grey). **B)** Schematic of genes involved in canonical NF$\kappa\beta$ pathway, adapted from KEGG. Gene expression levels upregulated (green) and unaffected (grey) by incubations with both BL21 and W3110 compared to media alone are shown.

2.5.3 BL21 and W3110 activate the NFκβ pathway and its negative feedback components.

The NF$\kappa\beta$ pathway is an integral part of the immune response, and functions as a protein complex that controls DNA transcription. To prevent uncontrolled inflammation, it is thought that

the negative feedback mechanisms associated with PAMP receptor activation are upregulated to suppress the over-production of inflammatory cytokines [77]. Consistent with this hypothesis, the canonical NF$\kappa\beta$ pathway was activated in both bacterial incubations, and the negative feedback components (i.e. NF$\kappa\beta$ -α inhibitor) were upregulated as well **(Figure 2.3B)**.

The function of the NF$\kappa\beta$ pathway is controlled by the NF$\kappa\beta$ kinase (IKK) complex, which consists of NEMO, IKK-α and IKK-β. The IKK complex phosphorylates the NF$\kappa\beta$ -α inhibitor, which causes its proteosomal degradation. The degradation of the NF$\kappa\beta$ -α inhibitor leads to the free movement of NF$\kappa\beta$ into the nucleus and subsequent initiation of gene transcription. In both BL21 and W3110 incubations, the end products of the canonical NF$\kappa\beta$ pathway were upregulated (inflammatory cytokines IL8, TNFα, and CXCL2) while the end products of the atypical NF$\kappa\beta$ pathway (e.g. apoptosis regulator Bcl-XL) were unchanged. This indicates that the bacterial secretomes stimulated the HCT-8 immune response through the canonical NF$\kappa\beta$ pathway, and possible microenvironmental conditions such as hypoxia, which activate the atypical NF$\kappa\beta$ pathway[78], did not elicit an immune response.

Critically, NF$\kappa\beta$ -α inhibitor, which is integral to the negative feedback in the NF$\kappa\beta$ pathway, was upregulated in both BL21 and W3110 incubations. Additionally, the NOD-like receptor pathway was inhibited in both pathways, with its negative feedback response regulator, TNFAIP3, also upregulated in both bacterial samples. NOD-like receptors (NLRs) act as cytosolic sensors, and once activated, subsequently activate a receptor-interacting protein (RIP). TNFAIP3 acts as the negative regulator of RIP, thereby quenching the signaling cascade despite the continued presence of agonists of NLRs [79]. TNFAIP3 has also been shown to be a critical negative feedback regulator to the NF$\kappa\beta$ pathway [80]. The activation of the NF$\kappa\beta$ pathway and the negative feedback regulators NF$\kappa\beta$ -α inhibitor and TNFAIP3 suggest that components of the bacterial secretions act as a stimulus to the immune system, and that the epithelial cells have

coincidently upregulated the negative feedback components to prevent uncontrolled inflammation from this nonpathogenic encounter.

2.5.4 Upregulation of gene expression by bacterial secretomes do not translate to increased cytokine protein expression.

Using a 12 cytokine multi-analyte ELISA kit, we surveyed two of the upregulated cytokines from incubations with BL21 and W3110 (TNF and IL8) as well as 10 other cytokines involved in inflammation. We found that while inflammatory cytokine gene expression was upregulated at the transcriptional level, there was no concomitant increase in secretion **(Supplementary Figure 2.3).** This finding is supported by Kamada et al. (2000), who similarly used a transwell model and found that IL-8 secretion was unchanged in IEC HCT15 when incubated with *E. coli* K-12 strain DH10β for 4 hours [63]. These results indicate that the transcriptomic upregulation is quenched either post-translationally or through the upregulation of negative feedback mechanisms such as NF$\kappa\beta$ and NOD-like signaling pathways.

2.5.5 BL21 and W3110 cause differential expression in genes responsible for tissue structure.

Since the bacterial secretome includes components such as LPS, an activator of osteoclastogenesis to enchance bone resorption in both *in vitro* and *in vivo* studies **[81,82],** differential expression of genes responsible for tissue structure was expected. Both BL21 and W3110 resulted in the activation of the osteoclast differentiation signaling pathway. CTSK, an end-product of this pathway, was upregulated in incubations with both BL21 and W3110 and encodes for the protein cathepsin K, a protease that breaks down elastin, gelatin and collagen, which are critical components of bone and cartilage. Furthermore, in the cytokine-cytokine receptor pathway, the downregulation of BMP4 induces the increased epithelial stem cell renewal. Collectively, these transcriptional differences indicate that the epithelial cells have been

insulted by the bacterial secretomes, causing the upregulation of genes responsible for cell renewal.

2.5.6 Strain-specific differentially expressed genes

BL21 and W3110 are derivatives of the B and K-12 strains of *E. coli*, respectively, and comprise the majority of all laboratory strains. Despite the similarity of their genomes, B strains and K-12 strains show marked phenotypic differences. B strains grow faster in minimal media, and have lower acetate production [66,67]. Furthermore, while B cells produce lower amounts of intracellular proteases (e.g. Lon, ClpA, ClpP), they secrete higher total levels of extracellular proteins, mainly through its Type II secretion pathway. K-12 strains have higher gene expression levels of heat shock proteins, flagella that provide motility, and they more ably survive stress insults (e.g. osmolarity, pH) than W3110 [66]. A closer investigation into the differential regulation caused by each strain illustrates that both affect the directionality (i.e. upregulated or downregulated) of differential expression in a similar manner. Of the 214 differentially expressed genes that BL21 and W3110 share in comparison to blank media, 100% of them were regulated in the same manner (i.e. upregulated or downregulated). **Figure 2.4** shows a heatmap of the two strains organized by the 25 most up and downregulated genes in the BL21 coincubation. The similarity in gene expression to incubations with W3110 was striking, with many cytokines as the most upregulated genes.

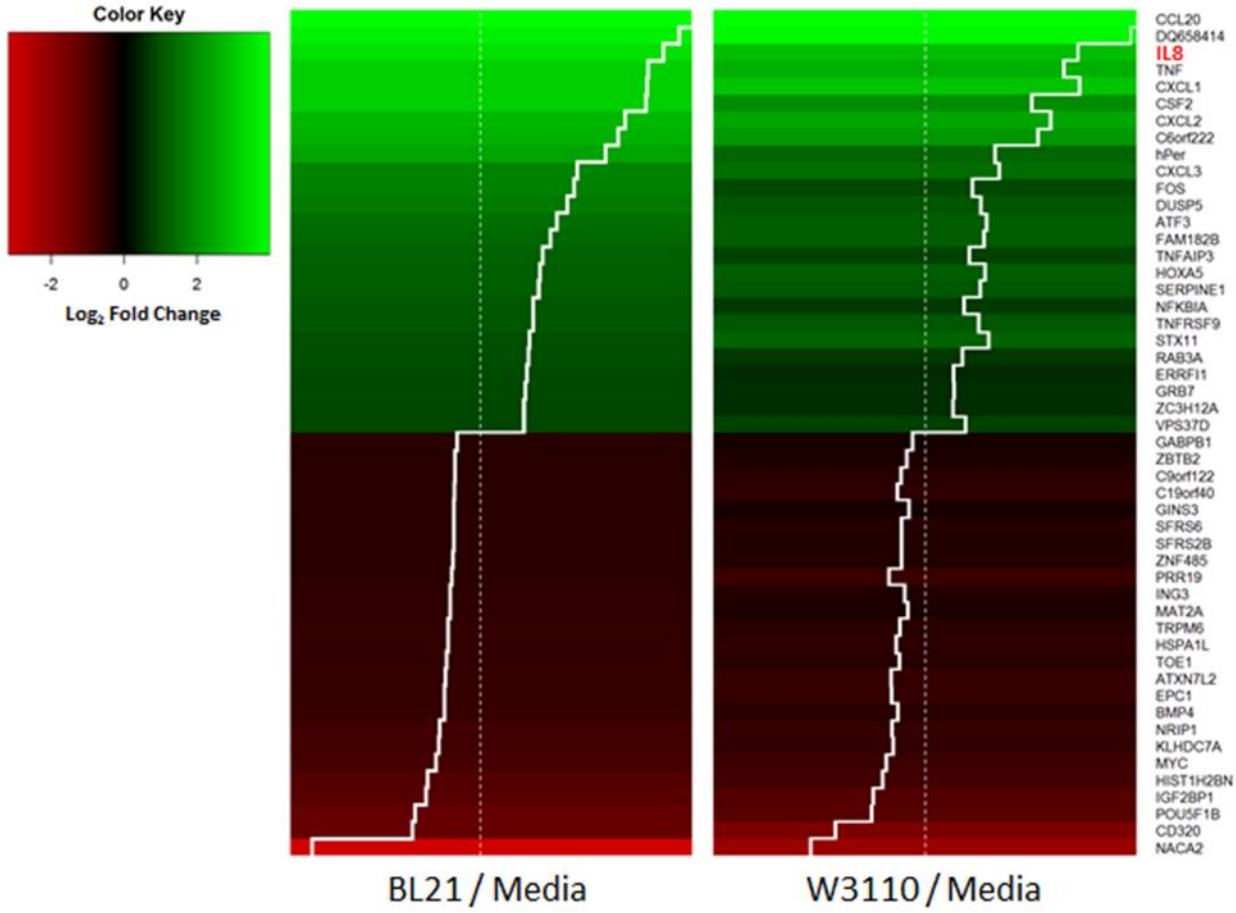

Figure 2.4: Heatmap. 25 most upregulated (green) and downregulated genes (red) in HCT-8 in incubations with BL21 compared to media alone and in incubations of W3110 compared to blank media. Trace line (white) indicates direction and extent of differential expression. Differential expression levels are similar between incubations of BL21 and W3110, and 100% of differential expression is regulated in the same manner (i.e. up or downregulated). DESeq was used to identify differential expression, and all genes listed have Benjamini-Hochberg-adjusted $p < 0.05$. Cytokines, including IL8 (red text), were among the genes most upregulated.

While both strains showed similarity in fold change expression levels and directionality of regulation, we found the amplitude of the up and/or downregulation was higher in BL21 incubations. This trend was also subtly revealed by more carefully considering the results from **Figure 2.1C**. Of the 214 genes that were commonly differentially expressed in both strains compared to blank media (**Figure 2.1C**), 96 were upregulated, and 76 of these (79.1%) were more upregulated in the BL21 sample. Of the 118 genes downregulated in common, 75 of these (63.5%) were more downregulated in the BL21 sample. Then, there were 280 genes differentially

expressed when comparing BL21 directly to W3110 (**Figure 2.1C**), and of these genes, 225 (80.3%) were differentially expressed at a greater amplitude in incubations with BL21. Of particular importance is IL-8, a proinflammatory cytokine, as it shows greater abundance in incubations with BL21 as opposed to W3110 **(Figure 2.5)**. These expression level differences indicate that secretions from BL21 induce a greater epithelial cell response than W3110. Importantly, cell densities of inocula were identical as were the final optical densities (data not shown).

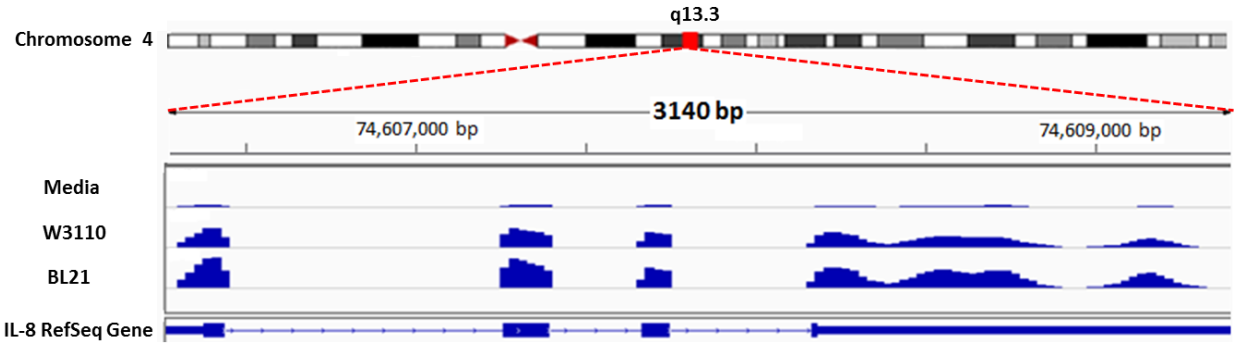

Figure 2.5: NGS sequenced reads mapped to annotated IL-8 gene as visualized in IGV. The IL-8 gene is shown at the bottom with four exons separated by three introns. Each read is represented by a blue square, and the abundance of reads at each condition (BL21, W3110 or media alone) is shown. HCT-8 incubations with W3110 show greater abundance of IL-8 transcription compared to media alone, while incubations with BL21 illustrate higher levels than W3110. One representative replicate sample of each condition is shown.

We then sought to investigate the cause of the greater perturbation caused by BL21 compared to W3110. Because of the use of the transwell, the phenotypic differences that would require direct interaction can be ignored, and we can focus on secretable substances. One possible candidate, LPS, is more highly expressed in BL21 than W3110 [66], and it is well known that LPS induces inflammatory effects on cytokines[83,84] and through it, the activation of the NF$\kappa\beta$ in colonic IECs [85]. However, in colonic epithelial cells, the addition of cytokine IFNγ to the IEC is needed to express myeloid differentiation protein-2 (MD-2), which is required for LPS responsiveness [75,83]. Furthermore, priming of IFNγ with subsequent LPS exposure shows a transient upregulation of IL-8 that returns to baseline levels after 6 hours, which is the time period

used in this study. On the other hand, BL21 produced much more extracellular AI-2 than W3110 (~ 35 μM compared to 8 μM, **Supplementary Figure 2.4**), and BL21 cells do not express the ABC transporter for uptake of quorum sensing signal molecule, autoinducer-2 (AI-2) or the intracellular kinase that sequesters AI-2 inside the cell [86]. BL21 showed much higher The effect of autoinducer-2 on colonic cells is of particular interest not only because the highest numbers of bacterial concentrations in the gut are found therein, but Eubacteria are almost entirely concentrated in this area of the GI tract [53]. Furthermore, the LuxS/AI-2 production system is highly conserved among the Eubacteria [9,87,88]; therefore we chose to investigate the effect of autoinducer-2 on IECs. While we have shown that the robust transcriptional response of epithelial cells to BL21 and W3110 is similar, the slightly greater amplitude shift in BL21 may be caused by the much higher levels of AI-2 in BL21. We then sought to tease out this smaller effect from the overall systematic response elicited from the secretome.

2.5.7 AI-2 initiates upregulation of inflammatory cytokines before downregulation.

Bacteria secrete and detect small molecules or autoinducers to coordinate gene expression in a cell density-dependent manner (known as quorum sensing, QS). These QS molecules are produced throughout the Eubacterial hierarchy and influence characteristics such as swarming motility, biofilm formation, virulence, among others (reviewed by [1-4]). The terminal synthase for one prevalent autoinducer, AI-2, has been found in over 80 species [9,87].

Studies have shown both beneficial and deleterious effects of QS molecules on human epithelial cells. N-3-(oxododecanoyl)-L-homoserine lactone (OdDHL) produced by *Pseudomonas aeruginosa* induces apoptosis in many mammalian cell types[89-91], while indole has been found to decrease inflammation in IECs by attenuating IL-8 production, reducing TNFα mediated NFκβ activation, and tightening cell junctions [49]. Investigations into interkingdom effects of AI-2 on human cells have been limited to one study where Bryan et al. (2010) performed

microarray studies of alveolar cells exposed to AI-2 at 50 μM, and found only 4 genes with over 2 fold changes in expression [22].

We chose to investigate the effect of AI-2 directly on IECs, and have performed a time course analysis using a range of AI-2 concentrations: 50, 150 and 400 μM. It must be noted that the levels of AI-2, or any other quorum sensing metabolite, is unknown in the GI tract. However, indole has been found in human feces at concentrations ranging from ~ 50-1100 μM [92,93], and interkingdom studies have used a range of concentrations from 0.4 to 250 μM for the AI-1 molecule OdDHL[22,90,91]. In our study, 50 μM of AI-2 was chosen as it is the concentration of the only previous interkingdom study [22], and is a level approximating our coincubation studies with BL21, which exposed the HCT-8 cells to much higher levels of AI-2 than W3110 **(Supplementary Figure 2.4).** 150 μM represents the upper limit reached by standard LB cultures of *E. coli* BL21 [94]. Finally, since it has been shown higher concentrations of Eubacteria can populate the colon than can be reached *in vitro* [53] and that QS molecules can reach much higher in biofilms (~600 μM) [95], we also selected 400 μM of AI-2 as a possible representation of high local QS molecule concentrations.

Thus, we exposed HCT-8 cells to 50, 150 and 400 μM AI-2 for 6, 12 and 24 hours. We performed AI-2 assays on samples after 24 hours and found that significant quantities of AI-2 were still present [data not shown]. After harvesting the RNA, we found that, IL-8, a proinflammatory cytokine that is chemotactic to neutrophils, was moderately upregulated with the average fold change for all three concentrations totaling 2.29 and 1.69 at 6 and 12 hour time points, respectively, before being downregulated (-1.98) compared to blank media for all three concentrations ranges at 24 hours (**Figure 2.6**). This trend was consistent with the secretomes and was found at all 3 concentrations. Interestingly, the same trend but at lower amplitude was found for TNF and CSF2 at some concentrations **(Supplementary Figure 2.5).** It is hypothesized that the interplay between host and the microbiota is tightly regulated, and that microbial metabolites

induce changes in the host signaling pathways, which are restored through negative feedback loops[68]. The initial upregulation of IL-8 expression levels with exposure of BL21 and W3110 to the HCT-8 cells, followed by abatement to lower levels is consistent with this hypothesis.

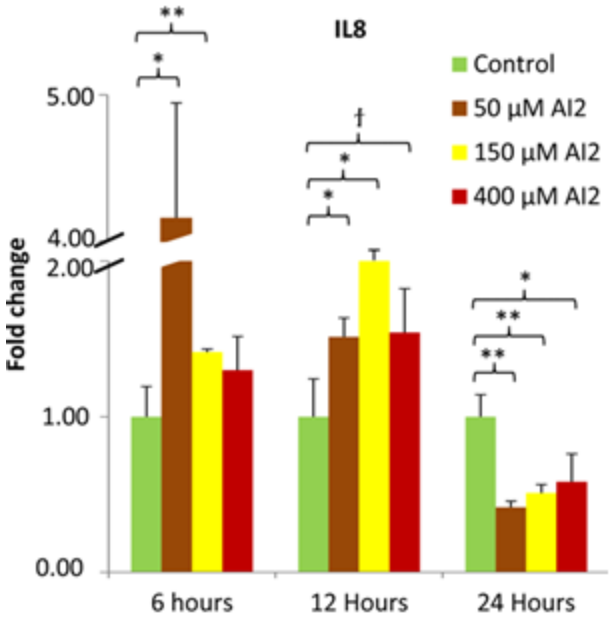

Figure 2.6 qPCR of IL-8. HCT-8 cells are incubated with AI-2 at 50, 150 and 400µM for 6, 12, and 24 hours, normalized to media alone. At early times (6 and 12 hours), incubations with AI-2 result in upregulation of IL-8 gene expression levels compared to media alone, while at 24 hours, IL-8 expression levels are downregulated compared to media alone. qPCR fold level changes are shown.
† $p < 0.10$, * $p < 0.05$, ** $p < 0.01$

2.6 Discussion

Investigations into interkingdom communication in the GI tract can aid in treatment for diseases such as inflammatory bowel disease, which arises from the immune system causing inflammation from commensal bacteria, and colorectal cancer, which is believed to be promoted through chronic inflammation. In this study, we have shown for the first time that bacterial secretions from non-pathogenic *E. coli* upregulated a number of proinflammatory pathways in IECs leading to the transcription of cytokines involved in recruiting leukocytes, particularly neutrophils. The activation of biological defense-related pathways from secretions of two

different strains of *E. coli*, BL21 and W3110, illustrate that direct contact from flagella, membrane bound proteins or secretion systems are not necessary to induce an immunological response from IECs. That is, we have shown that *E. coli* secretions cause the upregulation of pro-inflammatory cytokines through the activation of the mediation pathway, NF*κβ*, indicating that the immune response was elicited through bacterial secretions.

Our results also show that the negative feedback components of the NF*κβ* pathways (NF*κβ* -α inhibitor) and NOD-like receptor pathways (TNFAIP3) were upregulated in the HCT-8 cells, indicating a negative feedback loop to control the upregulation of cytokine gene expression from nonpathogenic *E. coli*. NF*κβ* -α inhibitor acts to block the canonical and atypical NF*κβ* pathways, and its upregulation directly inhibits the transcription of cytokines. TNFAIP3 is a negative regulator of the NOD-like receptor pathway, the intracellular sensing mechanism corollary to the extracellular TLR sensing mechanism. The inhibition of the NOD-like pathway suggests a response to block the signaling cascade of bacterial products that were transported into the mammalian environment. The upregulation of these negative feedback components may suggest the IEC is preventing the physiological response from developing into a pathological response.

While both bacteria elicited similar responses, BL21 appeared to cause greater perturbations in HCT-8 cells. As noted above, phenotypic differences between BL21 and W3110 include flagella, LPS, heat-shock proteins, metabolic byproduct secretions, and AI-2 production. Our investigations into the interkingdom effects of AI-2 revealed a moderate, but significant upregulation in IL-8 at both 6 and 12 hours, followed by a significant downregulation found at 24 hours. Like the results from the full secretome, this may indicate that AI-2 as a single signal molecule has an inflammatory effect, but after some period of modulation, the IEC inflammation is controlled through negative feedback to prevent a pathological response to a non-pathogenic stimulus.

In conclusion, while it may be expected that bacterial secretomes would affect IECs and immune function in the gut, our study has demonstrated that a bacterial-bacterial signaling molecule also influence the same. That is, IEC evidently "listen in" on the communication between bacteria that reside in the lumen and alter their behavior based on these signaling phenomena. Further exploration of the effects of bacterial soluble factors on IECs will aid in the understanding of microbial disease, and modulation of existing interkingdom signaling networks could result in novel methods to combat infections.

2.7 Supplemental Materials

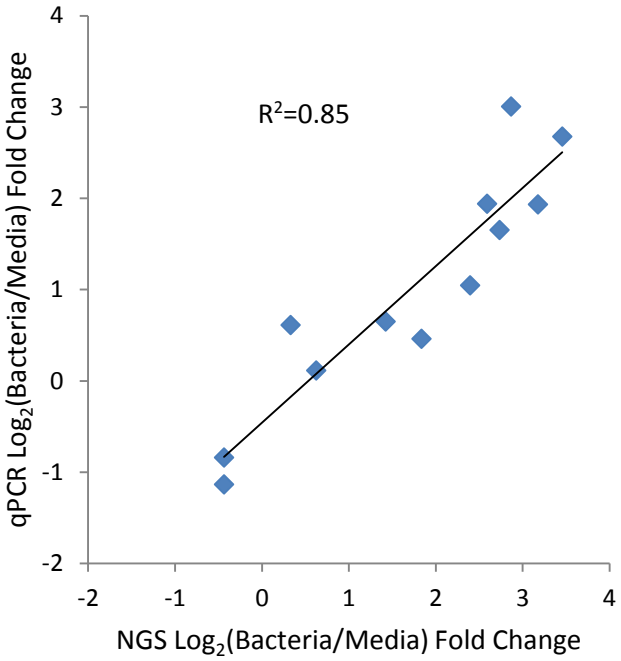

Figure S2.1: qPCR validation of RNA-Seq. Results shows high correlation for range of expression levels.

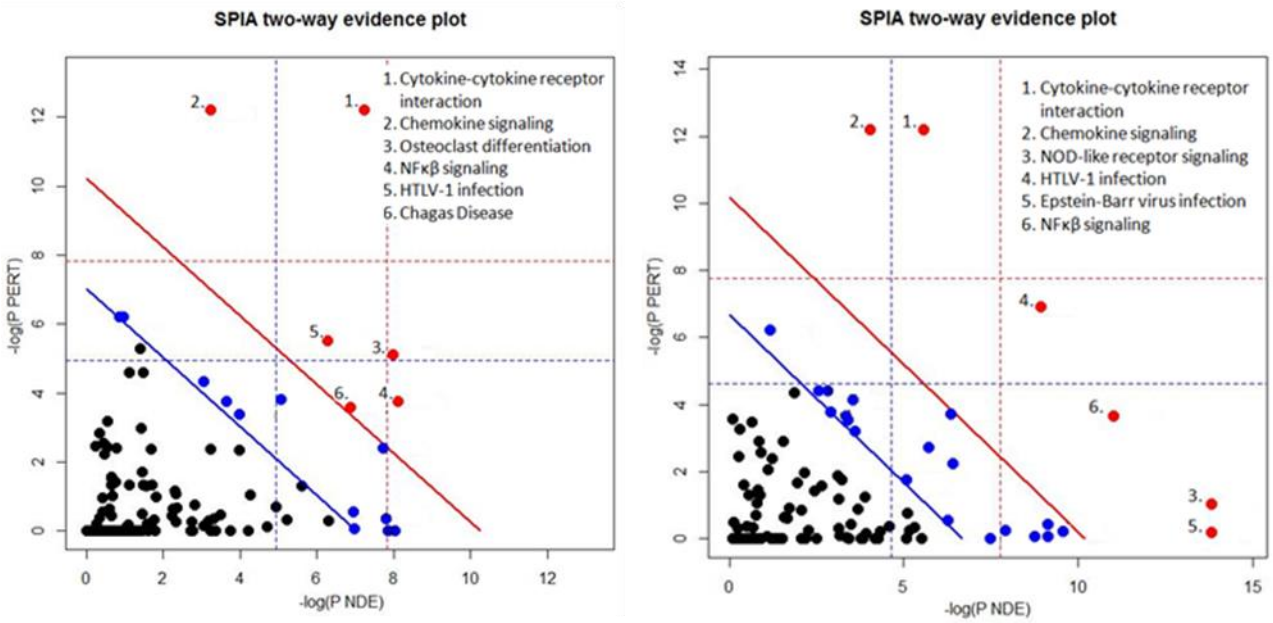

Figure S2.2: Signaling pathway analysis graphs. Significantly differentially expressed genes and expression levels from DESeq are inputted into SPIA (Signaling Pathway Impact Analysis) to determine activation and inhibition of entire biological pathways. All values to the right of the blue oblique line are significant after a False Discovery Rate adjustment of the global p-values. All values to the right of the red oblique line are significant after Bonferroni correction of the global p-values. a) HCT-8 cells incubated with BL21 compared to media significantly altered six biological pathways b) HCT-8 cells incubated with W3110 compared to media alone significantly altered six biological pathways. Common among both comparisons were the activation of the cytokine-cytokine receptor interaction, chemokine signaling pathway, osteoclast differentiation, NFκβ signaling pathway, human T-lymphotropic virus-1 (HTLV-I) infection, and the inactivation of the NOD-like receptor signaling pathway.

* pPERT probability of finding a greater total accumulation perturbation than compared to the preturbation accumulation in the pathway by chance
** pNDE probability of finding at least x number of DE genes on the pathway using a hypergeometric model

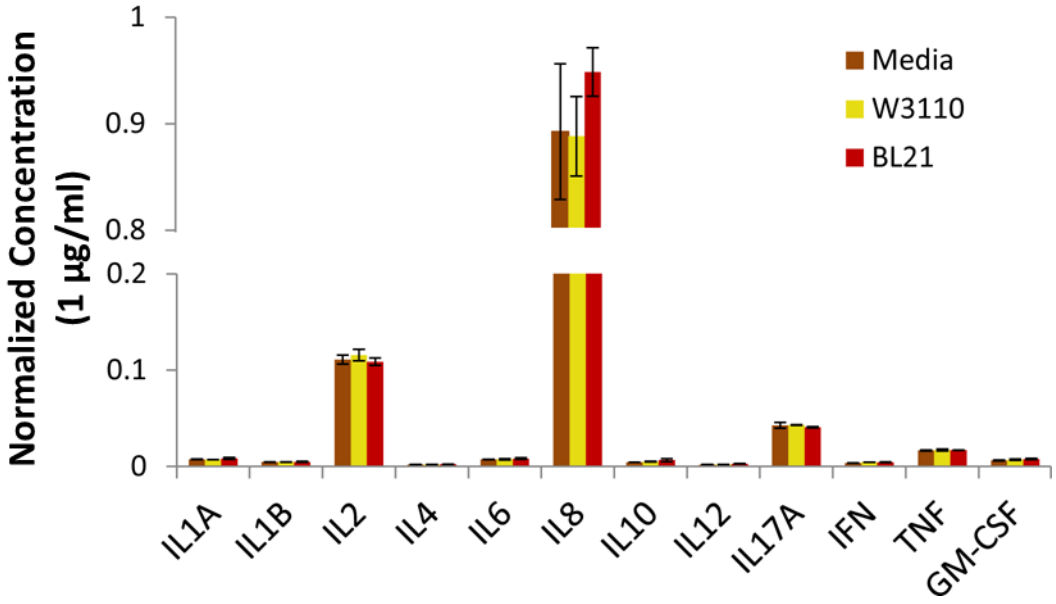

Figure S2.3: Multi-analyte ELISA. ELISAs were performed on cell culture supernatants of HCT-8 cells in transwell coincubations with BL21, W3110, and media alone. Values are normalized to positive control (1µg/mL). ELISA data show no translational modulation in inflammatory cytokines with incubations of either W3110 or BL21 compared to media alone.

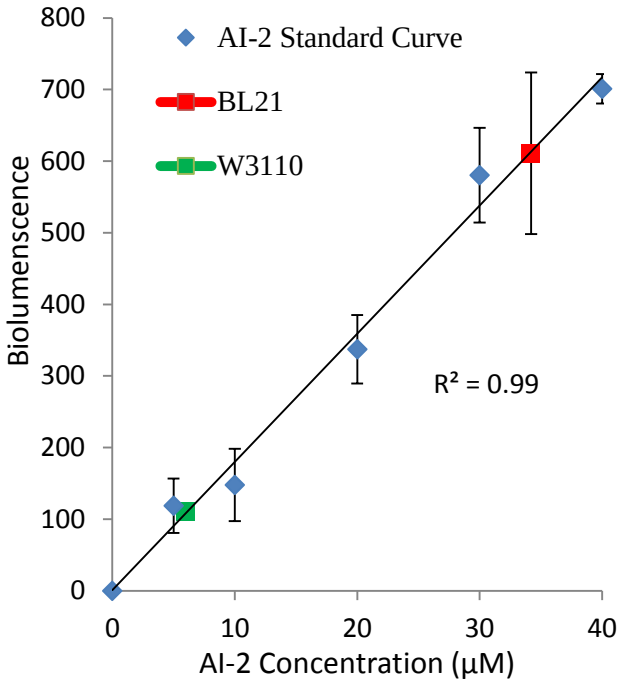

Figure S2.4: AI-2 standard curve. AI-2 concentration levels in HCT-8 supernatant from incubations with BL21 and W3110, respectively. An AI-2 standard curve was created from AI-2 activity assays (see methods) with known AI-2 concentrations, and a best fit linear regression is shown ($R^2 = 0.99$). AI-2 concentration levels in the supernatant of the lower transwell (HCT-8 supernatant) are shown in incubations with BL21 (red) and W3110 (green).

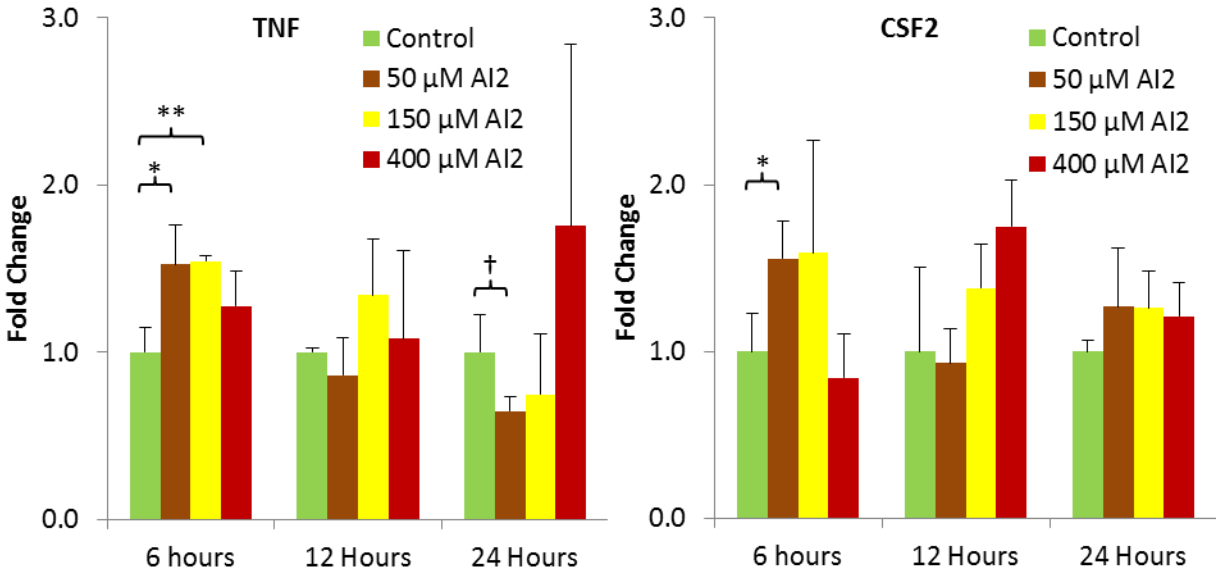

Figure S2.5: qPCR of TNF and CSF2. HCT-8 cells are incubated with AI-2 at 50, 150 and 400µM for 6, 12, and 24 hours. qPCR fold level changes are shown for colony stimulating factor-2 (CSF2) and tumor necrosis factor (TNF) and normalized to blank media (0 µM AI-2).
† $p < 0.10$, * $p < 0.05$, ** $p < 0.01$

728

Gene	Primers
CXCL2	Upstream primer: TCCAAAGTGTGAAGGTGAAGTCCC Downstream primer: GGTTGAGACAAGCTTTCTGCCCAT
CXCL3	Upstream primer: CTGCAGGGAATTCACCTCAAGAAC Downstream primer: AGTGTGGCTATGACTTCGGTTTGC
PDGFB	Upstream primer: GGTGGGTTAGAGATGGAGTTTG Downstream primer: GAACCAGAGGAAGAGGTGAATC
IL8	Upstream primer: TCCTGATTTCTGCAGCTCTGTGTG Downstream primer: AATTTCTGTGTTGGCGCAGTGTGG
TNF	Upstream primer: AGCCCATGTTGTAGCAAACC Downstream primer: TGAGGTACAGGCCCTCTGAT
NFKB1	Upstream primer: GTGACAGGAGACGTGAAGATG Downstream primer: TGAAGGTGGATGATTGCTAAGT
B2M	Upstream primer: TGTGTCTGGGTTTCATCCATCCGA Downstream primer: TCACACGGCAGGCATACTCATCTT
CSF2	Upstream primer: AAATGTTTGACCTCCAGGAGCCGA Downstream primer: GGTGATAATGTGGGTTGCACAGGA

729 **Table S2.1 Primers used for SYBR green qPCR**
730

731

Chapter 3: Rational design of ‘controller cells’ to manipulate protein and phenotype expression

This chapter was primarily reproduced directly or adapted from Zargar, Amin et al. " Rational design of ‘controller cells’ to manipulate protein and phenotype expression " *Metabolic Engineering [96]*

3.1 Abstract

Coordination between cell populations via prevailing metabolic cues has been noted as a promising approach to connect synthetic devices and drive phenotypic or product outcomes. However, there has been little progress in developing ‘controller cells’ to modulate metabolic cues and guide these systems. In this work, we developed ‘controller cells’ that manipulate the molecular connection between cells by modulating the bacterial signal molecule, autoinducer-2, that is secreted as a quorum sensing (QS) signal by many bacterial species. Specifically, we have engineered *E. coli* to overexpress components responsible for autoinducer uptake (*lsrACDB*), phosphorylation (*lsrK*), and degradation (*lsrFG*), thereby attenuating cell-cell communication among populations. Further, we developed a simple mathematical model that recapitulates experimental data and characterizes the dynamic balance among the various uptake mechanisms. This study revealed two controller “knobs” that serve to increase AI-2 uptake: overexpression of the AI-2 transporter, LsrACDB, which controls removal of extracellular AI-2, and overexpression of the AI-2 kinase, LsrK, which increases the net uptake rate by limiting secretion of AI-2 back into the extracellular environment. We find that the overexpression of *lsrACDBFG* results in an extraordinarily high AI-2 uptake rate that is capable of completely silencing QS-mediated gene expression among wild-type cells. We demonstrate utility by modulating naturally occurring processes of chemotaxis and biofilm formation. We envision that ‘controller cells’ that modulate bacterial behavior by manipulating molecular communication, will find use in a variety of applications, particularly those employing natural or synthetic bacterial consortia.

3.2 Highlights

- ‘Modular’ quorum sensing systems manipulate the extracellular AI-2 environment
- Mathematical model characterizes mechanics of AI-2 signal transduction
- ‘Controller cells’ can modulate protein expression in synthetic QS-dependent systems
- Natural bacterial processes (chemotaxis and biofilm production) can be altered

3.3 Introduction

Metabolic engineering exploits the genetic modification of cellular pathways to improve production of metabolites and proteins [97,98]. Many noteworthy examples have been demonstrated wherein these cells serve as ‘factories’ for the environmentally sustainable production of energy, materials, and chemicals [99]. Towards this aim, metabolic engineering has incorporated finely tuned synthetic controllers and cells in the creation of artificial networks [100-104]. The general structure of these synthetic networks is based on control devices that respond to specific stimuli in a predictable fashion [105,106]. However, the task of coordinating among and between cell populations remains a critical challenge that can limit the production of desired end-products [13,107]. A further challenge is controlling the partitioning of resources that (i) maintain native metabolism and (ii) adequately support product synthesis [108,109]. One creative approach to address both of these challenges is through the leveraging of cell-cell communication networks, and these have been the target of a variety of dynamic control systems [110-112]. Using the native bacterial signaling network known as quorum sensing [113,114], we have previously shown the ability to reduce the metabolic burden [115,116] and “program” cell populations through the metabolic cue, autoinducer-2 [14,117]. However, while there has been much development in multicellular systems that respond to metabolic cues [118-121], control of the intensity of these metabolic cues to fulfill the potential of spatiotemporal control has not been realized.

In this work, we have developed bacterial AI-2 consumers, 'controller cells', which can be deployed to control AI-2 in a predictable fashion using the now well-characterized quorum sensing mechanisms of *E. coli* (**Scheme 1A**). AI-2 is synthesized and recognized by a wide variety of bacteria [9,87]; correspondingly its use as a potential target for modulating QS activities among different cell types is of interest. The use of genetically engineered bacteria to 'quench' extracellular AI-2 was first described by Xavier et al. [35], where genetic deletions of its synthase (*luxS*) and its repressor (*lsrR*) were used to interfere with bacterial communication. However, the interrelated complexity of QS networks renders the elucidation of its mechanisms difficult, and the production of simple, "modular" networks would enrich the understanding of these actions [122]. We have addressed this through the model-based design, construction, and characterization of these 'controller cells' to modulate the external AI-2 environment. These cells are designed via the compartmentalization of different aspects of AI-2 processing: uptake (*lsrACDB*), phosphorylation (*lsrK*), and degradation (*lsrFG*) **(Scheme 1B-1C)**.

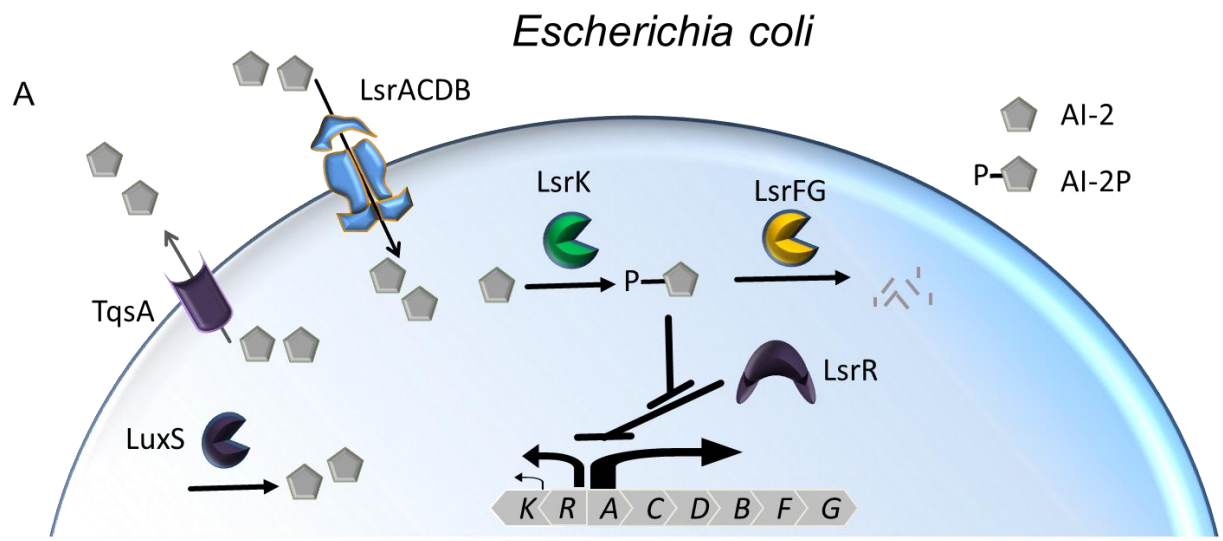

B

	LsrACDB	LsrK	LsrFG
LW12 pTrcHisB	Native	Native	Native
LW12 pLsrFG	Native	Native	**Induced**
LW12 pLsrK	Native	**Induced**	Native
LW12 pLsrACDB	**Induced**	Native	Native
LW12 pLsrACDBFG	**Induced**	Native	**Induced**

C

Strain	Genotype	Source
LW12	W3110 ΔluxS::Kan T	(Liang et al., 2005)
Plasmid	**Description**	**Source**
pTrcHisB	Cloning Vector Ap^r	Invitrogen
pLsrFG	pTrcHisB derivative, containing *lsrFG*, Ap^r	This study
pLsrK	pTrcHisB derivative, containing *lsrK*, Ap^r	This study
pLsrACDB	pTrcHisB derivative, containing *lsrACDB*, Ap^r	This study
pLsrACDBFG	pTrcHisB derivative, containing *lsrACDBFG*, Ap^r	This study

Scheme 3: *E. coli lsr*-system: Panel (A) depicts the AI-2 quorum sensing network. LuxS generates AI-2 from metabolic precursors, which is then exported out of the cell by TqsA. AI-2 is primarily taken up through the ABC-type transporter Lsr, and then phosphorylated by LsrK to AI-2P. AI-2P depresses the response regulator LsrR, thereby activating transcription of the *lsr* operon. AI-2P is degraded by LsrF and LsrG. Panel (B) depicts the 'controller cells' that are engineered through the overexpression of distinct components of the *lsr* system. "Native" indicates native production, while 'Induced' indicateso over-expression. Panel (C) illustrates the strains, plasmids, descriptions and sources used for these 'controller cells'.

These 'controller cells' provide the ability to regulate extracellular AI-2 and modulate synthetic circuits. Further, we show that the ability to quench extracellular AI-2 through 'controller cells' can attenuate the native cell-cell behaviors of chemotaxis and biofilm formation. By teasing apart the regulatory network for AI-2, we have enhanced our understanding of the collective population-scale response to AI-2. In this way, systems can be designed wherein we decouple the consumption of AI-2 from bacterial population density and its emergent behavior. With the addition of 'controller cells', we provide an orthogonal means to modulate QS activity,

demonstrate their use as mediators of heterologous protein and phenotype expression, and provide a modeling foundation to guide QS-communication.

3.4 Materials and Methods

3.4.1 Plasmid construction

The bacterial strains and plasmids used in this study are listed in **Table S3.1**, and were constructed according to standard procedures [123]. Briefly, plasmid pTrcHisB (Invitrogen) was used as the backbone to construct plasmids pLsrFG, pLsrK, pLsrACDB, and pLsrACDBFG. The sequences for *lsrFG*, *lsrK*, *lsrACDB*, and *lsrACDBFG* were amplified by PCR using Q5 polymerase (New England Biolabs) from *E. coli* K-12 strain W3110. These PCR inserts were ligated into XhoI-digested pTrcHisB using Gibson assembly [124] and then transformed into LW12 (W3110 Δ*luxS*) [125]. Oligonucleotide primers were obtained from Integrated DNA Technologies (Coralville, IA) and are listed in **Table S3.2**. Cloning was verified with sequencing and Western Blot.

3.4.2 AI-2 assay

Cultured media was tested for the presence of AI-2 by inducing luminescence in *Vibrio harveyi* reporter strain BB170 [69]. Briefly, BB170 was grown for 16 hours with shaking at 30°C in AB (AI-2 Bioassay) media. AB media is made by adjusting 400 mL of distilled (DI) water to pH 7.5, and adding 7 grams of NaCl, 2.4 grams of $MgSO_4$, 0.8 grams casamino acid, and 8 mL of glycerol. AB media is supplmented with 400 μL of potassium phosphate buffer (K_2HPO_4 10.71g and 5.24g KH_2PO_4 in 100 mL of DI water), 400 μL of 0.1M L-arginine (0.1742g in 10 mL of DI water), 40 μL of riboflavin (10 μg/mL), 40 μL of thiamine (1 mg/mL) and 40 μL kanamycin (50 mg/mL).

Overnight cultures were diluted 1:5,000 in fresh AB media with kanamycin, and aliquoted into sterile 12 x 75-mm tubes (Fisher Scientific). Test samples were added to BB170 cultures at a final concentration of 10% (vol/vol). Luminescence was measured by quantifying light production with a luminometer (EG&G Berthold LB 9509 Jr) and assays were adjusted, if needed, so that values were in the linear range. Data are presented as "fold change" compared to negative controls. All conditions were tested in triplicate. In experiments with supplemented chemically-synthesized AI-2, we report AI-2 activity normalized to the initial concentration, as our previous study showed a linear correlation between AI-2 concentration and resultant bioluminescent AI-2 activity [126].

3.4.3 AI-2 uptake profiles of 'controller cells'

Chemically synthesized AI-2 [127] was generously provided by the Sintim research group. Each strain was reinoculated by diluting an overnight culture to 3% volume in 10 mL of LB; these cells were grown in a 50 mL culture flask to an optical density (OD) ~ 0.4-0.6 at 30ºC with 250 RPM shaking. Isopropyl β-D-1-thiogalactopyranoside (IPTG) and AI-2 were added to a final concentration of 1 mM and 50 μM, respectively. Every half hour, optical density was measured (**Supplementary Figure 3.1**) and samples were harvested for analysis. The average bioluminescence for samples at t = 0 was denoted 50 μM, and subsequent AI-2 activity values were normalized to this concentration.

3.4.4 Modulation of AI-2 in co-cultures

BL21 pTrcHisB, LW12 pTrcHisB, and LW12 pLsrACDBFG were reinoculated at 3% of overnight culture in 25 mL of LB in 125 mL culture flasks and grown to an OD ~ 0.4-0.6 at 37ºC with ampicillin. Co-cultures of BL21 pTrcHisB incubated with either LW12 pTrcHisB or LW12 pLsrACDBFG were aliquoted in culture test tubes at ratios of 9:1, 3:1, 1:1, 1:3, and 1:9. IPTG (1

mM) was added and every 30 minutes optical density (**Supplementary Figure 3.2**) was measured and samples were harvested, on which AI-2 activity assays were performed.

3.4.5 Silencing of autoinduced protein expression

LW12 pTrcHisB and LW12 pLsrACDBFG were reinoculated at 3% overnight culture into 25 mL of LB in 125 mL flasks and grown to an OD ~ 0.4-0.6. The samples were induced with IPTG (1 mM) for three hours, before being resuspended (2000 RPM for 10 minutes) to an OD ~ 1. W3110 pCT6 pET-GFP_{uv} [14], a strain of *E.coli* that responds to the level of the AI-2 concentration by expressing GFP, was grown to an OD ~ 0.2, and then incubated with LW12 pTrcHisB or LW12 pLsrACDBFG. Flow cytometric analysis was performed using a FACSCanto II™ Flow Cytometer (Becton Dickinson) and all raw data was analyzed with BD FACSDiva™ 6.0 software (Becton Dickinson).

3.4.6 Biofilm studies and evaluation

W3110 pTrcHisB, LW12 pTrcHisB, and LW12 pLsrACDBFG were diluted to OD ~ 0.05 and reinoculated at a total volume of 200 μL at a 1:1 (v/v) ratio. IPTG (1 mM) was added at OD ~ 0.4, and biofilms were cultured for ~ 24 hours (+/- 30 minutes) at 30ºC in static conditions. After incubation, optical density was read on a plate reader (Molecular Devices SpectraMax M2) at 600 nm. The supernatant was gently decanted, and each well was washed 3 times with 300 μL of sterile PBS to detach loosely adhered cells. The plate was then incubated at 60ºC with the lid off for 60 minutes, and afterwards, 250 μL of 0.1% crystal violet was added to each well and incubated for 15 minutes at room temperature. Crystal violet stain was aspirated with a pipette and excess stain was washed off by gently submerging and mixing in a tray filled with distilled water until washings were free of the stain. After the microplate was air-dried, the dye was resolubilized by adding 250 μL of 95% ethanol, and incubated at room temperature with shaking

for 30 minutes. The optical density of each well stained with crystal violet was measured at 540 nm.

3.4.7 Chemotaxis studies and assay

Preparation of conditioned media: LW12 pTrcHisB and LW12 pLsrACDBFG were inoculated from frozen cell stock in 20 mL of LB with ampicillin in a 125 mL culture flask and grown overnight to OD ~ 0.4 at 23 ºC with 150 RPM shaking. The cultures were induced with IPTG (1 mM) for two hours (23 ºC, 150 RPM shaking) before being washed and resuspended with DPBS (with calcium and magnesium) to OD ~ 0.4. LW12 pTrcHisB and LW12 pLsrACDBFG cultures were incubated at 37 ºC with 250 RPM shaking with 0 µM and 20 µM AI-2. The cell cultures were spun down, and the supernatant ("conditioned media") was syringe-filtered and stored at -20 ºC.

Transwell chemotaxis assay: CT104 pCT6 pET-dsRed cultures [128] were inoculated from frozen stock into 30 mL of LB in 250 mL culture flasks and grown overnight to an OD ~ 0.4-0.6 at 23 ºC with 150 RPM shaking. The cells were spun down at 1500 RPM with a fixed rotor for 15 minutes and washed twice with DPBS (supplemented with calcium and magnesium) to an optical density ~ 0.4-0.6. A 3.0 µm transwell was placed in four wells of a 6-well plate (Corning). CT104 pCT6 pET-dsRed cells were first pipetted into the bottom of the wells with a volume of 2.5 mL per well, followed by 1.5 mL of each of the "conditioned media" fluids added to the top of the transwell. The plate was incubated at 30 ºC for three hours; cells accumulating in the upper transwell had swum vertically [129]. This method yields fewer motile cells than the reverse scenario (swimming down), but precludes settling in negative controls. The optical density of each sample from the top chamber of the transwell was measured at 600 nm. The experiment was repeated in triplicate.

3.5 Results

3.5.1 Design of modular QS elements

As illustrated in **Scheme 1A**, the three steps involved in the processing of AI-2 from the extracellular environment are (i) uptake, primarily through the LsrACDB transporter [125,130,131], (ii) LsrK-mediated phosphorylation of AI-2 (to AI-2P), which blocks export back to the extracellular milieu so that accumulated AI-2P binds the regulatory protein LsrR [132,133], derepressing the Lsr transporter as well as enzymes, LsrF and LsrG, and (iii) degradation of AI-2P through the two step process from isomerase LsrG followed with cleaving and thiolation by LsrF [133,134]. In this study, we cloned *lsrFG*, *lsrK*, *lsrACDB*, and *lsrACDBFG* into the plasmid pTrcHisB to enable overexpression of all proteins associated with these AI-2 processing mechanisms **(Scheme 1B-1C).** We subsequently transformed each plasmid into LW12, a *luxS* null mutant that cannot synthesize AI-2.

We first characterized the uptake rate of AI-2 by adding a fixed amount of exogenous AI-2 and monitoring the extracellular concentration. Each strain was grown to mid-logarithmic phase (OD ~ 0.4) with the subsequent addition of 50 μM AI-2 and 1 mM IPTG (see Methods) and optical density was recorded throughout **(Supplementary Figure 3.1)**. **Figure 3.1A** shows the uptake profile of each strain (colored dots), as well as the results of a topologically simple mathematical model (black trendlines) comprised of several ordinary differential equations **(Table 3.1)** for state variables AI-2, the molecular species that contribute to AI-2 uptake, and optical density for each cell type**.** Note, we have included an empty vector control LW12 pTrcHisB that will consume AI-2 (Δ*luxS*), but not in an accelerated fashion. We found that overexpression of *lsrACDB* and *lsrACDBFG* genes showed the highest rate of uptake, indicating that AI-2 transport into the cell is the slowest step involved in the processing of extracellular AI-2 into phosphorylated intracellular AI-2. Further, overexpression of *lsrK* resulted in an extracellular

AI-2 removal rate slower than overexpression of the transporter, but still faster than the host strain, LW12, with an empty vector or pLsrFG.

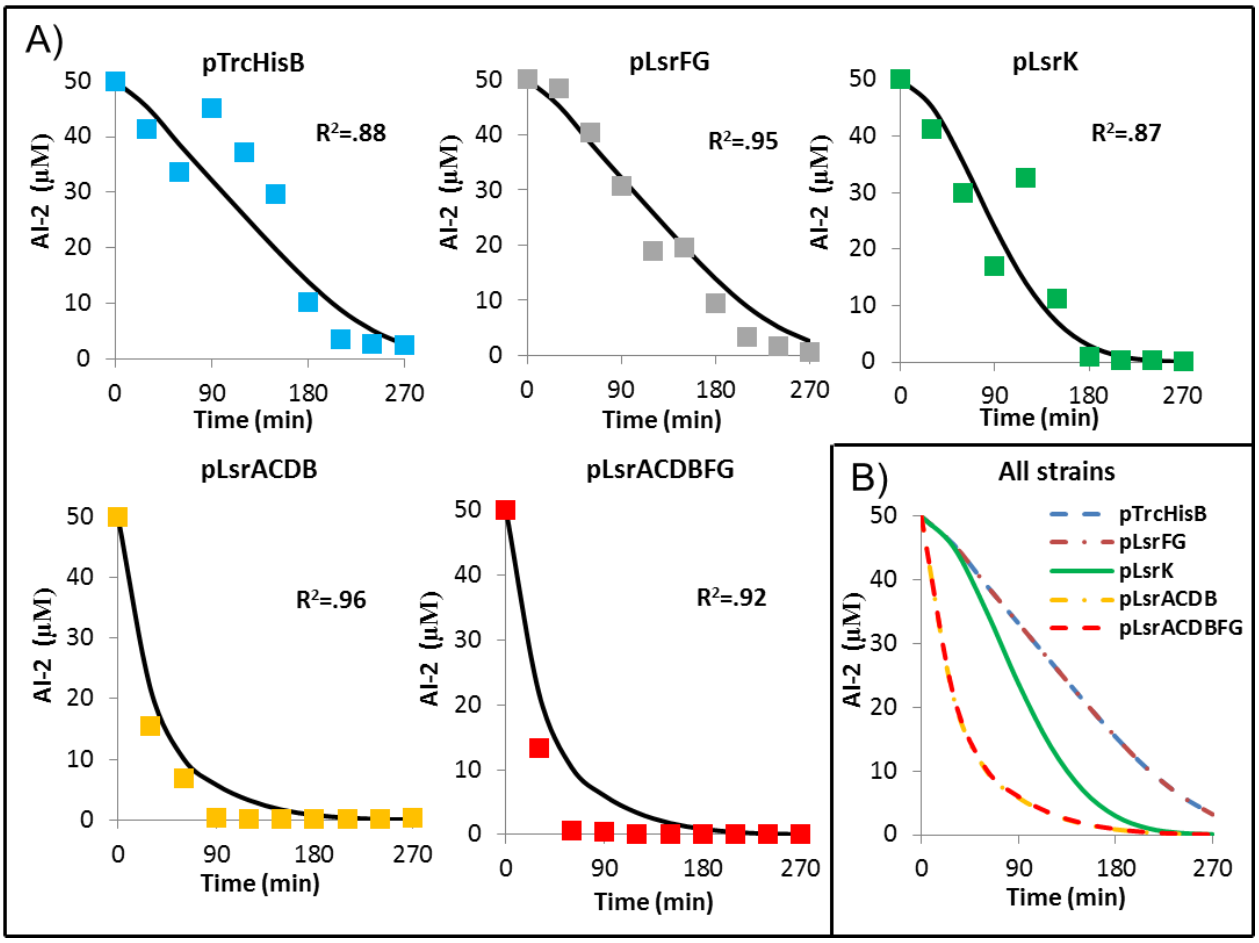

Figure 3.1 AI-2 uptake profiles of 'controller cells' A) Each plasmid was transformed into LW12 (W3110 Δ*luxS*) and grown to OD ~ 0.4 before the addition of IPTG (1 mM) and AI-2 (50 µM). AI-2 levels were measured with AI-2 activity assays (see Methods) every 30 minutes (data points) and a mathematical model was created (black trendlines) to fit the data. **B)** Collation of mathematical models of each strain. Each experiment is performed in triplicate.

Reaction	Differential Equation
AI-2 outside the cell	$\frac{dAI2_{out}}{dt} = -k_{in} * (LsrACDB) * (AI2_{out}) + k_{out} * (AI2_{in})$
AI-2 inside the cell	$\frac{dAI2_{in}}{dt} = k_{in} * (LsrACDB) * (AI2_{out}) - k_{out} * (AI2_{in}) - k_p * (LsrK) * (AI2_{in})$
ACDB protein synthesis	$\frac{dLsrACDB}{dt} = [K_{nat} + K_I * (IPTG_{ACDB})] * (OD_{600}^{ACDB}) - k_d * (LsrACDB)$
Lsr kinase synthesis	$\frac{dLsrK}{dt} = [K_{nat} + K_I * (IPTG_K)] * (OD_{600}) - k_d * (LsrK)$
Cell density (LsrACDB overexpression)	$\frac{dOD_{600}^{ACDB}}{dt} = \mu_T * (OD_{600}^{ACDB})$
Cell density	$\frac{dOD_{600}}{dt} = \mu * (OD_{600})$

Table 3.1: Ordinary differential equations of model. Uptake of exogenously added AI-2 by each plasmid in the strain LW12

Using the described network architecture, our deterministic model yielded simulation results that closely matched the experimental data (**Figure 3.1A**). The simulated values of AI-2 uptake for each 'controller cell' is illustrated in **Figure 3.1B** and these indicate a broad distribution in the rate of AI-2 uptake through the overexpression of the various uptake mechanisms, and also enrich our understanding of the kinetic balances basis for these phenomena.

In all cases, this is a phenomenological "best fit" model that incorporates the molecular features contributing to uptake, and it is a simplification of our previous stochastic model for AI-2 uptake [135] and deterministic model for *lsr* gene expression [130]. The AI-2 transport into the cell is described as an interaction of the protein complex LsrACDB with extracellular AI-2, and the phosphorylation of AI-2 to AI-2P (a sequestered form of AI-2 that cannot be secreted back outside the cell) is dependent on the interaction of enzyme LsrK with intracellular AI-2. The induction parameter $IPTG_x$ is used as an input (1 or 0) to specify if a plasmid-encoded protein is overexpressed (e.g. pLsrACDBFG has $IPTG_{ACDB}$ value of 1, and $IPTG_K$ value of 0) in the presence of IPTG (strains without induction showed reduced AI-2 uptake, **Supplementary Figure** 3.3). Our prior work on *lsr* gene expression and AI-2 synthesis [130,135] provided an initial range of kinetic parameters; a parameter estimation routine was used to fit the model based

on a least squares minimization of the distance between the experimental and modeled data **(Table 3.2)**. A detailed discussion of rate equations, growth rates, and kinetic parameters can be found in the **Supplementary material**.

Species	Description	Initial Condition/Range
t	Time	[0, 270] min
$AI2_{out}$	Extracellular AI-2	50 μM
$AI2_{in}$	Intracellular AI-2	0 μM
$IPTG_K$	Plasmid-encoded LsrK	[1,0]
$IPTG_{ACDB}$	Plasmid-encoded LsrACDB	[1,0]
$LsrK$	Kinase	0 μM
$LsrACDB$	ACDB transporter	0 μM
OD_{600}^{ACDB}	Cell density (LsrACDB,LsrACDBFG)	0.4-0.6
OD_{600}	Cell density (LsrK, LsrFG, empty)	0.4-0.6
Parameters	**Description**	**Best fit value**
k_{in}	AI-2 import by LsrACDB complex	0.008 μM^{-1} min^{-1}
k_{out}	AI-2 export	0.045 min^{-1}
k_p	AI-2 phosphorylation	0.006 μM^{-1} min^{-1}
K_I	Induced expression	0.9 μM min^{-1}
K_{nat}	Native expression	0.1 μM min^{-1}
k_d	Protein decay	0.02 min^{-1}
μ	Growth rate	0.0056 min^{-1}
μ_T	Growth rate (LsrACDB expression)	0.0044 min^{-1}

Table 3.2: Model species and kinetic rate constants in model of exogenously added AI-2 uptake by each plasmid in the strain LW12

3.5.2 Quenching of QS-dependent protein expression

We sought to "shut off" W3110 pCT6 pET-GFP_{uv}, a strain that produces and responds to AI-2 by producing GFP, to provide an independent means to alter heterologous gene expression [14]. In **Figure 3.2**, we show that a 1:1 mixture of W3110 pCT6 pET-GFP_{uv} with LW12 pLsrACDBFG almost completely suppresses QS-activated gene expression from the WT (AI-2 producing) cells for 10 hours. This is in stark contrast to the empty vector results, which found that over 50% of the total population was observed to synthesize GFP over the same time period. Intermediate timepoints show a steady rise in the production of GFP in co-incubations with the empty vector, while co-incubations with LW12 pLsrACDBFG remained low throughout

(**Supplementary Figures 3.S4-S5**). "Since both the 'controller cells' and W3110 pCT6 pET-EGFP have the same antibiotic resistance, relative population dynamics could not be determined throughout the incubation. However, since LW12 pTrcHisB has a faster growth rate than LW12 pLsrACDBFG **(Table 3.2)**, purely growth rate dynamics would favor decreased fluorescence in cultures of LW12 pTrcHisB than LW12 pLsrACDBFG. Because we chose the 'controller cell' strain having the greatest uptake rate, LW12 pLsrADCBFG, we would expect that by either using a lower inoculum fraction or by selecting LW12 pLsrK (the strain that significantly reduced AI-2 levels through overexpression of the kinase) at 50% inoculum we would observe gradations in the overall fraction of QS positive activity. These results demonstrate "programmed" attenuation of heterologous protein expression as an indicator of QS phenotype and typically this is an outcome we seek to maximize. However, such control of the metabolic cue may also have positive implications for guiding synthetic networks of small populations of cells assembled to coordinate to produce a desired outcome [13].

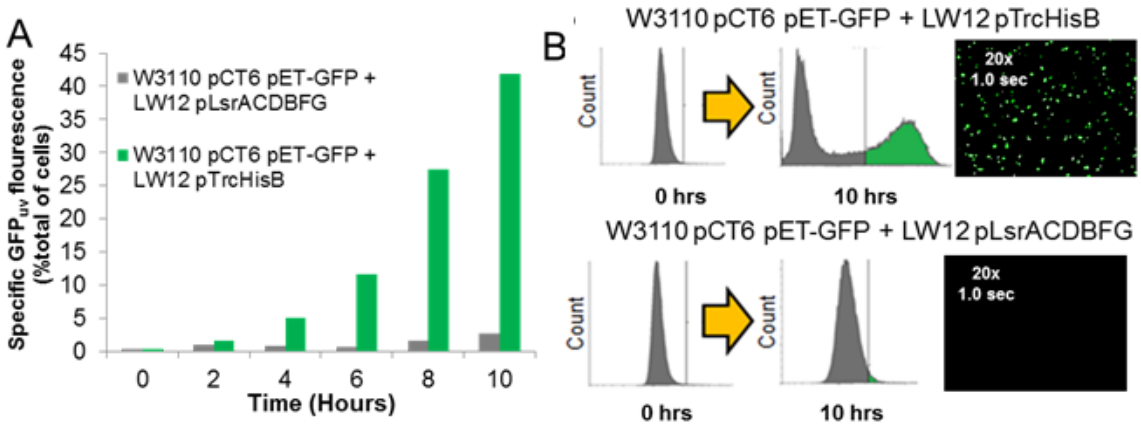

Figure 3.2 Cell-cell modulation of protein expression. Panel (A) shows results for two cultures with an initial state of non-fluorescence. A 1:1 mixture of OD~1 of LW12 pLsrACDBFG or LW12 pTrcHisB is mixed with OD~0.2 of reporter strain W3110 pCT6 pET-GFP. Panel (B) shows FACS data of the non-fluorescing population of both mixtures and the results 10 hours later. Microscopic images of the cells at 10 hours are shown, adjusted for clarity.

3.5.3 Manipulation of 'producer cell' in co-cultures and extension of model

Previously, we illustrated that the *E. coli* strain, BL21 *luxS*$^{+}$, can act as 'producer cell' to increase protein expression in QS-dependent systems [14]. To enable the use of these cells to dynamically modulate metabolic cues, we investigated the interaction of the most effective 'controller cell', pLsrACDBFG, and the empty vector with strain BL21 *luxS*$^{+}$. We note that BL21 does not take up AI-2 from the medium [86], hence the removal of AI-2 here is due solely to the added Δ*luxS* 'controller cells'. In this experiment, BL21 pTrcHisB, LW12 pTrcHisB, and LW12 pLsrACDBFG were grown to an OD ~ 0.4 and co-cultures of BL21 pTrcHisB were incubated with either LW12 pTrcHisB or LW12 pLsrACDBFG and aliquoted in culture test tubes at ratios of 9:1, 3:1, 1:1, 1:3, and 1:9. At this point, IPTG (1 mM) was added and samples were harvested every 30 minutes on which AI-2 activity assays were performed and optical density was measured **(Supplementary Figure 3.2)**.

The data in Figure 3.3A depict the AI-2 levels over time for each initial condition (the initial ratio of BL21 to 'controller cell' ranging from 9:1 to 1:9). The initial level of AI-2 is due to wild-type BL21 in the inoculums (they had secreted AI-2 in precultures). As expected, cultures with more BL21 initially had higher AI-2 activity levels and remained highest throughout the incubation. Also, we note that for the control culture, LW12 pTrcHisB (Figure 3.3A blue bars), there was an appreciable consumption of AI-2 so that we did not find a consistent threefold decrease in AI-2 as the population shifted in three-fold increments from 9:1 to 1:9. Nonetheless, a nearly linear decrease was observed with increasing LW12 pTrcHisB cells and this would be expected. In contrast, the rapid uptake rate of LW12 pLsrACDBFG is perhaps most evident in cultures where the consumer culture strain was present at an initial ratio of 1:1 or higher. In these cases, LW12 pLsrACDBFG (Figure 3.3A red bars), prevented significant quantities of AI-2 from accumulating to even measurable levels in the extracellular environment throughout the time period, while the empty vector control showed increased accumulation of AI-2 over time at all

ratios. Hence, the co-cultured LW12 pLsrACDBFG cells effectively cleared all QS signaling among the ‘producer’ cells at these ratios.

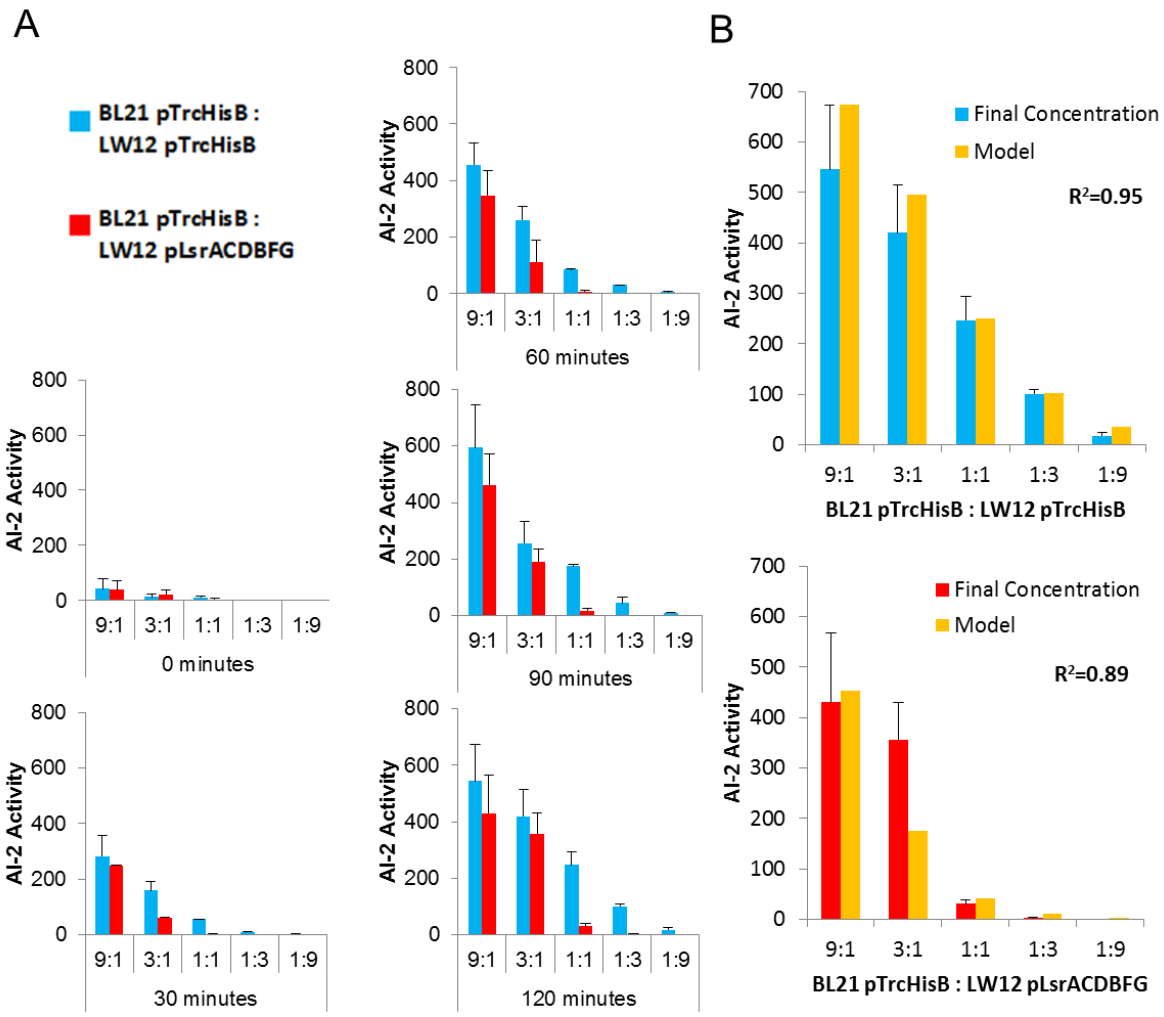

Figure 3.3 LW12 pLsrACDBFG modulates AI-2 in the microenvironment. Panel (A) illustrates the AI-2 in co-cultures of *E. coli* BL21 (*luxS*$^{+}$) with LW12 pTrcHisB (blue) and LW12 pACDBFG (red), respectively, over time in a range of concentration ratios. AI-2 levels were measured with AI-2 activity assays every 30 minutes. Each experiment is performed in triplicate with error bars indicating standard error. Panel (B) compares the AI-2 activities at 120 minutes with the mathematical model generated.

The mathematical model developed in **Table 3.1** was extended to characterize these co-cultures (Figure 3.3B), as opposed to the addition of exogenous AI-2 to the earlier simulations where AI-2 was exogenously added to 'controller cell' cultures (Figure 3.1). We found good agreement between the model and the experimental data, and detailed discussion of all rate equations, growth rates, and kinetic parameters is provided in the Supplementary material. We

note all rate equations and kinetic parameters used in the uptake profile for exogenously added AI-2 were unchanged for the co-incubation experiments.

3.5.4 Chemotaxis and biofilm attenuation

While this methodology provides a tool to regulate synthetic systems, it may also serve as a modifier of natural processes such as antibiotic susceptibility, motility, and biofilm formation. It has been shown that AI-2 has a contributing effect on biofilm formation in the *E. coli* W3110 [136]; therefore, we investigated if LW12 pLsrACDBFG, could interfere with biofilm formation from this biofilm producer. Co-incubations of W3110 pTrcHisB were reinoculated with either LW12 pTrcHisB or LW12 pLsrACDBFG and grown in a 96-well plate for 24 hours. In certain wells, exogenous AI-2 was added to produce greater biofilm formation, and homocysteine, a side-product of AI-2 synthesis, was added as an additional negative control. Optical density measurements showed no significant variation in growth (**Figure 3.4A**), thereby suggesting that this method to obtain biofilm reduction does not exert selective pressure. Biofilm production was normalized to the final cell density and LW12 pLsrACDBFG showed reduced biofilm formation by about 20% compared to identical incubations with LW12 pTrcHisB (**Figure 3.4B**). A two-tailed unpaired Student's t-test was performed between the groupings, and a p-value of 0.0000485 was determined, indicating that the biofilm reduction is significant. Further, the addition of exogenous AI-2 to the co-incubations (bar 'D') showed a restoration of biofilm formation in co-culture of LW12 pLsrACDBFG while homocysteine (bar 'E') does not, which further illustrates that the direct removal of AI-2 by LW12 pLsrACDBFG caused the resultant biofilm reduction.

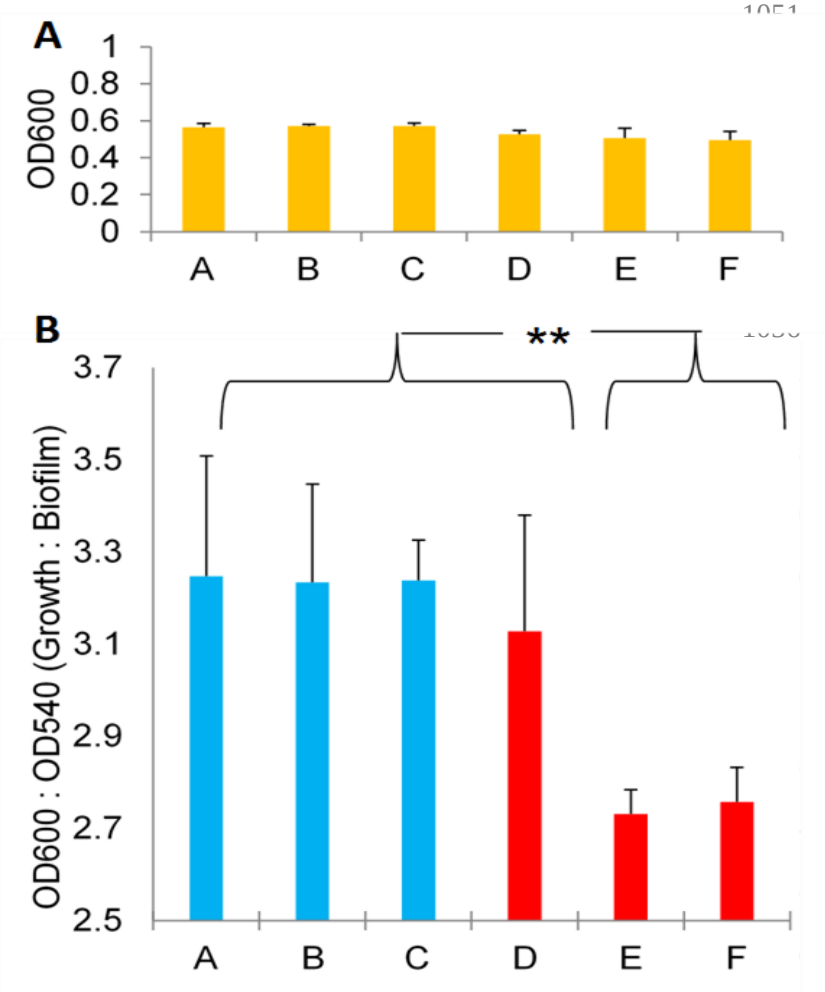

Figure 3.4: Effects of AI-2 on biofilm production. Co-incubations of **(A)** W3110 pTrcHisB : LW12 pTrcHisB **(B)** W3110 pTrcHisB : LW12 pTrcHisB + homocysteine (50 µM) **(C)** W3110 pTrcHisB : LW12 pTrcHisB + AI-2 (50 µM) **(D)** W3110 pTrcHisB : LW12 pLsrACDBFG **(E)** W3110 pTrcHisB : LW12 pLsrACDBFG + homocysteine (50 µM) **(F)** W3110 pTrcHisB : LW12 pLsrACDBFG + AI-2 (50 µM) are mixed at a 1:1 ratio at OD ~ 0.05 and IPTG (1 mM) is added at OD ~ 0.4. Homocysteine is added as a negative control to evaluate the effect of exogenous AI-2. Biomass is measured in technical triplicate after 24 hours, and each experiment is performed in biological duplicate. **Figure 3.4A** illustrates optical density at OD_{600} after 24 hours. **Figure 3.4B** shows the ratio of cell density at OD_{600} to biomass measured at OD_{540}. A Student's two tailed unpaired t-test was used to compare the groupings shown and a significance value of $p = 4.85 \times 10^{-5}$ was determined. All error bars indicate one standard deviation.

Similarly, AI-2 acts as a chemoattractant for *E. coli* [137], and we show that LW12 pLsrACDBFG can interfere with chemotaxis through the removal of AI-2. Conditioned media

with exogenously added AI-2 incubated with LW12 pTrcHisB or LW12 pLsrACDBFG was used in a transwell assay where a culture of "seeker" cells, W3110 *ΔluxS ΔlsrFG*, in the bottom chamber traverse the permeable membrane towards the conditioned media with AI-2 in the top chamber (see Methods). As shown in **Figure 3.5**, a greater population of "seeker" cells chemotaxed upwards towards conditioned media from incubations with LW12 and the empty vector supplemented with AI-2 than LW12 pLsrACDBFG supplemented with AI-2, illustrating that the clearing of AI-2 by LW12 pLsrACDBFG can block AI-2 mediated chemotaxis.

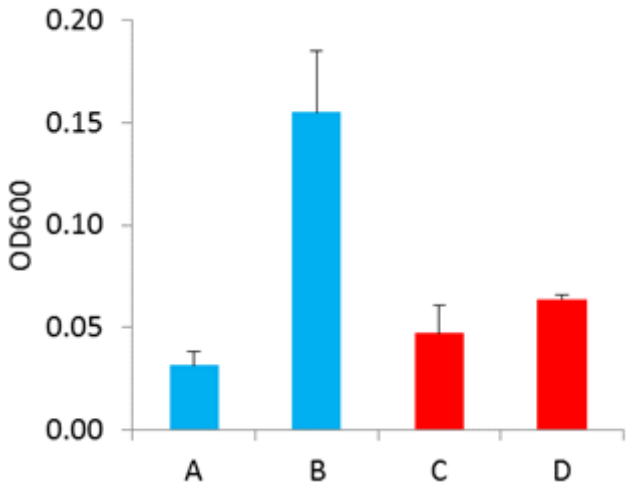

Figure 3.5: Effects of AI-2 on chemotaxis. Migration of CT104 (ΔluxS ΔlsrFG) in a transwell incubated for two hours (see Methods) with induced (1 mM IPTG) conditioned media of **(A)** LW12 pTrcHisB **(B)** LW12 pTrcHisB + AI-2 (20 µM) **(C)** LW12 pLsrACDBFG and **(D)** LW12 pLsrACDBFG + AI-2 (20 µM). Each experiment is performed in biological triplicate. Error bars indicate one standard deviation.

3.6 Discussion

Connecting both natural and synthetic networks, quorum sensing is widely used for a variety of processes and applications. When we developed the first population based example of a native regulatory circuit that was rewired to sense and transduce AI-2 to produce proteins, we looked forward to its potential to be used for "throttled" protein expression[14]. This dynamic control could help lead to the development of a 'synthetic switchboard' to control multiple genes in industrial bioprocesses [138], and the 'universal' signaling molecule AI-2, could be a natural choice to guide this kind of consortia. Traditional metabolic engineering could also benefit from microbial consortia, where a division of labor between two communities decreases the net metabolic load, creates new compounds, and increases productivity [139]. Synthetic communication systems would provide population-level coordination [140], and by developing an orthogonal method to control these QS systems, we provide another useful tool to guide microbial consortia in metabolic engineering applications.

We have previously demonstrated that both native [125] and artificial transcriptional circuits [14,117] are dependent on the level of signal and that this potentially has widespread application [27,141,142]. In this work, we developed 'controller cells, the application of which can actively modulate extracellular AI-2 concentrations. We show that the most effective 'controller cell', LW12 pLsrACDBFG, can silence heterologous gene expression. Also, this 'controller cell' can independently remove the signal generated from a 'producer cell', BL21, revealing the possibility of dynamic modulation (i.e. up- and down-regulation). We extended the application from synthetic networks to the naturally occurring processes of biofilm formation and chemotaxis.

Further, the deterministic model developed here helps to delineate the mechanistic underpinnings that guide QS phenomena. While the increased rate of AI-2 uptake due to LsrACDB overexpression was expected, increased uptake coincident with LsrK overexpression

was not (**Figure 3.1B**). By examining our model results in the context of the roles of the various components, we hypothesize that enhanced AI-2 uptake was due to a combination of two related factors. The first was that phosphorylated AI-2, unlike AI-2, cannot be transported across the bacterial membrane [32]. Thus, increased LsrK converts more intracellular AI-2 into AI-2P, increasing net AI-2 influx into the cell. Second, phosphorylated AI-2 acts to derepress LsrR, consequently resulting in greater expression of the *lsr*-operon from the genome (that is, AI-2P is assumed to be in rapid equilibrium with LsrR and this level corresponds to the prevailing rate of LsrK expression). So, faster accumulation of AI-2P should result in faster activation of *lsr* – mediated components. Of these two factors, we believe that the dominant is that the increased AI-2P prevents AI-2 from leaking back out of the cell. This was supported by the uptake profile of cells with pLsrFG, which was not significantly different than the uptake profile of cells with the empty vector. Theoretically, overexpression of *lsrFG* should result in faster degradation of AI-2P, which should cause a concomitant decreased expression of the genomic *lsr*-operon and resultantly, a slower uptake of AI-2. Since the uptake rate was not significantly altered, which suggests sufficient AI-2P levels in LW12 pLsrFG to maintain transcription of the genomic *lsr*-operon, then increased levels of AI-2P in LW12 pLsrK from overexpression of LsrK was correspondingly unlikely to cause much greater activation of the genomic *lsr*-operon.

While we have only simulated conditions that describe the experiments shown, its use as a predictive tool for further work is envisioned. That is, the intentional modulation of quorum-sensing molecules by the inclusion of static or growing ‘controller cells’ can provide an additional level of control for synthetic networks. Further understanding of the kinetic parameters of the uptake system would guide future manipulation using this control methodology; one might estimate the quantities of ‘controller cells’ needed to guide protein expression or other processes. Alternatively, we suggest that similarly engineered commensal *E. coli* may provide a means for altering behavior in natural ecosystems such as the gut microbiome. Analogously, by extension,

other bacterial species similarly engineered may provide a means to alter the balance of native niches. To our knowledge these concepts have not been reported. Among the many phenotypes controlled by AI-2 [8] at least two have been demonstrated in *E. coli* [136,143], and we have shown here that LW12 pLsrACDBFG can guide these phenotypes (biofilm formation and chemotaxis). We envision such cells might find utility in minimally disturbing cell-cell processes. We recognize that the current system uses a "charged" bacterium (induced with IPTG to overexpress transporter); the advantage being a well-controlled 'controller cell'. There may be instances where a completely autonomous system would be more advantageous; it might interrogate and interact within ecological niches. While challenges clearly remain for tailoring metabolic cues to spatiotemporally control cell populations, this work provides one additional potent tool for guiding phenotype among bacterial populations.

3.7 Supplemental material on mathematical model

3.7.1 Mathematical model of 'controller cells' with exogenously added AI-2

The expression of LsrACDB and LsrK are presented as 1st order dependent on cell density; this presumes that LsrR binding kinetics are rapid relative to the transcription rate and that LsrR is effectively unbound to the DNA because of the high levels of AI-2P. Since it has been shown that the alternative transport system is far slower than the *lsr*-mediated system to uptake AI-2 [130], we have assumed that flux through the alternative pathway is negligible. The secretion of AI-2 back into the extracellular environment through the transporter TqsA [144] is assumed to be 1st order. Lastly, the growth rates are fitted to experimental measurements (R^2 > 0.90), and it was found that overexpression of the LsrACDB and LsrACDBFG resulted in growth rates that were slower compared to the other strains **(Supplementary Figure 3.1)**.

3.7.2 Extension of deterministic model to co-incubations with BL21

The mathematical model developed with exogenous AI-2 is extended to account for co-incubations with AI-2 producer, BL21 pTrcHisB. All strains were grown to an OD ~ 0.4 and co-cultures of BL21 pTrcHisB were incubated with either LW12 pTrcHisB or LW12 pLsrACDBFG and aliquoted in culture test tubes at ratios of 9:1, 3:1, 1:1, 1:3, and 1:9. Rate equations for incubations of BL21 pTrcHisB with LW12 pTrcHisB or LW12 pLsrACDBFG are listed in **Table S3.3** and **Table S3.4,** respectively. We note that kinetic rate coefficients are unchanged from incubations with exogenous AI-2 (**Table S3.5**). Further, the production of AI-2 from BL21 is modeled as a 1st order process, since it has been shown that BL21 accumulates AI-2 in the extracellular environment with a similar dependence on cell density during exponential growth [94]. The resuspension of the cultures in various ratios results in various degrees of disturbance, and a phenomena known as an intermediate lag phase has been found to occur when cells are disturbed during exponential growth [145-147]. Therefore, a microbial lag phase is included in the model for strains that were diluted to below a 50% initial co-culture ratio. It is well-known that the length of the microbial lag phase is dependent on various parameters, including the deviation from the prior state and the bacterium [145,148]. We used the commonly used growth model from Baranyi and Roberts (1994) [149], resulting in an adjustment function dependent on the deviation from the previous state (denoted here as physiological state). The adjustment function, $\left(\frac{\boldsymbol{Q_i}}{\boldsymbol{1+Q_i}}\right)$, has an initial higher deviance for strains with 10% of the co-culture ratio compared to strains with 25% of the co-culture ratio. The adjustment function approaches a value of 1 at a rate dependent on the cell density growth rate. Since LW12 pLsrACDBFG has a slower growth rate than LW12 pTrcHisB and BL21 pTrcHisB, the adjustment function returns to a value of 1 slower for LW12 pLsrACDBFG than the other cultures. Lastly, the optical density rates are fitted from the experimental measurements and show good agreement ($R^2 > 0.87$) **(Supplementary Figure 3.2)**.

3.8 Supplemental figures

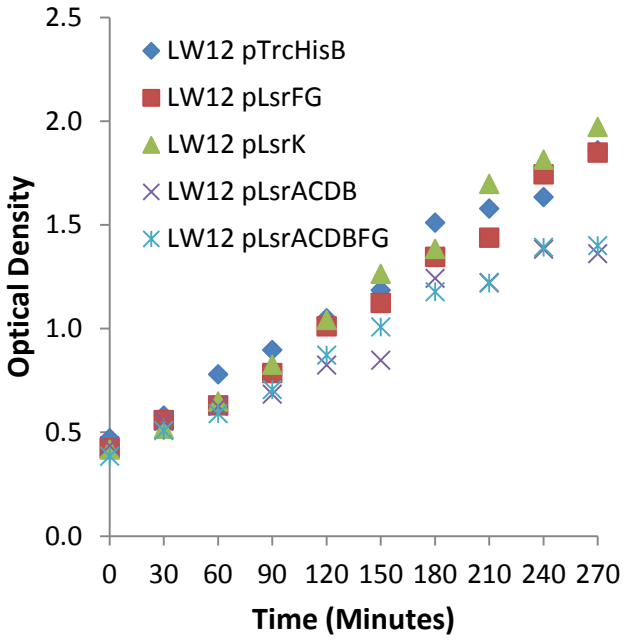

Figure S3.1: Optical density of individual strains. OD_{600} of respective strains after reinoculation and growth to OD ~ 0.4 before the addition of IPTG (1 mM) and AI-2 (50 µM).

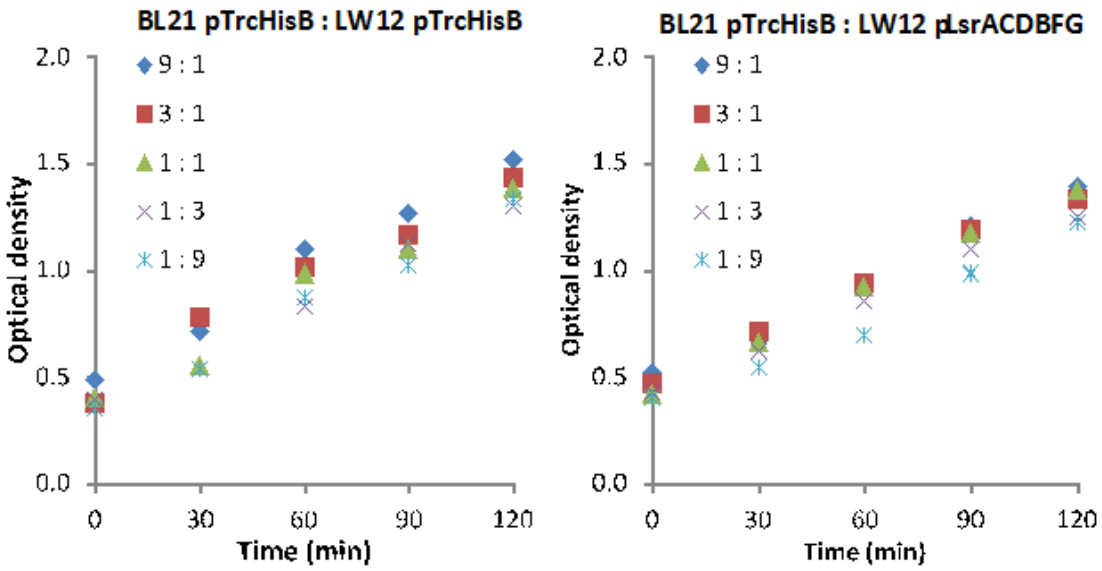

Figure S3.2: Optical density of co-cultures. OD_{600} of co-cultures of *E. coli* BL21 with LW12 pTrcHisB or LW12 pLsrACDBFG, respectively, over time at range of concentration ratios

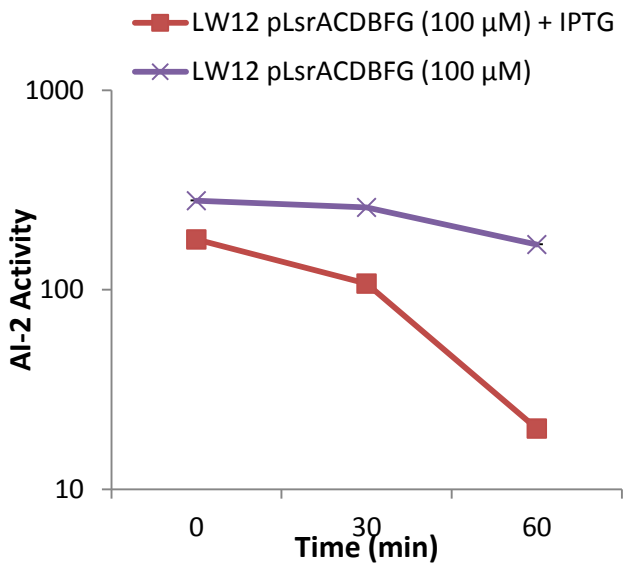

Figure S3.3: Uninduced uptake rate. Uptake rate of LW12 pLsrACDBFG with or without the presence of IPTG (1 mM)

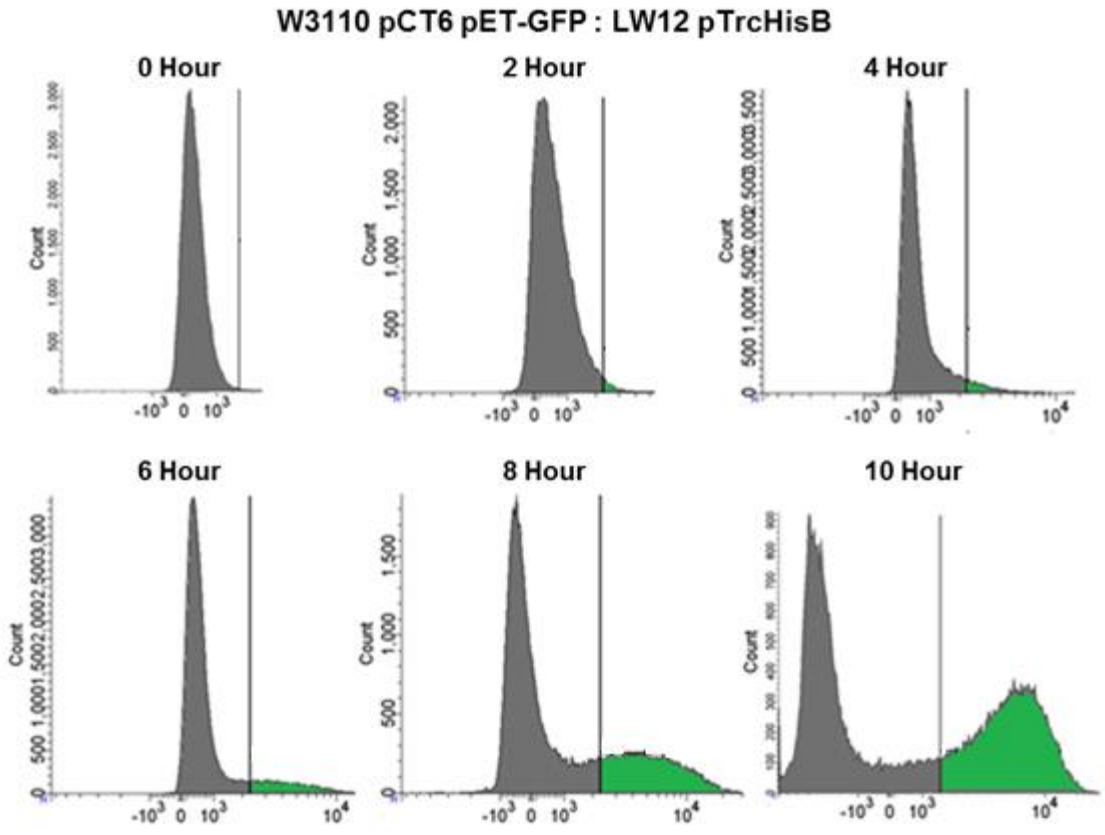

Figure S3.4: QS reporter with control. A 1:1 mixture of OD~1 of LW12 pTrcHisB is mixed with OD~0.2 of reporter strain W3110 pCT6 pET-GFP. Panel shows FACS data of the non-fluorescing population of both mixtures over time.

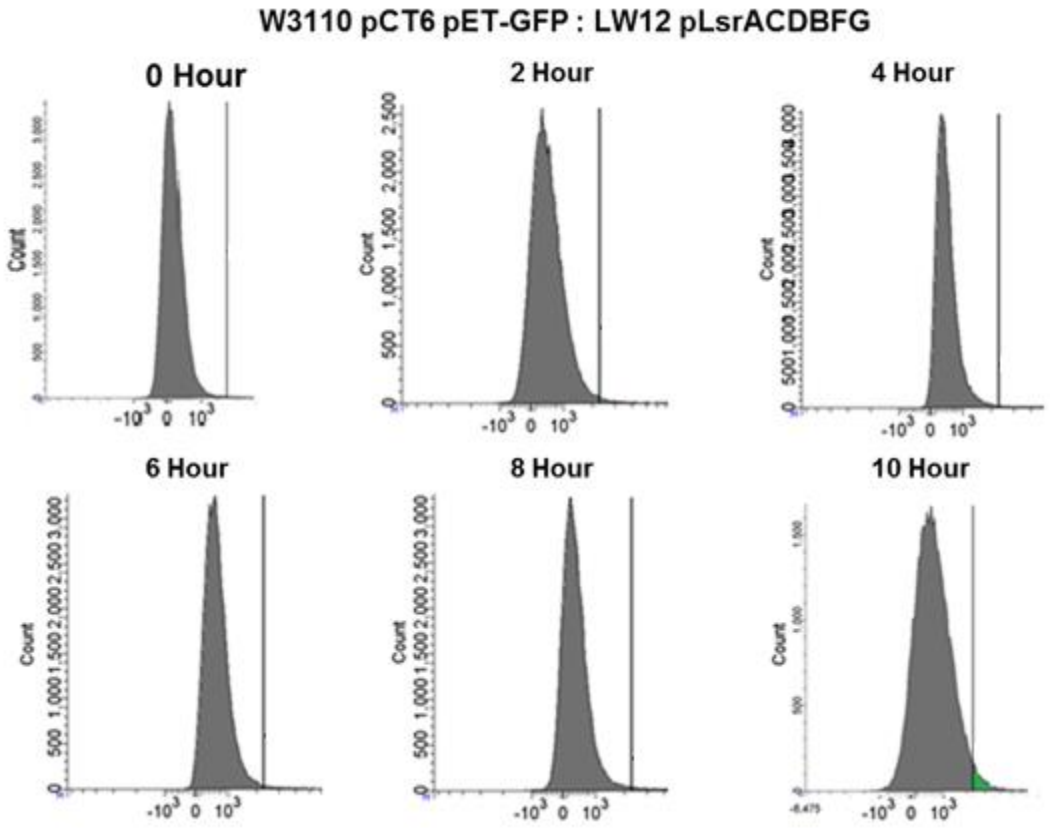

Figure S3.5: QS reporter with controller cell. A 1:1 mixture of OD~1 of LW12 pLsrACDBFG is mixed with OD~0.2 of reporter strain W3110 pCT6 pET-GFP. Panel shows FACS data of the non-fluorescing population of both mixtures over time.

3.9 Supplemental Tables

Strains	Description	Source
E. coli		
W3110	K12 strain, wild type, l^-, F^-, IN(*rrnD-rrnE*)1, *rph-1*s	Genetic Stock Center Yale University, New Haven, CT
LW12	W3110 ΔluxS::Kan T	[125]
BL21	B strain, F^-*ompT [dcm][lon]hsdS*($r_B^-M_B^-$)*gal*	Novagen
V. harveyi		
BB170	BB120 *luxN*::Tn5 (sensor 1^- ,sensor 2^+), Km^r	[69]
Plasmids	Description	Source
pFZY1	*galK'-lacZYA* transcriptional fusion vector, Ap^r	[150]
pET200/D-TOPO	Cloning vector, containing *T7* promoter, Km^r	Invitrogen
pTrcHisB	pTrcHis derivative, Ap^r	Invitrogen
pET200/dsRed	pET200 derivative, containing *dsRed*, Km^r	[129]
pCT6	pFZY1 derivative, containing lsrR and lsrR promoter region fused with T7RPol, Ap^r	[14]
pLsrFG	pTrcHisB derivative, containing lsrFG, Ap^r	This study
pLsrK	pTrcHisB derivative, containing lsrK, Ap^r	This study
pLsrACDB	pTrcHisB derivative, containing lsrACDB, Ap^r	This study
pLsrACDBFG	pTrcHisB derivative, containing lsrACDBFG, Ap^r	This study

Table S3.1: All strains and plasmids used in Chapter 3

Name	Sequence	Relevant Description
pLsrFG Fwd	CGATAAGGATCCGAGCATGGCAGATTTAGACGATATTAAAG	Forward primer for cloning *lsrFG*
pLsrFG Rev	GTACCAGCTGCAGATCTCACGGCATCAAACCATTG	Reverse primer for cloning *lsrFG*
pLsrK Fwd	CGATAAGGATCCGAGCTGAGATGGCTCGACTCTTTACC	Forward primer for cloning *lsrK*
pLsrK Rev	GTACCAGCTGCAGATCTCGAGCTATAACCCAGGCGCTTTC	Reverse primer for cloning *lsrK*
pLsrACDB Fwd	CGATAAGGATCCGAGCTCGAGATGCAAACGAGTGATACC	Forward primer for cloning *lsrACDB*
pLsrACDB Rev	GTACCAGCTGCAGATCTGAGTCAGAAATCGTATTTGCCG	Reverse primer for cloning *lsrACDB*
pLsrACDBFG Fwd	CGATAAGGATCCGAGCATGCAAACGAGTGATACC	Forward primer for cloning *lsrACDBFG*
pLsrACDBFG Rev	GTACCAGCTGCAGATCCTCACGGCATCAAACCATTG	Reverse primer for cloning *lsrACDBFG*

1231 **Table S3.2: Oligonucleotide primers used in Chapter 3**

1232

Reaction	Differential Equation
AI-2 outside the cell	$\frac{dAI2_{out}}{dt} = -k_{in} * (LsrACDB) * (AI2_{out}) + k_{out} * (AI2_{in}) + k_{lux} * (OD_{BL21})$
AI-2 inside the cell	$\frac{dAI2_{in}}{dt} = k_{in} * (LsrACDB) * (AI2_{out}) - k_{out} * (AI2_{in}) - k_p * (LsrK) * (AI2_{in})$
ACDB protein synthesis	$\frac{dLsrACDB}{dt} = K_{nat} * \left(OD_{LW12}^{pTrcHisB}\right) - k_d * (LsrACDB)$
Lsr kinase synthesis	$\frac{dLsrK}{dt} = K_{nat} * \left(OD_{LW12}^{pTrcHisB}\right) - k_d * (LsrK)$
Cell density (BL21)	$if\ r_b \geq 0.5,\ \frac{dOD_{BL21}}{dt} = r_b * \mu * (OD_{BL21})$ $else\ \frac{dOD_{BL21}}{dt} = r_b * \mu * (OD_{BL21}) * \left(\frac{Q_{BL21}}{1 + Q_{BL21}}\right)$
Cell density (LW12 pTrcHisB)	$if\ r_h \geq 0.5,\ \frac{dOD_{LW12}^{pTrcHisB}}{dt} = r_h * \mu * \left(OD_{LW12}^{pTrcHisB}\right)$ $else\ \frac{dOD_{LW12}^{pTrcHisB}}{dt} = r_h * \mu * \left(OD_{LW12}^{pTrcHisB}\right) * \left(\frac{Q_{LW12}^{pTrcHisB}}{1 + Q_{LW12}^{pTrcHisB}}\right)$
Physiological state (BL21)	$\frac{dQ_{BL21}}{dt} = \mu * (Q_{BL21})$
Physiological state (LW12 pTrcHisB)	$\frac{dQ_{LW12}^{pTrcHisB}}{dt} = \mu * \left(Q_{LW12}^{pTrcHisB}\right)$

Table S3.3: Rate equations used in co-incubations of BL21 pTrcHisB with LW12 pTrcHisB

Reaction	Differential Equation
AI-2 outside the cell	$\frac{dAI2_{out}}{dt} = -k_{in} * (LsrACDB) * (AI2_{out}) + k_{out} * (AI2_{in}) + k_{lux} * (OD_{BL21})$
AI-2 inside the cell	$\frac{dAI2_{in}}{dt} = k_{in} * (LsrACDB) * (AI2_{out}) - k_{out} * (AI2_{in}) - k_p * (LsrK) * (AI2_{in})$
ACDB protein synthesis	$\frac{dLsrACDB}{dt} = K_I * \left(OD_{LW12}^{pLsrACDBFG}\right) + K_{nat} * \left(OD_{LW12}^{pLsrACDBFG}\right) - k_d * (LsrACDB)$
Lsr kinase synthesis	$\frac{dLsrK}{dt} = K_{nat} * \left(OD_{LW12}^{pLsrACDBFG}\right) - k_d * (LsrK)$
Cell density (BL21)	$if\ r_b \geq 0.5,\ \frac{dOD_{BL21}}{dt} = r_b * \mu * (OD_{BL21})$ $else\ \frac{dOD_{BL21}}{dt} = r_b * \mu * (OD_{BL21}) * \left(\frac{Q_{BL21}}{1 + Q_{BL21}}\right)$
Cell density (LW12 pTrcHisB)	$if\ r_v \geq 0.5,\ \frac{dOD_{LW12}^{pLsrACDBFG}}{dt} = r_v * \mu_v * \left(OD_{LW12}^{pLsrACDBFG}\right)$ $else\ \frac{dOD_{LW12}^{pLsrACDBFG}}{dt} = r_v * \mu_v * \left(OD_{LW12}^{pLsrACDBFG}\right) * \left(\frac{Q_{LW12}^{pLsrACDBFG}}{1 + Q_{LW12}^{pLsrACDBFG}}\right)$
Physiological state (BL21)	$\frac{dQ_{BL21}}{dt} = \mu * (Q_{BL21})$
Physiological state (LW12 pTrcHisB)	$\frac{dQ_{LW12}^{pLsrACDBFG}}{dt} = \mu_v * \left(Q_{LW12}^{pLsrACDBFG}\right)$

Table S3.4: Rate equations used in co-incubations of BL21 pTrcHisB and LW12 pLsrACDBFG

Species	Description	Initial Condition/Range
t	Time	[0, 120] min
$AI2_{out}$	Extracellular AI-2	[0, 4] μM
$AI2_{in}$	'Controller' intracellular AI-2	0 μM
$IPTG_K$	Overexpression of LsrK	[1,0]
$IPTG_{ACDB}$	Overexpression of LsrACDB	[1,0]
$LsrK$	Kinase	0 μM
$LsrACDB$	ACDB transporter	0 μM
$OD_{LW12}^{pTrcHisB}$	Cell density (LW12 pTrcHisB)	0.04-0.54
$OD_{LW12}^{pLsrACDBFG}$	Cell density (LW12 LsrACDBFG)	0.04-0.54
OD_{BL21}	Cell density (BL21 pTrcHisB)	0.04-0.54
r_b	Ratio of BL21 pTrcHisB	[.90, .75, .50, .25, .10]
r_h	Ratio of LW12 pTrcHisB	[.10, .25. .50, .75, .90]
r_v	Ratio of LW12 pLsrACDBFG	[.10, .25. .50, .75, .90]
Q_{BL21}	Physiological state BL21 pTrcHisB	[0, 0, 0, 1.5, 1]
$Q_{LW12}^{pTrcHisB}$	Physiological state LW12 pTrcHisB	[1, 1.5, 0, 0, 0]
$Q_{LW12}^{pLsrACDBFG}$	Physiological state LW12 pLsrACDBFG	[1, 1.5, 0, 0, 0]
Parameters	**Description**	**Best fit value**
k_{in}	AI-2 import by LsrACDB complex	0.008 μM^{-1} min^{-1}
k_{out}	AI-2 export	0.045 min^{-1}
k_p	AI-2 phosphorylation	0.006 μM^{-1} min^{-1}
K_I	Induced expression	0.9 μM min^{-1}
K_{nat}	Native expression	0.1 μM min^{-1}
k_{lux}	AI-2 production	0.45 μM min^{-1}
k_d	Protein decay	0.02 min^{-1}
μ	Growth rate (BL21 / LW12, pTrcHisB)	0.010 min^{-1}
μ_v	Growth rate (LW12 pLsrACDBFG)	0.007 min^{-1}

Table S3.5: Kinetic rate constants and parameters used in co-cultures

3.10 Supplemental Material on Mathematical Model

Mathematical model of 'controller cells' with exogenously added AI-2

The expression of LsrACDB and LsrK are presented as 1st order dependent on cell density; this presumes that LsrR binding kinetics are rapid relative to the transcription rate and that LsrR is effectively unbound to the DNA because of the high levels of AI-2P. Since it has been shown that the alternative transport system is far slower than the *lsr*-mediated system to uptake AI-2 [130], we have assumed that flux through the alternative pathway is negligible. The secretion of AI-2 back into the extracellular environment through the transporter TqsA [144] is assumed to be 1st order. Lastly, the growth rates are fitted to experimental measurements ($R^2 > 0.90$), and it was found that overexpression of the LsrACDB and LsrACDBFG resulted in growth rates that were slower compared to the other strains **(Supplementary Figure 3.1)**.

Extension of deterministic model to co-incubations with BL21

The mathematical model developed with exogenous AI-2 is extended to account for co-incubations with AI-2 producer, BL21 pTrcHisB. All strains were grown to an OD ~ 0.4 and co-cultures of BL21 pTrcHisB were incubated with either LW12 pTrcHisB or LW12 pLsrACDBFG and aliquoted in culture test tubes at ratios of 9:1, 3:1, 1:1, 1:3, and 1:9. Rate equations for incubations of BL21 pTrcHisB with LW12 pTrcHisB or LW12 pLsrACDBFG are listed in **Table S3.3** and **Table S3.4,** respectively. We note that kinetic rate coefficients are unchanged from incubations with exogenous AI-2 (**Table S3.5**). Further, the production of AI-2 from BL21 is modeled as a 1st order process, since it has been shown that BL21 accumulates AI-2 in the extracellular environment with a similar dependence on cell density during exponential growth [94]. The resuspension of the

cultures in various ratios results in various degrees of disturbance, and a phenomena known as an intermediate lag phase has been found to occur when cells are disturbed during exponential growth [145-147]. Therefore, a microbial lag phase is included in the model for strains that were diluted to below a 50% initial co-culture ratio. It is well-known that the length of the microbial lag phase is dependent on various parameters, including the deviation from the prior state and the bacterium [145,148]. We used the commonly used growth model from Baranyi and Roberts (1994) [149], resulting in an adjustment function dependent on the deviation from the previous state (denoted here as physiological state). The adjustment function, $\left(\frac{Q_i}{1+Q_i}\right)$, has an initial higher deviance for strains with 10% of the co-culture ratio compared to strains with 25% of the co-culture ratio. The adjustment function approaches a value of 1 at a rate dependent on the cell density growth rate. Since LW12 pLsrACDBFG has a slower growth rate than LW12 pTrcHisB and BL21 pTrcHisB, the adjustment function returns to a value of 1 slower for LW12 pLsrACDBFG than the other cultures. Lastly, the optical density rates are fitted from the experimental measurements and show good agreement ($R^2 > 0.87$) **(Supplementary Figure 3.2)**.

Chapter 4: Generation of 'quantized quorums' through dose-dependent encapsulated bacteria

The following work is prepared to be submitted into *ACS Synthetic Biology*.

4.1 Abstract

Bacteria secrete and recognize communication molecules to coordinate action in a process known as quorum sensing (QS), which plays a role in natural processes such as biofilm formation, antibiotic susceptibility, and motility. QS is used to connect synthetic networks with QS molecules such as acyl homoserine lactones, autoinducer-2 and oligopeptides. Previously, we engineered a suite of 'controller cells' that elucidated the dynamics of the uptake mechanisms and were used to quench QS and modulate QS dependent phenotypes such as biofilm formation. However, these 'controller cells' required an equivalent ratio of induced controller cell population to target QS cell population, an undesirable scenario in many microbiological applications. In this work, we rationally design a high-efficiency (HE) 'controller cell' that provides the most rapid uptake of the quorum sensing molecule autoinducer-2 (AI-2), without the addition of an exogenous inducing agent, to guide QS populations in a sequestered, encapsulated environment. This is done through the expression of every element of the *lsr*-system, with the exception of the *lsr* repressor, on a two-promoter constitutive plasmid. In addition to greatly increased uptake rate, this HE 'controller cell' is unaffected by the presence of glucose, thereby providing the possibility to affect cell processes in diverse, polymicrobial environments as well as glucose feedstock bioreactors. We show that these HE cells can silence quorum sensing at much lower cell populations than previous 'controller cells', and then show that through HE encapsulation inside the well-studied alginate-chitosan capsule motif, we can quench quorum sensing in target QS populations from a sequestered environment. Lastly, we sought to enable quantized subpopulation of QS-activated cells and in a dose-dependent fashion, tune QS-mediated gene expression. We have previously described the generation of 'quantized quorums' through

differences in AI-2 sensitivity[151], and here, we build on this by producing these quorums in a user-mediated fashion. These encapsulated bacteria provide orthogonal control to drive protein expression while maintaining minimal interaction and interference with the system, with applications in metabolic engineering and human disease.

4.2 Introduction

Quorum sensing (QS) is a process used by many microorganisms to coordinate action in a cell-density dependent manner through small signaling molecules. Microorganisms survey their local environment through the production and transduction of QS molecules. This coordination is necessary in natural bacterial networks such as biofilm formation, virulence factor secretion, and antibiotic production which can be critical to survival, but are fruitless if only enacted by a single member of the community. When the critical threshold for QS molecules is reached, indicating a sufficient cell population, a 'quorum' is obtained and bacteria can initiate gene expression as a community to coordinate behavior of a population on a larger scale[152]. Extending beyond natural processes, synthetic biologists have incorporated these QS components into synthetic circuits to generate sophisticated systems such as bistable networks, pulse generators, spatio-temporal activation of gene expression, and predator-prey ecosystems [106].

Recently, we developed "controller cells" to quench QS-dependent protein expression and phenotypic outcomes such as biofilm formation and chemotaxis (in review). These cells provided an orthogonal means of manipulation of natural and synthetic gene networks and phenotypes. However, these controller cells needed large amounts of bacteria directly interacting with the system to block communication, required the addition of an exogenous inducing agent, functioned only in the absence of glucose—a common nutrient in a variety of environments. The requirement of an induced, direct interaction of a large controller cell population to actuate quorum sensing suppression may not be suitable for many applications. Ideally, we could not

only quench, but tune QS-dependent response in a target population through a sequestered, separated controller cell population.

In this work, we sought to extend our prior work to encapsulate a controller cell inside a multifunctional polysaccharide capsule to tune protein expression of QS-dependent protein expression systems, without direct interaction with the QS culture, the need for an inducing agent, or the exclusion of glucose. We rationally designed a high-efficiency (HE) 'controller cell' that would provide rapid uptake of AI-2 without the need for an inducing agent, such as IPTG. In this design, we build off of our prior work where we separately overexpressed the three main components responsible for the uptake and degradation of AI-2 from the environment (**Scheme 1**): AI-2 transport into the cell through the protein complex LsrACDB, phosphorylation of AI-2 to AI-2P, a form of AI-2 that cannot cross the cell membrane, by the kinase LsrK, and degradation of AI-2P by the isomerase LsrG and cleavage by LsrF.

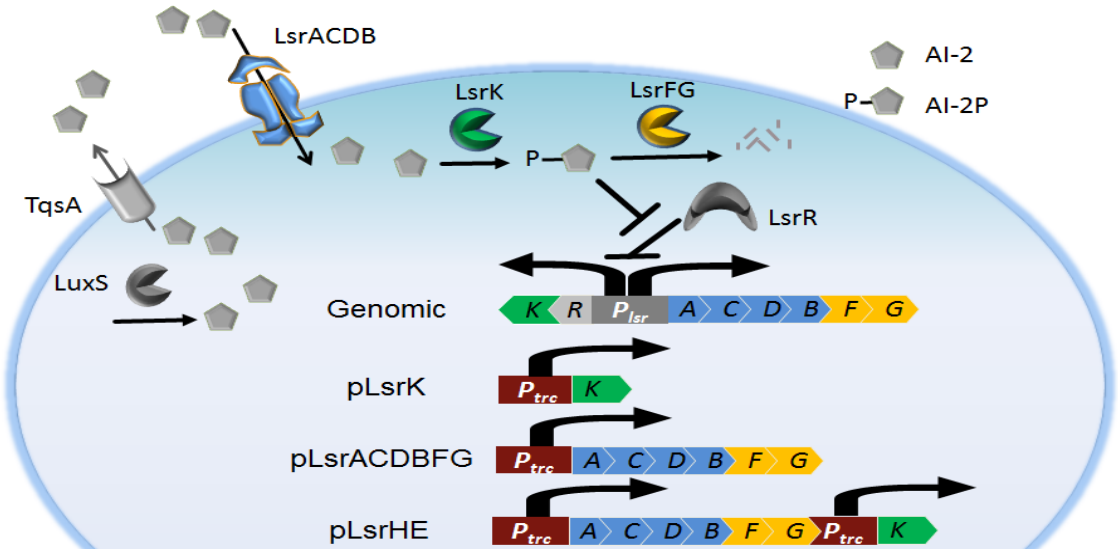

Scheme 4: Schematic of the *lsr*-system in *E. coli* and engineered plasmids. LuxS generates AI-2, which is exported out of the cell by TqsA. The ABC-transporter complex, LsrACDB, brings AI-2 into the cell where it is subsequently phosphorylated by LsrK into AI-2P. AI-2P derepresses LsrR, the global regulator of the lsr operon, from the genome allowing transcription of the *lsr*-genes. AI-2P is degraded through a two-step process by enzymes LsrG and LsrF. The engineered plasmids pLsrK, pLsrACDBFG, and pLsrHE are illustrated with constitutive transcription through the leakiness of the P_{trc} promoter.

Our previous work revealed that the separate overexpression of LsrK and LsrACDB both resulted in increased uptake, and we hypothesized that the overexpression of both mechanisms would result in greater uptake than overexpression of each separately. Therefore, a two promoter system on a single plasmid was designed to overexpress all aspects of the *lsr*-system, save the *lsr* repressor, and we rely on 'leaky' transcription from the *trc* promoter (i.e. IPTG is not added). As a host strain, we previously used a Δ*luxS* synthase knockout to enable investigation of the kinetics involved in AI-2 uptake. In this study, to fully enable AI-2 uptake, we used the strain SH1c, a Δ*luxS* Δ*lsrR* double knockout that does not require a quorum of phosphorylated AI-2 to activate the *lsr* system. Further, since the metabolic pathway that is responsible for AI-2 uptake and phosphorylation is greatly impaired when glucose is present due to the reduction of transcription factor cAMP-CRP [125], our previously engineered 'controller cells' could not be applied in glucose-rich environments. The HE 'controller cell' constitutively expresses the *lsr*-system using the *trc* promoter, independently of genomic transcription of the *lsr* system through the *lsr* promoter, which removes the need for the cAMP-CRP transcription factor.

We show that the HE 'controller cell' provides the most rapid uptake of AI-2 compared to all previously engineered cells, and that it is the only one to effectively remove all AI-2 from the extracellular environment in the presence of glucose. Further, the HE cells can silence QS-dependent protein expression communication not only at very low cell quantities, but also when encapsulated inside a biocompatible capsule. We sought to encapsulate these cells to maintain population separation while being able to effectively remove AI-2 and interfere with quorum sensing. Recent work has shown that 'engineered' population control through killer proteins can achieve adjustable steady state populations [16,153,154], and we aim to engineer quantized active subpopulations with minimal interaction. To achieve this, the 'controller cells' were encapsulated in a porous chitosan-alginate capsule. The improved HE controller cell is needed to overcome the diffusion limits of small molecules into capsules and the comparatively small bacterial

populations encapsulated to effectively uptake AI-2, as empty vector controls show no significant reduction in AI-2 levels.

We show that higher dosages of these encapsulated HE controller cells can quench QS signaling, which can be envisioned to be used as a quorum quenching [35,155] treatment to reduce the expression of harmful phenotypes while maintaining separation from the encapsulated bacteria. Our overarching goal was to not only quench protein expression, but to guide a QS-dependent system that would minimally interact with the controller cell populations. Tunable protein expression is a highly desired property and has been pursued through methods such as proteases [156,157], riboregulators[158], and RNAi[159]. We show here that we can tune protein expression by adjusting the quorum activated population through capsule dosage. We also envision that by enabling controlled manipulation of quorums, this tool could be used to assay threshold responses[159], manipulate complex genetic circuits [138], and develop and interrogate spatially-patterned cell populations[160,161].

4.3 Materials and Methods

4.3.1 Plasmid construction

Plasmids were constructed according to standard procedures[123]. Briefly, plasmid pLsrACDBFG (Invitrogen) was used as the backbone to construct plasmids pLsrHE. The plasmid plsrK was used as template to PCR the promoter to the termination region, inclusive of the lsrK gene using Q5 polymerase (New England Biolabs). This PCR insert was ligated into XhoI-digested pLsrACDBFG using Gibson assembly[124] and then transformed into SH1c (W3110 Δ*luxS* Δ*lsrR*) (Cite). Oligonucleotide primers were obtained from Integrated DNA Technologies (Coralville, IA) and are listed in **Table S1** (Supplementary Information).

4.3.2 AI-2 Assay

Cultured media was tested for AI-2 activity through the assay using *Vibrio harveyi* reporter strain BB170 [69]. In short, BB170, supplemented with kanamycin (50 ug/mL), was grown for 16 hours with shaking at 30°C in AB media. These cultures were diluted 1:5,000 in fresh AB media, and aliquoted into 12 x 75-mm tubes (Fisher Scientific). Cultured media samples were added to these BB170 cultures to obtain a final concentration of 10% (vol/vol). The resulting bioluminescence was measured by quantifying light production with a lumenometer (Glomax Multi- Jr) and assays points were selected so that values were in the linear range. Data are presented as "fold change" compared to the negative control, and all conditions were tested in triplicate. In experiments with supplemented chemically-synthesized AI-2, we report AI-2 activity normalized to the initial concentration, and subsequent points are correlated to AI-2 concentration using a prepared standard curve, as performed in prior studies (CITE mBIO).

4.3.3 Synthetic AI-2 uptake profiles

Chemically synthesized AI-2 [127] was generously provided by the Sintim research group. Each strain was reinoculated by diluting an overnight culture to 3% volume in 10 mL of LB and 10 mL of LB supplemented with 1% glucose, respectively. These cells were grown in a 50 mL culture flask to an optical density (OD) ~ 0.4 at 30^{o}C with 250 RPM shaking. AI-2 was then added to obtain a final concentration of 100μM.. Optical density was measured and samples were harvested every half hour for AI-2 activity assays. The average bioluminescence for samples at t = 0 were denoted as 100 μM, and subsequent AI-2 activity values were normalized to the standard curve generated.

4.3.4 Modulation of autoinduced protein expression

SH1c pTrcHisB, and SH1c pLsrSV were reinoculated at 3% of overnight culture in 4 mL of LB in 15 mL culture tubes and grown to an OD ~ 0.4-0.6 at 37^{o}C with ampicillin. W3110

pCT6 pET_EGFP [14], a strain of *E.coli* that responds to the level of the AI-2 concentration by expressing GFP, was grown to an OD ~ 0.1, was reinoculated at 3% overnight culture in 10 mL of LB in 50 mL culture flasks and grown to OD ~ 0.2. Co-cultures of W3110 pCT6 pET-EGFP incubated with either LW12 pTrcHisB or LW12 pLsrACDBFG were aliquoted in culture test tubes at ratios of 1:1, 2:1, 3:1, 6:1 and 8:1. Fluorescence was measured with a **plate reader.**

4.3.5 Capsule preparation

SH1c pTrcHisB and SH1c pLsrSV were reinoculated at 3% overnight culture in and grown to an OD~0.4-0.6 in 4 mL of LB supplemented with ampicillin (50 μg/mL) and 4 mL LB supplemented with 1% glucose and ampicillin (50 μg/mL), respectively. Cells were concentrated (5x) in their respective medias before being mixed with a 1:1 mixture of 2% alginate. A 1:1 mixture of 2% alginate with bacteria in LB is added dropwise with a 22 gauge needle into a stirring mixture of 4 mL of 1.5% chitosan and 2 ml of 0.25 M $CaCl_2$ in 10 mL beaker. Each capsule is then washed 3 times with 200 uL of DPBS supplemented with 0.1 M $CaCl_2$.

4.3.6 AI-2 uptake profile in capsules

Capsules were placed in 12 well plates (**Corning**) with 2 mL of LB supplemented with 20 μM AI-2, 50 μM Amp and 0.1 M $CaCl_2$ and 2 mL of LB supplemented with 20 μM AI-2, 1% glucose, 50 μM Amp and 0.1 M $CaCl_2$. A 150 μL sample is harvested every 30 minutes for for AI-2 activity assays.

4.3.7 Modulation of protein expression through encapsulated bacteria

W3110 pCT6 pET-EGFP was grown to OD ~ 0.2 and then resuspended in an equivalent volume of LB supplemented with ampicillin (50μg/mL). Capsules were added in each well of a 48 well plate (Corning) that contained 0.25 mL the W3110 pCT pET-EGFP culture. Flow cytometric

analysis was performed using a FACSCanto II™ Flow Cytometer (Becton Dickinson) and all raw data were analyzed with BD FACSDiva™ 6.0 software (Becton Dickinson).

4.4 Results and Discussion

4.4.1 AI-2 uptake profiles of controller cells with and without glucose

We characterized the uptake rates of our 'controller cells' by adding a fixed amount of exogenous AI-2 and monitoring AI-2 activity levels over time (**Figure 4/1A**). To determine this, we grew each culture in LB or LB supplemented with 1% glucose to an OD~0.4 and then added 100 µM of AI-2. While all controller cells displayed uptake of AI-2 in the presence of LB (left panel), the SH1c pLsrHE was clearly the fastest, with a rapid quenching by the first 30 minute timepoint. The uptake rate of SH1c pLsrACDBFG, which showed the most rapid uptake in our prior work, illustrated faster uptake dynamics than the empty vector, but clearly slower than SH1c pLsrHE. The controller cell SH1c pLsrK showed no significant uptake differences than the empty vector. Our prior work had shown that overexpression of LsrK provides a significant increase in uptake rate in the Δ*luxS* knockout strain LW12, but we find here that in the Δ*luxS* Δ*lsrR* double knockout strain, that plasmid expression of LsrK does not alter the uptake rates. This suggests by deleting *lsrR*, the gene responsible for the repression of the lsr-operon, the constant genomic transcription of *lsrK* already rapidly reduces intracellular AI-2 levels, so that additional overexpression of the kinase through pLsrK has negligible effects.

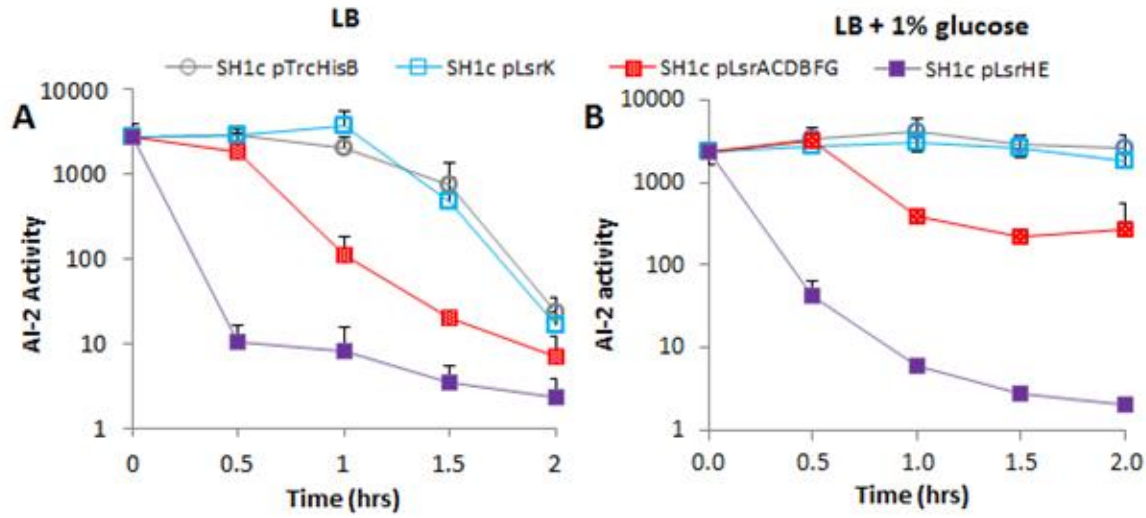

Figure 4.1: AI-2 uptake profiles. Each plasmid was transformed into SH1c (W3110 *ΔlsrR ΔluxS*) and grown to OD~0.4 in either LB (Panel A) or LB supplemented with 1% glucose (Panel B) before the addition of 100 µM of AI-2. AI-2 activity assays (see Methods) were used to measure AI-2 levels. Experiment performed in biological triplicate.

While all controller cells removed AI2 from the environment in LB, we expected the addition of 1% glucose (**Figure 4.1B**) to interfere greatly with uptake in strains relying on genomic transcription of at least one component of the *lsr*-system (i.e. SH1c with all plasmids except pLsrHE). This effect on genomic transcription of the *lsr*-operon is attributed to the export of cAMP out of the cell and down-regulation of catabolite repressor protein (CRP), which are transcription factors for *lsr* gene transcription[125]. As expected, in the empty vector, the extracellular AI-2 levels were not significantly reduced. Likewise, SH1c pLsrK showed no significant drop in AI-2 levels, as the downregulation of the ABC-transporter did not allow significant uptake of AI-2 for subsequent intracellular phosphorylation. While AI-2 can also enter through the slower intracellular transport of the alternative system [130], these dynamics were likely too slow to overcome the downregulation of genomic *lsrACDB*. Surprisingly, despite the downregulation of genomic *lsrK*, SH1c pLsrACDBFG did reduce AI-2 from the extracellular environment, albeit at a much slower rate compared to incubations with LB alone. Prior studies have shown that *lsrK* knockouts do not reduce extracellular AI-2 concentrations, as the phosphorylation of AI-2 by LsrK is needed to prevent secretion of AI-2 back into to the

extracellular environment [32]. Therefore, we expected that SH1c pLsrACDBFG would exhibit a similar uptake profile as the empty vector in glucose due to the down-regulation of *lsrACDB*. This surprising reduction by SH1c pLsrACDBFG may be due to the second independent promoter of LsrK [125], and suggests that this promoter may not be directly influenced by CRP-cAMP. As expected, SH1c pLsrHE exhibited only a small reduction in uptake rate since the downregulation of genomic transcription of *lsr*-components was supplemented with the unaffected transcription from the two-promoter plasmids.

4.4.2 Quenching of protein expression

To demonstrate that the HE 'controller cell' can interfere with QS-dependent actions, we sought to interfere with W3110 pCT6 pET-EGFP, a reporter strain that generates and transduces the AI-2 signal to produce GFP. Previously, we have shown that we can quench protein expression in this reporter system, by inducing the controller cell culture for 3 hours and resuspending in a 1:1 mixture with the reporter system (in review). In **Figure 4.2**, we grew W3110 pCT6 pET-EGFP, SH1c pTrcHisB, and SH1c pLsrHE to OD~0.4, and co-cultured W3110 pCT6 pET-EGFP with SH1c pTrcHisB and SH1c pLsrHE for 6 hours at a range of mixture ratios. The empty vector could quench AI-2 at ratios of 1:1 compared to the reporter strain, but in proportions with higher amounts of the reporter strain, the amount of protein expression shifts higher. In contrast, co-cultures with our improved 'controller cell' SH1c pLsrHE quenched protein expression even at proportions as high as 8:1.

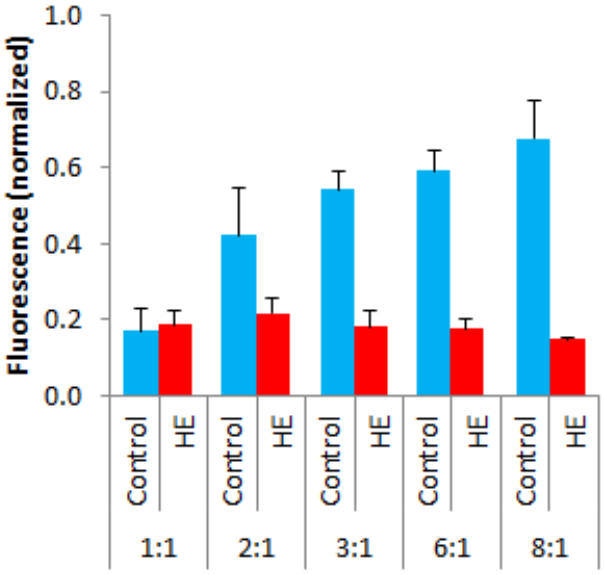

Figure 4.2. Modulation of protein expression. A range of concentration ratios of W3110 pCT6 pET-EGFP and SH1c pTrcHisB or SH1c pLsrHE are incubated for six hours before fluorescence intensity is measured on a plate reader and normalized to pure cultures of W3110 pCT6 pET-EGFP (positive control) and SH1c pTrcHisB (negative control). Experiment performed in biological duplicate.

4.4.3 Encapsulated bacteria remove extracellular AI-2

We have previously shown the ability to encapsulate fusion proteins that could produce AI-2 from the precursor, SAH, that would secrete from the capsule and signal QS-sensitive cells [162]. Here, we sought to encapsulate controller cells to modulate QS expression through the removal of AI-2 from the QS-dependent protein expression system. With an estimated pore size of less than 17nm [163], bacteria are easily retained inside the alginate matrix [164,165], and we used the well-studied alginate chitosan capsule method made through the extrusion technique [166]. Alginate entraps the bacteria and is surrounded by a hard chitosan shell. The pores in the alginate-chitosan allow small molecules such as AI-2 to pass, but contains larger items such as enzymes and bacteria within. Briefly, bacteria were grown to an OD ~ 0.4-0.6, concentrated 5X, and then mixed with a 2% alginate solution. The resulting mixture was added dropwise to a stirring chitosan/$CaCl_2$ solution (see Methods). To confirm that the bacteria are contained within the alginate matrix, we stained the bacterial membranes with calcein and used rhodamine dyed chitosan to visualize the orientation of the capsule. As **Figure 4.3A** and 4.**3B** illustrate, these

chitosan forms a thin layer at the edge to provide support, and the bacteria are within the alginate inner core [162].

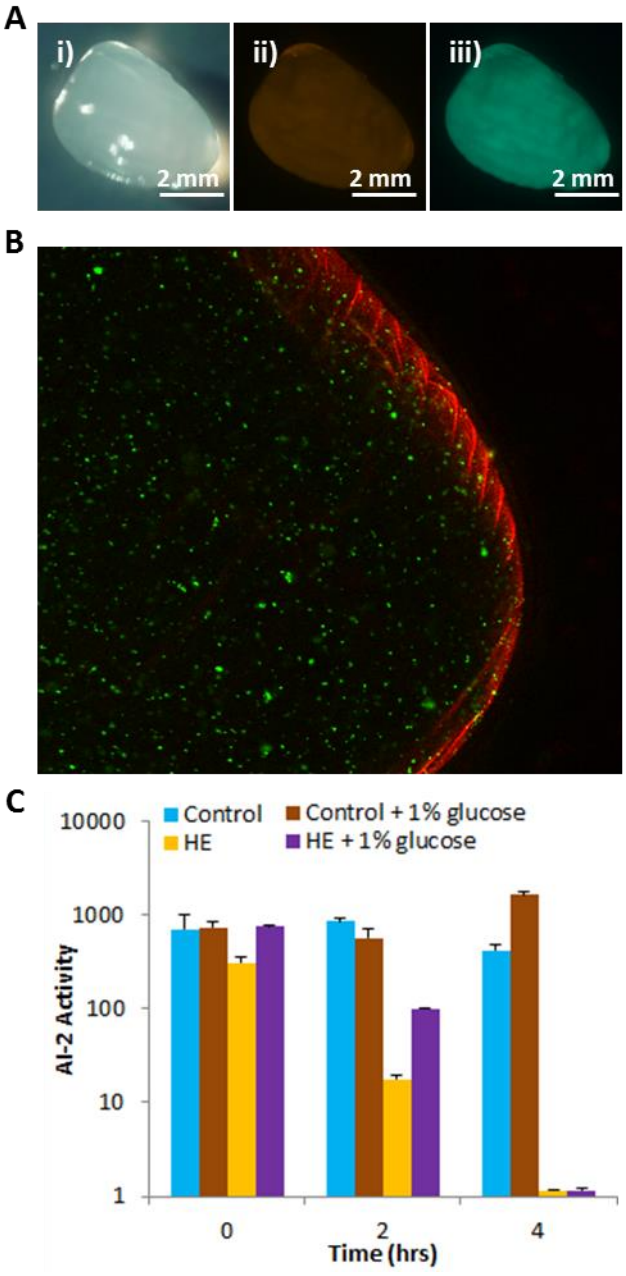

Figure 4.3: Encapsulated bacteria uptake profiles. Bacteria are mixed with 2% alginate in a 1:1 ratio before being dropped into a chitosan-$CaCl_2$ mixture. Panel (A) shows a stereomicroscopic (i) bright field image of the capsule (ii) RFP-filtered image of the rhodamine-labeled chitosan, and (iii) GFP-filtered image of Syto9 labeled bacteria. Panel (B) is a confocal image of the capsule with Syto9 labeled bacteria (green) and rhodamine labeled chitosan (red). Panel (C) shows the AI-2 uptake profile of encapsulated bacteria. Concentrated (5X) SH1c pTrcHisB and SH1c pLsrHE cultures in LB and LB supplemented with 1% glucose are mixed at a 1:1 ratio with 2% alginate before being dropped into a mixture of chitosan and $CaCl_2$ to encapsulate bacteria. Four capsules are then placed in 2 mL of LB supplemented with 20 µM of AI-2, and samples are harvested every 2 hours to measure AI-2 activity with AI-2 assays. Experiment performed in biological triplicate and a representative sample is illustrated.

Based on our prior work where entrapped enzymes inside the alginate-chitosan capsule could synthesize AI-2 that diffused out of the capsule [162], we encapsulated bacteria and tested the AI-2 uptake rate. Four capsules of SH1c pTrcHisB and SH1c pLsrHE were mixed with 20 μM of exogenous AI-2, and AI-2 levels were monitored over time. As **Figure 4.3C** illustrates, encapsulated HE 'controller cells' remove exogenous AI-2 from the environment, either with or without glucose, while the empty vector did not show any detectable reduction in the AI-2 environment. As in **Figure 4.1**, glucose only causes a small reduction in AI-2 uptake rate in SH1c pLsrHE. Bacterial load in each capsule was determined by dissolving each capsule in sodium citrate before and after incubation and streaking diluted portions on antibiotic selective plates. Colony-forming units (CFU) count showed an initial cell load of ~ 1.1 x 10^7 cells that grew to a final count of ~ 1.4 x 10^8 cells (data not shown).

4.4.4 Encapsulated HE 'controller cell' can quench and tune quorum sensing

We have shown that SH1c pLsrHE can quench protein expression of a QS-dependent system with a comparatively small amount of bacteria (**Figure 4.2**) and that encapsulated SH1c pLsrHE can remove exogenous AI-2 despite a limited bacterial load **(Figure 4.4)**. We applied the encapsulated bacteria to growing cultures of W3110 pCT6 pET-EGFP to silence QS dependent communication (see Methods). As **Figure 4.5** shows, no capsules, alginate capsules and SH1c pTrcHisB encapsulated capsules all resulted in bimodal cell populations. Each of these cultures displayed a bimodal population, and microscopic images show a bright, fluorescent population. In incubations with SH1c pLsrSV, however, a unimodal population was observed and microscopic images display a much smaller and dimmer fluorescent population.

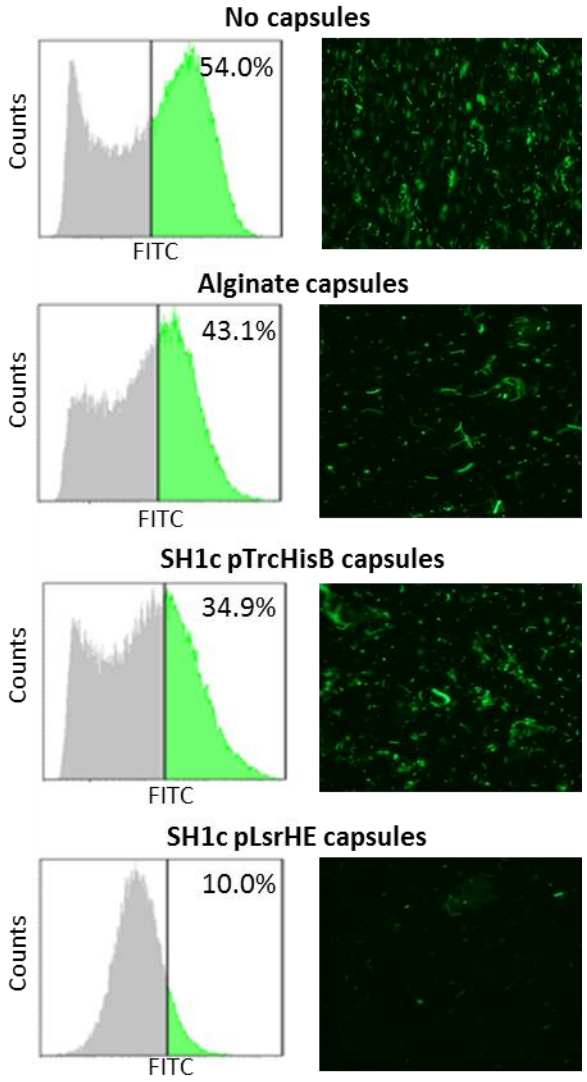

Figure 4.4: Encapsulated bacteria silence cell-cell communication. Cultures of W3110 pCT6 pET-EGFP were grown to an OD~0.1, and then incubated for 10 hours alone or with 8 capsules of alginate, SH1c pTrcHisB, and SH1c pLsrS.V. Cultures were then evaluated using flow cytometry (left panels) and microscopic images (right panels).

Finally, we sought to externally "tune" autonomous protein expression through encapsulated controller cells to obtain graduations of QS active subpopulations. Growing cultures of W3110 pCT6 pET-EGFP were grown in the presence of 8, 4, and 2 capsules of HE 'controller cells', as well as a culture without capsules. Capsules loaded with the HE 'controller cell' showed a dose-dependent guiding of protein expression with the doubling of capsule dose from 2 to 4 to 8 causing a concomitant reduction in brightness and fluorescent cell population (**Figure 4.6**). A

linear reduction in fluorescent population was observed (R^2 = 0.94), and a linear fit found a 22% reduction in population with the doubling of capsule dosage. **Supplementary Figure 4.1** shows the graduated reductions from a bimodal system (0 capsules) to a unimodal system (8 capsules)**.** **Supplementary Figure 4.2** displays the same information graphed on forward and side scatter. Through the further development of mathematical models, we can envision the *a priori* determination of QS-active subpopulations. While there has been promising work to develop adjustable threshold switches through direct mediation of transcription or translation, this work shows the first tunable protein expression system through the use of biocompatible capsules that provide minimal interaction to the system.

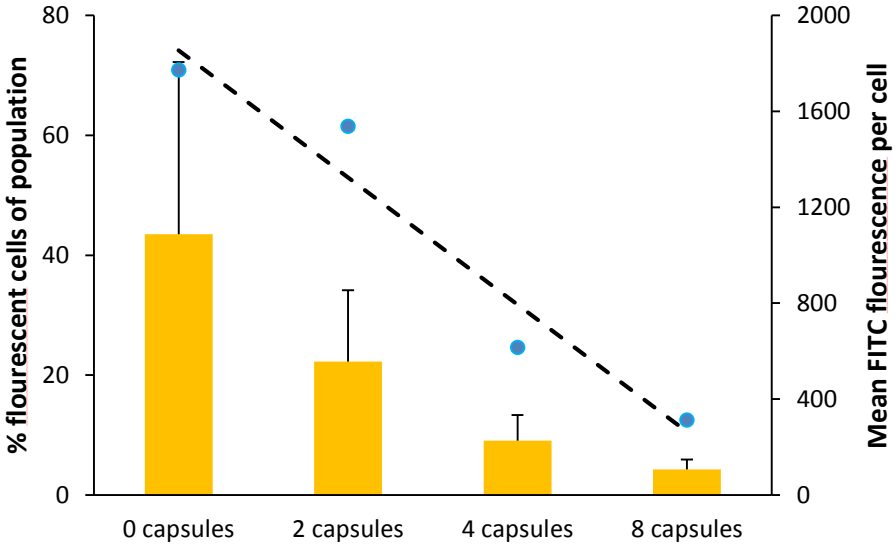

Figure 4.5: Tuning protein expression with varying doses of encapsulated bacteria. Cultures of W3110 pCT6 pET-EGFP were grown to an OD~0.1, and then incubated for 10 hours alone or with 8, 4 and 2 capsules of SH1c pLsrHE. Cultures were then evaluated using flow cytometry with data points (blue) representing the fluorescent population and bar graphs (yellow) representing the mean fluorescence. A linear trendline is fitted to the fluorescent population and an R^2 value is provided.

1600

4.5 Supplemental Figures

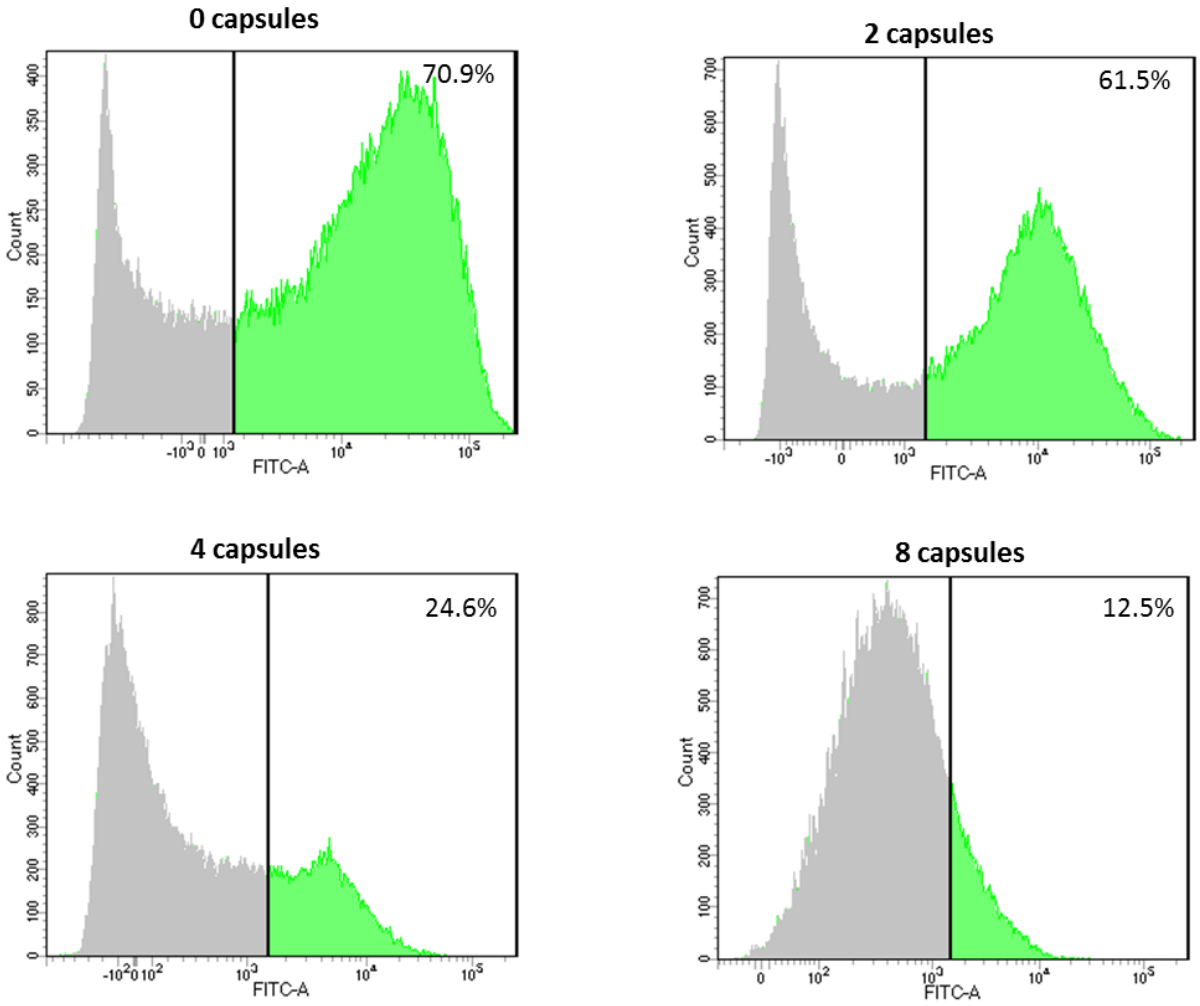

Figure S1: FACS histogram of EGFP expression with doses of encapsulated bacteria. Cultures of W3110 pCT6 pET-EGFP were grown to an OD~0.1, and then incubated for 10 hours alone or with 8, 4 and 2 capsules of SH1c pLsrHE. Cultures were then evaluated using flow cytometry. Percentages of fluorescent populations through gating is noted in the top right hand corner of each panel.

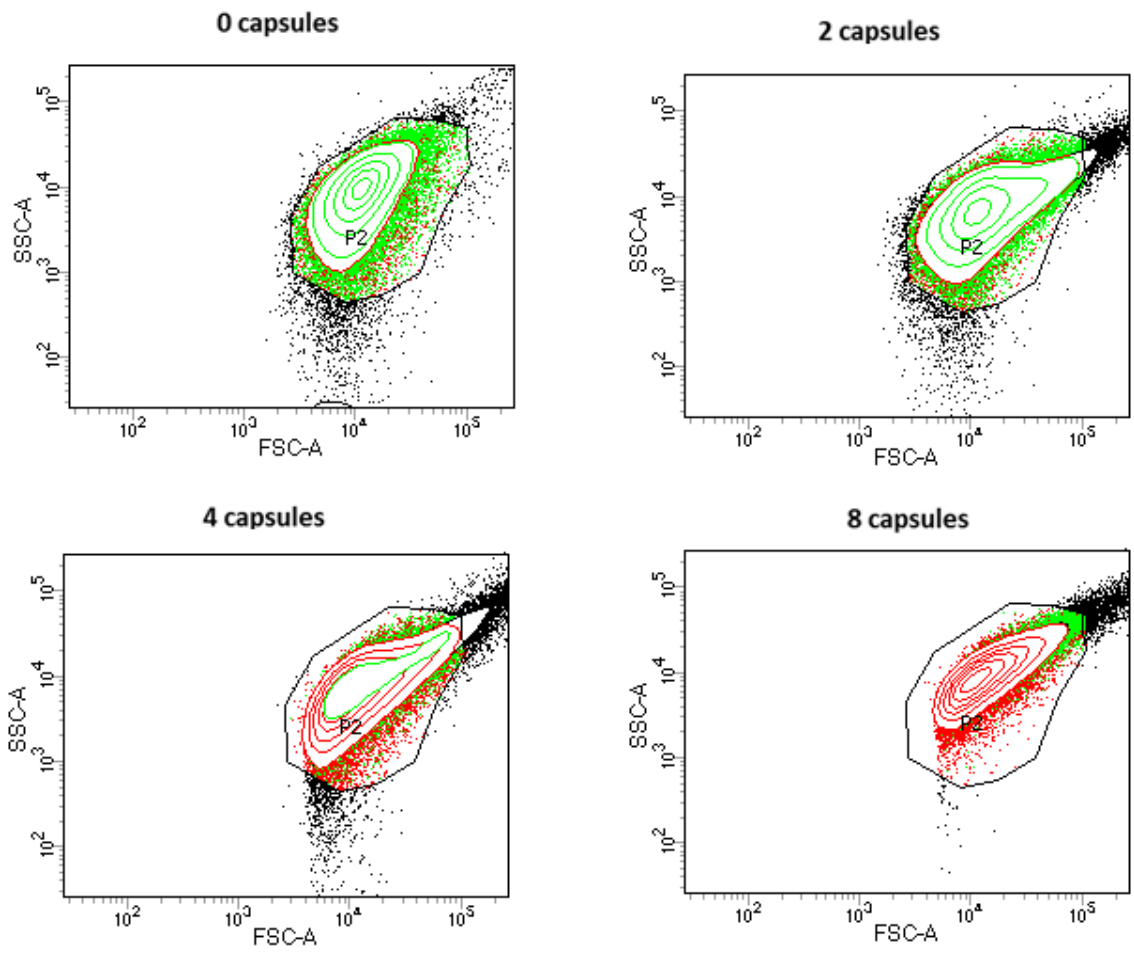

Figure S2: FACS histogram of EGFP expression with gating on side and forward scatter illustrated. Illustrated is Figure S1 graphed on gating for side and forward scatter. Black dots indicate all events, red dots indicate a non-fluorescent event, and green dots indicate a fluorescent event.

Chapter 5: Autonomous cell-guided quorum quenching

In our group, we have leveraged QS systems to engineer protein expression systems that are driven by QS signaling molecules [14]. A central challenge in metabolic engineering is balancing the distribution of microbial resources to maximize overexpression pathways come at the expense of endogenous pathways, which has been described as a 'zero-sum game'[109]. *E. coli*, the bacterium of choice for recombinant protein production, conveys the stress of overexpressing heterologous genes through AI-2 [116]. A creative approach to leveraging this behavior for protein production is to use QS to autonomously produce recombinant proteins, which we have done using *E. coli* and its 'universal' QS molecule, autoinducer-2 [167]. We wish to use this same approach to develop an autonomous 'controller cell'. This is a direction that will provide a useful tool in situations where the use of autonomous "cell-mediated" cells is more preferable to the "user-mediated' approach as outlined in this work (Chapers 3 and 4), such as the use of "surveillance bacteria" in GI tracts.

5.2.1 Autonomous controller cell generates positive feedback loop

In Chapters 3 and 4, we developed controller cells that were characterized with inducible or constitutive expression. While we believe these 'user-mediated' controller cells are useful in a variety of applications, one could envision autonomous 'cell-mediated' controller cells that are only active in the presence of the QS molecule AI-2. Used to interrogate and alter their environments, these autonomous controller cells would ideally be activated and sensitive to the the presence of AI-2, report a signal indicating the presence of the QS molecule, and actuate a response by uptaking AI-2 and processing the signal. We sought to enable this through the pCT6 systme. **Figure 5.1** shows the schematic, where phosphorylated AI-2 derepresses the pCT6 plasmid causing the transcription of the pET plasmid. The pET plasmid, in this case makes LsrK or LsrACDB, instead of GFP. Phosphorylated AI-2 would cause the upregulation of the components responsible for the generation of phosphorylated AI-2.

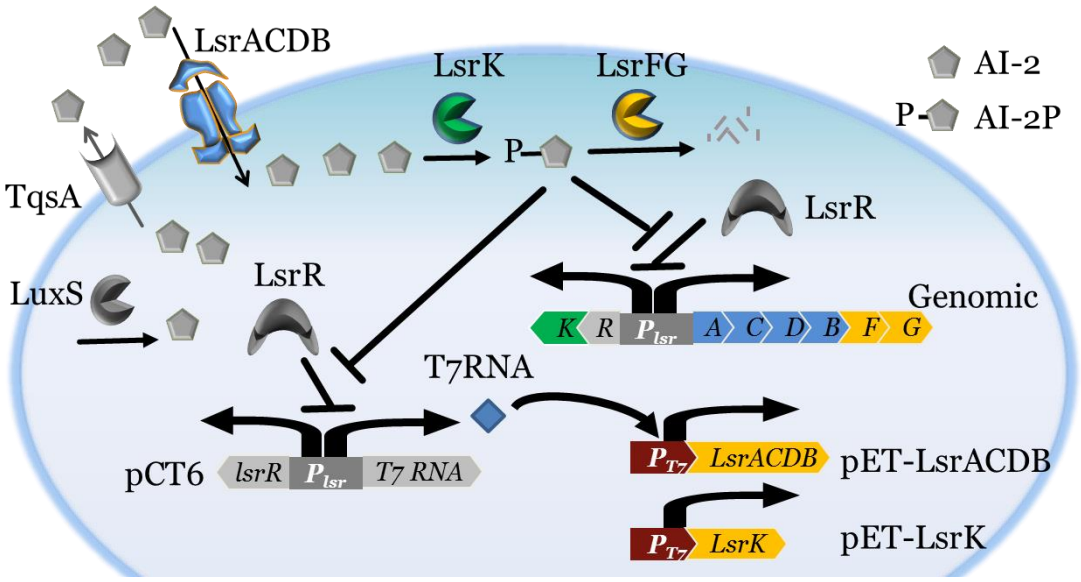

Figure 5.1: Schematic of 'autonomous controller cell'. Phosphorylated AI-2 causes the expression of T7RNA polymerase that transcribes LsrACDB and LsrK.

We first show that this positive feedback loop indeed cause greater activation of the pET plasmid, through qPCR, as seen in **Figure 5.2**. Strains were grown to an OD~0.4 and exogenous AI-2 at 40 and 4 µM were added. qPCR results show greater expression of the pET transgene in the pET-LsrK and pET-LsrACDB plasmids, than the empty vector pET200 control at both concentrations. As expected, the extent of upregulation in the autonomous controller cells is higher at 40 µM than 4 µM.

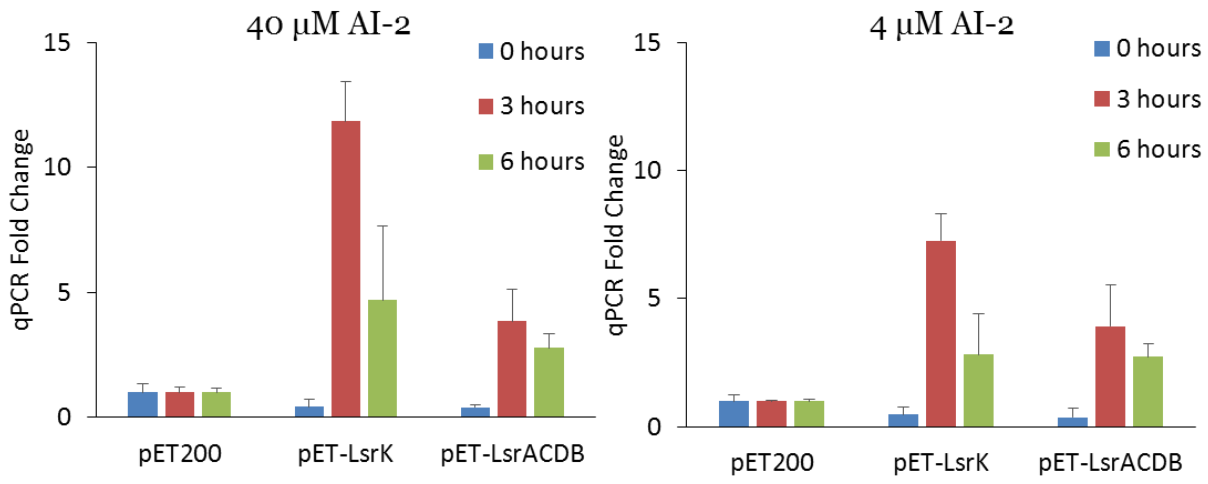

Figure 5.2: qPCR of autonomous controller cells. MDAI2 pCT6 with plasmids pET200, pET-LsrK and pET-LsrACDB are grown to OD~0.4. Left panel shows qPCR results of pET transgene when 40 µM of AI-2 is added. Right panel shows qPCR results pET transgene when 4 µM of AI-2 is added.

5.2.2 Autonomous controller uptake AI-2 in accelerated fashion and increases sensitivty

We measured actuation by also monitoring the AI-2 levels in the experiment above (OD~ 0.4 with the addition of exogenous AI-2). As **Figure 5.3** illustrates, when 40 µM of AI-2 is added, the empty vector pET200 control shows a slow removal of AI-2 over the course of 6 hours. The autonomous controller cells, both rapidly clear AI-2 within 3 hours. When 4 µM of AI-2 is added, the pET200 control is virtually unresponsive to the level AI-2, while the autonomous cells once again remove AI-2 within 3 hours, illustrating the increased sensitivity of these cells.

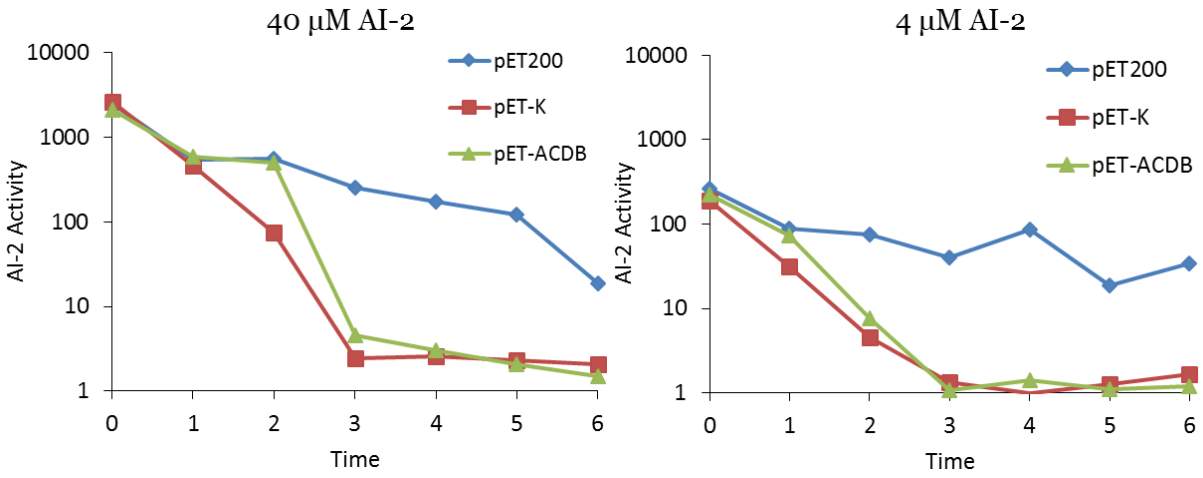

Figure 5.3: AI-2 uptake of autonomous controller cells. MDAI2 pCT6 with plasmids pET200, pET-LsrK and pET-LsrACDB are grown to OD~0.4. Left panel shows AI-2 levels when 40 µM of AI-2 is added. Right panel shows AI-2 levels when 4 µM of AI-2 is added.

5.2.3 Autonomous controller uptake provides signal of AI-2 uptake

Lastly, we would like these autonomous cells to secrete a signal when they uptake AI-2. To enable this, we cloned a GFP reporter gene upstream of the *lsrACDB* and *lsrK* genes. We grew the strains to OD~0.4 and added 40 µM of exogenous AI-2. Fluorescence was measured with flow cytometry every 2 hours and the results are shown in **Figure 5.4**. By creating this positive feedback loop that increases transcription of the pET transgene, the reporter gene is expressed at much higher levels in the autonomous controller cells than in the empty vector control.

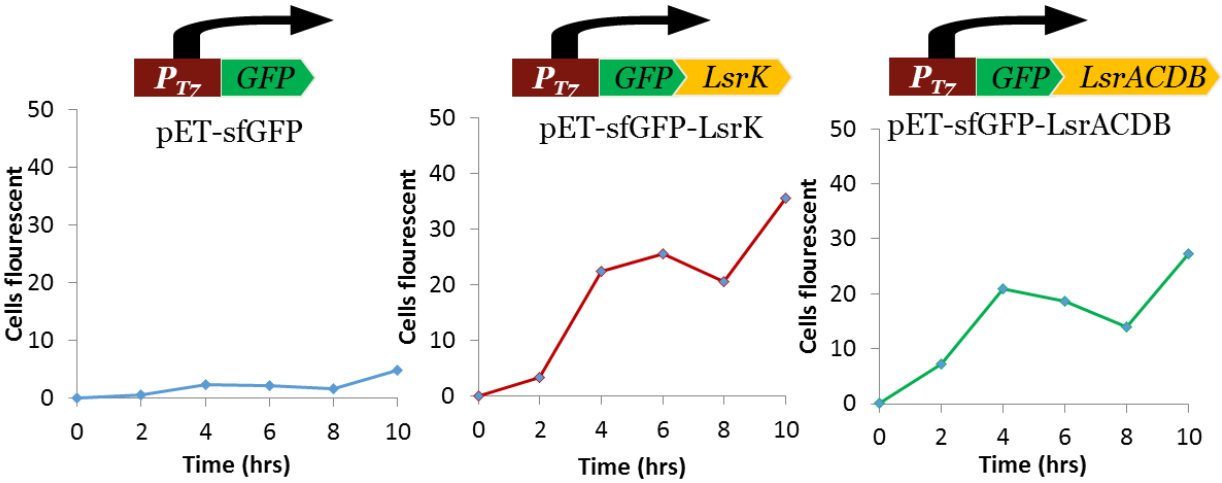

Figure 5.4: AI-2 uptake of autonomous controller cells. MDAI2 pCT6 with plasmids pET-sfGFP, pET-sfGFP-LsrK and pET-sfGFP-LsrACDB are grown to OD~0.4. Exogenous AI-2 (40 µM) is added and fluorescence is measured every 2 hours with flow cytometry.

5.3 Applications of autonomous controller cell

We believe the autonomous controller cells would be useful as a tool in both synthetic and natural networks. We hope to input these bacteria inside an animal model and show that these cells can interfere with QS-dependent phenotypes such as bioluminescence inside a living system.

Chapter 6: Conclusions, contributions and future directions

6.1 Summary

This dissertation details our work to investigate the interkingdom effects of the nonpathogenic *E. coli* secretome, including AI-2, on colonic epithelial cells, and the development of controller cells to guide intrakingdom phenotypes. This work has currently generated two published papers in mBio and Metabolic Engineering, an additional paper in preparation, and 5 international conferences.

We have shown here for the first time the global transcriptomic effects of the *E. coli* secretome on human epithelial cells. The secretome was shown to have an inflammatory response, with the upregulation of many genes in the cytokine-cytokine receptor pathway, the chemokine signaling pathway, and others, while also upregulating negative feedback regulators of the NOD-like signaling pathway and the NFkB pathway. We further show that AI-2 may also have a transcriptional inflammatory response that is initially upregulated at 6 hours before being downregulated at 24 hours. We hypothesize that this pattern fits the motif of a tight interplay between the host and microbiota, where metabolites can cause perturbations in the host cell which are restored through negative feedback elements[68].

After determining the AI-2 may contribute an initial inflammatory response to IECs, we progressed to the second aim of our work, to develop 'controller cells' that could rapidly remove AI-2 and affect QS-dependent phenotypes. We selected a *luxS* null mutant that could not generate AI-2 as a host strain, and transformed inducible plasmids that overexpressed each aspect of the AI-2 uptake mechanism. We found two 'knobs' for AI-2 uptake: phosphorylation of AI-2 by LsrK and transport into the cell by LsrACDB. Our mathematical model closely recapitulated the experimental results, and our work provides a clearer elucidation of the dynamics involved in the *lsr*-system. We provide phenotypic applications such as chemotaxis and biofilm formation.

Our overall goal was to develop controller cells that could modulate the target QS population while being sequestered in a separate environment. To do this, we extended the work by creating a HE controller cell that overexpresses every component of the *lsr*-system, save the repressor. We transform this inside a *luxS lsrR* double knockout mutant strain, a strain shown by Xavier et al, to provide more rapid uptake of AI-2 than a *luxS* null mutant alone [35]. We chose a single *luxS* mutant in the previous work to more clearly investigate the *lsr* dynamics, but in this work, to fully enable AI-2 uptake, we chose the double knockout strain. This HE controller cell provides the most rapid uptake of AI-2, without the addition of an inducing agent or the absence of glucose. This HE controller cell provides the needed rapid uptake to not only quench, but tune QS response while sequestered inside an alginate-chitosan capsule. This capsule provides a proof-of-concept to deliver encapsulated bacteria to modulate QS.

Lastly, we developed an autonomous quorum quenching system that rapidly removes AI-2 without a stimulus. We have characterized the system with AI-2 kinetic rates, transcriptional profiles and protein expression. We plan to further characterize the system with a detailed mathematical model, and apply the system to *in vivo* murine models.

6.2 Contributions to Science

We provide the first global transcriptomic analysis of nonpathogenic *E. coli* secretome on epithelial cells, and reveal that IECs respond to secretomes by activating defense-related pathways. We found that IECs "listen in" on QS molecule AI-2, but modulate response at later times.

We developed induced 'controller cells' that quench synthetic QS networks and applied these induced 'controller cells' to modulate QS-dependent phenotypes, including biofilm formation and chemotaxis. Through a mathematical model of our "controller cells', we elucidated the mechanisms of AI-2 processing in the *lsr* system.

Using the mathematical model we generated in our induced controller cells, we set about developing high-efficiency controller cells that uptake AI-2 at a fastest rate, without an inducing agent. In this application, we encapsulated HE cells inside biocompatible capsules and illustrated that it can quench and guide QS networks in discrete 'quantized quorums'. Not only can this method be used to quench QS and study QS dependent phenotypes such as antibiotic resistance, but as the capsules hold in bacteria and most proteins, the effects of secretome on IECs may be minimized in *in vivo* applications.

Lastly, we provide a quorum quenching platform that is self-directed. This provides the first quorum quenching application that is autonomous, and by rewiring the system, improve protein production yield. This system may be used in W3110 cells to improve the autonomous protein production system previously developed by our laboratory.

6.3 Future directions

We feel there are many exciting new directions and applications from this work. One application already mentioned is that the directed quantized quorums can be used to study quorum sensing dependent phenotypes. Previously, we have shown that by adding discrete quantities of AI-2, we can develop 'self-assembled' quorums using *luxS* knockout *E. coli* [151]. However, this system requires knocking out the gene *luxS*, a vital gene in *E. coli* metabolism. Studying QS by removing *luxS* confounds the conclusions that can be drawn [168]. The HE-capsules allow a general platform to manipulate any lsr-autoinduction system, as well as possibly any AI-2 producing bacterial species, which numbers over 80 different species. By allowing the gradual reduction in QS population, we can determine answer QS questions, such as, "How many QS cells are needed to defend the population against an antibiotic?"

While we have already mentioned using the autoinduced quorum quenching cells for an *in vivo* application, we could also use them as a rapid dynamic gene expression system. These systems have been hypothesized for use in microfluidic chips, where they are combined in a plug

and play application [161]. Further, these cells could be used in a breadboard like production switchboard, where cells are localized [169] and respond rapidly to different intensities of the 'universal' AI-2 signal.

References

1. Ng WL, Bassler BL (2009) Bacterial quorum-sensing network architectures. Annual review of genetics 43: 197-222.
2. Jayaraman A, Wood TK (2008) Bacterial quorum sensing: signals, circuits, and implications for biofilms and disease. Annu Rev Biomed Eng 10: 145-167.
3. Ahmer BMM (2004) Cell-to-cell signalling in Escherichia coli and Salmonella enterica. Molecular Microbiology 52: 933-945.
4. Walters M, Sperandio V (2006) Quorum sensing in Escherichia coli and Salmonella. International Journal of Medical Microbiology 296: 125-131.
5. Nealson K, Hastings JW (1979) Bacterial bioluminescence: its control and ecological significance. Microbiological reviews 43: 496.
6. Nasser W, Reverchon S (2007) New insights into the regulatory mechanisms of the LuxR family of quorum sensing regulators. Analytical and bioanalytical chemistry 387: 381-390.
7. Fuqua C, Greenberg EP (2002) Listening in on bacteria: acyl-homoserine lactone signalling. Nature Reviews Molecular Cell Biology 3: 685-695.
8. Pereira CS, Thompson JA, Xavier KB (2013) AI-2-mediated signalling in bacteria. FEMS microbiology reviews 37: 156-181.
9. Quan DN, Bentley WE (2012) Gene network homology in prokaryotes using a similarity search approach: Queries of quorum sensing signal transduction. PLoS computational biology 8: e1002637.
10. Monod J, Jacob F. General conclusions: teleonomic mechanisms in cellular metabolism, growth, and differentiation; 1961. Cold Spring Harbor Laboratory Press. pp. 389-401.
11. Gardner TS, Cantor CR, Collins JJ (2000) Construction of a genetic toggle switch in Escherichia coli. Nature 403: 339-342.
12. Khalil AS, Collins JJ (2010) Synthetic biology: applications come of age. Nature Reviews Genetics 11: 367-379.
13. Cameron DE, Bashor CJ, Collins JJ (2014) A brief history of synthetic biology. Nature Reviews Microbiology 12: 381-390.
14. Tsao C-Y, Hooshangi S, Wu H-C, Valdes JJ, Bentley WE (2010) Autonomous induction of recombinant proteins by minimally rewiring native quorum sensing regulon of E. coli. Metabolic engineering 12: 291-297.
15. Prindle A, Samayoa P, Razinkov I, Danino T, Tsimring LS, et al. (2012) A sensing array of radically coupled genetic /`biopixels/'. Nature 481: 39-44.
16. Balagaddé FK, Song H, Ozaki J, Collins CH, Barnet M, et al. (2008) A synthetic Escherichia coli predator–prey ecosystem. Molecular systems biology 4.
17. Swofford CA, Van Dessel N, Forbes NS (2015) Quorum-sensing Salmonella selectively trigger protein expression within tumors. Proceedings of the National Academy of Sciences 112: 3457-3462.
18. Duan F, March JC (2010) Engineered bacterial communication prevents Vibrio cholerae virulence in an infant mouse model. Proceedings of the National Academy of Sciences 107: 11260-11264.
19. Silver PA, Way JC, Arnold FH, Meyerowitz JT (2014) Synthetic biology: Engineering explored. Nature 509: 166-167.

20. Telford G, Wheeler D, Williams P, Tomkins P, Appleby P, et al. (1998) The Pseudomonas aeruginosaQuorum-Sensing Signal MoleculeN-(3-Oxododecanoyl)-l-Homoserine Lactone Has Immunomodulatory Activity. Infection and Immunity 66: 36-42.
21. Williams SC, Patterson EK, Carty NL, Griswold JA, Hamood AN, et al. (2004) Pseudomonas aeruginosa autoinducer enters and functions in mammalian cells. Journal of bacteriology 186: 2281-2287.
22. Bryan A, Watters C, Koenig L, Youn E, Olmos A, et al. (2010) Human transcriptome analysis reveals a potential role for active transport in the metabolism of< i> Pseudomonas aeruginosa</i> autoinducers. Microbes and Infection 12: 1042-1050.
23. Kendall MM, Sperandio V (2007) Quorum sensing by enteric pathogens. Current opinion in gastroenterology 23: 10-15.
24. Sperandio V, Torres AG, Jarvis B, Nataro JP, Kaper JB (2003) Bacteria–host communication: the language of hormones. Proceedings of the National Academy of Sciences 100: 8951-8956.
25. Shiner EK, Rumbaugh KP, Williams SC (2005) Interkingdom signaling: Deciphering the language of acyl homoserine lactones. FEMS Microbiology Reviews 29: 935-947.
26. Arias CA, Murray BE (2009) Antibiotic-resistant bugs in the 21st century—a clinical super-challenge. New England Journal of Medicine 360: 439-443.
27. Roy V, Adams BL, Bentley WE (2011) Developing next generation antimicrobials by intercepting AI-2 mediated quorum sensing. Enzyme and Microbial Technology 49: 113-123.
28. García-Contreras R, Maeda T, Wood TK (2013) Resistance to quorum-quenching compounds. Applied and environmental microbiology 79: 6840-6846.
29. Duan F, March JC (2008) Interrupting Vibrio cholerae infection of human epithelial cells with engineered commensal bacterial signaling. Biotechnology and bioengineering 101: 128-134.
30. Wright JS, Jin R, Novick RP (2005) Transient interference with staphylococcal quorum sensing blocks abscess formation. Proceedings of the National Academy of Sciences of the United States of America 102: 1691-1696.
31. LaSarre B, Federle MJ (2013) Exploiting Quorum Sensing To Confuse Bacterial Pathogens. Microbiology and Molecular Biology Reviews 77: 73-111.
32. Roy V, Fernandes R, Tsao C-Y, Bentley WE (2010) Cross species quorum quenching using a native AI-2 processing enzyme. ACS chemical biology 5: 223-232.
33. Roy V, Smith JA, Wang J, Stewart JE, Bentley WE, et al. (2010) Synthetic analogs tailor native AI-2 signaling across bacterial species. Journal of the American Chemical Society 132: 11141-11150.
34. Thompson JA, Oliveira RA, Djukovic A, Ubeda C, Xavier KB (2015) Manipulation of the Quorum Sensing Signal AI-2 Affects the Antibiotic-Treated Gut Microbiota. Cell Reports.
35. Xavier KB, Bassler BL (2005) Interference with AI-2-mediated bacterial cell–cell communication. Nature 437: 750-753.
36. Wang Z, Gerstein M, Snyder M (2009) RNA-Seq: a revolutionary tool for transcriptomics. Nature Reviews Genetics 10: 57-63.
37. Ewing B, Hillier LD, Wendl MC, Green P (1998) Base-calling of automated sequencer traces usingPhred. I. Accuracy assessment. Genome research 8: 175-185.
38. Volkman SK, Sabeti PC, DeCaprio D, Neafsey DE, Schaffner SF, et al. (2006) A genome-wide map of diversity in Plasmodium falciparum. Nature genetics 39: 113-119.
39. Trapnell C, Pachter L, Salzberg SL (2009) TopHat: discovering splice junctions with RNA-Seq. Bioinformatics 25: 1105-1111.

40. Langmead B, Trapnell C, Pop M, Salzberg SL (2009) Ultrafast and memory-efficient alignment of short DNA sequences to the human genome. Genome Biol 10: R25.
41. Thorvaldsdóttir H, Robinson JT, Mesirov JP (2012) Integrative Genomics Viewer (IGV): high-performance genomics data visualization and exploration. Briefings in bioinformatics.
42. Anders S, Huber W (2010) Differential expression analysis for sequence count data. Genome Biol 11: R106.
43. Tarca AL, Draghici S, Khatri P, Hassan SS, Mittal P, et al. (2009) A novel signaling pathway impact analysis. Bioinformatics 25: 75-82.
44. Dwyer DJ, Kohanski MA, Collins JJ (2009) Role of reactive oxygen species in antibiotic action and resistance. Current opinion in microbiology 12: 482-489.
45. Zargar A, Quan DN, Carter KK, Guo M, Sintim HO, et al. (2015) Bacterial Secretions of Nonpathogenic Escherichia coli Elicit Inflammatory Pathways: a Closer Investigation of Interkingdom Signaling. mBio 6: e00025-00015.
46. Sekirov I, Russell SL, Antunes LCM, Finlay BB (2010) Gut microbiota in health and disease. Physiological reviews 90: 859-904.
47. Peterson LW, Artis D (2014) Intestinal epithelial cells: regulators of barrier function and immune homeostasis. Nature Reviews Immunology 14: 141-153.
48. Rakoff-Nahoum S, Paglino J, Eslami-Varzaneh F, Edberg S, Medzhitov R (2004) Recognition of Commensal Microflora by Toll-Like Receptors Is Required for Intestinal Homeostasis. Cell 118: 229-241.
49. Bansal T, Alaniz RC, Wood TK, Jayaraman A (2010) The bacterial signal indole increases epithelial-cell tight-junction resistance and attenuates indicators of inflammation. Proceedings of the National Academy of Sciences 107: 228-233.
50. Medzhitov R (2001) Toll-like receptors and innate immunity. Nature Reviews Immunology 1: 135-145.
51. Inohara N, Nunez G (2003) NODs: intracellular proteins involved in inflammation and apoptosis. Nature Reviews Immunology 3: 371-382.
52. Creagh EM, O'Neill LA (2006) TLRs, NLRs and RLRs: a trinity of pathogen sensors that co-operate in innate immunity. Trends in immunology 27: 352-357.
53. Nord CE, Kager L, Heimdahl A (1984) Impact of antimicrobial agents on the gastrointestinal microflora and the risk of infections. The American journal of medicine 76: 99-106.
54. Lyte M (2013) Microbial Endocrinology in the Microbiome-Gut-Brain Axis: How Bacterial Production and Utilization of Neurochemicals Influence Behavior. PLoS pathogens 9: e1003726.
55. Curtis MM, Sperandio V (2011) A complex relationship: the interaction among symbiotic microbes, invading pathogens, and their mammalian host. Mucosal immunology 4: 133-138.
56. Hughes DT, Sperandio V (2008) Inter-kingdom signalling: communication between bacteria and their hosts. Nature Reviews Microbiology 6: 111-120.
57. Iyer LM, Aravind L, Coon SL, Klein DC, Koonin EV (2004) Evolution of cell–cell signaling in animals: did late horizontal gene transfer from bacteria have a role? TRENDS in Genetics 20: 292-299.
58. Rutherford ST, Bassler BL (2012) Bacterial quorum sensing: its role in virulence and possibilities for its control. Cold Spring Harbor perspectives in medicine 2: a012427.
59. Rasko DA, Sperandio V (2010) Anti-virulence strategies to combat bacteria-mediated disease. Nature Reviews Drug Discovery 9: 117-128.

60. Borruel N, Casellas F, Antolín M, Llopis M, Carol M, et al. (2003) Effects of nonpathogenic bacteria on cytokine secretion by human intestinal mucosa. The American journal of gastroenterology 98: 865-870.
61. Kelly D, Campbell JI, King TP, Grant G, Jansson EA, et al. (2004) Commensal anaerobic gut bacteria attenuate inflammation by regulating nuclear-cytoplasmic shuttling of PPAR-γ and RelA. Nature immunology 5: 104-112.
62. Haller D, Bode C, Hammes WP, Pfeifer AMA, Schiffrin EJ, et al. (2000) Non-pathogenic bacteria elicit a differential cytokine response by intestinal epithelial cell/leucocyte co-cultures. Gut 47: 79-87.
63. Kamada N, Maeda K, Inoue N, Hisamatsu T, Okamoto S, et al. (2008) Nonpathogenic Escherichia coli Strain Nissle 1917 Inhibits Signal Transduction in Intestinal Epithelial Cells. Infection and Immunity 76: 214-220.
64. Lammers K, Helwig U, Swennen E, Rizzello F, Venturi A, et al. (2002) Effect of probiotic strains on interleukin 8 production by HT29/19A cells. The American journal of gastroenterology 97: 1182-1186.
65. Martinez-Medina M, Aldeguer X, Lopez-Siles M, González-Huix F, López-Oliu C, et al. (2009) Molecular diversity of Escherichia coli in the human gut: New ecological evidence supporting the role of adherent-invasive E. coli (AIEC) in Crohn's disease. Inflammatory Bowel Diseases 15: 872-882.
66. Yoon SH, Han M-J, Jeong H, Lee CH, Xia X-X, et al. (2012) Comparative multi-omics systems analysis of Escherichia coli strains B and K-12. Genome Biol 13: R37.
67. Yoon S, Jeong H, Kwon S-K, Kim J (2009) Genomics, Biological Features, and Biotechnological Applications of Escherichia coli B: “Is B for better?!”. In: Lee S, editor. Systems Biology and Biotechnology of Escherichia coli: Springer Netherlands. pp. 1-17.
68. Lozupone CA, Stombaugh JI, Gordon JI, Jansson JK, Knight R (2012) Diversity, stability and resilience of the human gut microbiota. Nature 489: 220-230.
69. Bassler BL, Greenberg EP, Stevens AM (1997) Cross-species induction of luminescence in the quorum-sensing bacterium Vibrio harveyi. Journal of bacteriology 179: 4043-4045.
70. Baruch M, Belotserkovsky I, Hertzog BB, Ravins M, Dov E, et al. (2014) An Extracellular Bacterial Pathogen Modulates Host Metabolism to Regulate Its Own Sensing and Proliferation. Cell 156: 97-108.
71. Kendall MM, Gruber CC, Parker CT, Sperandio V (2012) Ethanolamine controls expression of genes encoding components involved in interkingdom signaling and virulence in enterohemorrhagic Escherichia coli O157: H7. MBio 3: e00050-00012.
72. Swamy M, Jamora C, Havran W, Hayday A (2010) Epithelial decision makers: in search of the'epimmunome'. Nature immunology 11: 656-665.
73. Abreu MT, Vora P, Faure E, Thomas LS, Arnold ET, et al. (2001) Decreased expression of Toll-like receptor-4 and MD-2 correlates with intestinal epithelial cell protection against dysregulated proinflammatory gene expression in response to bacterial lipopolysaccharide. The Journal of Immunology 167: 1609-1616.
74. Naik S, Kelly EJ, Meijer L, Pettersson S, Sanderson IR (2001) Absence of Toll-like receptor 4 explains endotoxin hyporesponsiveness in human intestinal epithelium. Journal of pediatric gastroenterology and nutrition 32: 449-453.
75. Suzuki M, Hisamatsu T, Podolsky DK (2003) Gamma Interferon Augments the Intracellular Pathway for Lipopolysaccharide (LPS) Recognition in Human Intestinal Epithelial Cells through Coordinated Up-Regulation of LPS Uptake and Expression of the Intracellular Toll-Like Receptor 4-MD-2 Complex. Infection and Immunity 71: 3503-3511.

76. Jeon HJ, Choi J-H, Jung I-H, Park J-G, Lee M-R, et al. (2010) CD137 (4–1BB) deficiency reduces atherosclerosis in hyperlipidemic mice. Circulation 121: 1124-1133.
77. Liew FY, Xu D, Brint EK, O'Neill LA (2005) Negative regulation of toll-like receptor-mediated immune responses. Nature Reviews Immunology 5: 446-458.
78. Perkins ND (2007) Integrating cell-signalling pathways with NF-[kappa]B and IKK function. Nat Rev Mol Cell Biol 8: 49-62.
79. Ma A, Malynn BA (2012) A20: linking a complex regulator of ubiquitylation to immunity and human disease. Nature Reviews Immunology 12: 774-785.
80. Vereecke L, Beyaert R, van Loo G (2009) The ubiquitin-editing enzyme A20 (TNFAIP3) is a central regulator of immunopathology. Trends in immunology 30: 383-391.
81. Hausmann E, Raisz L, Miller W (1970) Endotoxin: stimulation of bone resorption in tissue culture. Science 168: 862-864.
82. Ishihara Y, Nishihara T, Maki E, Noguchi T, Koga T (1991) Role of interleukin-1 and prostaglandin in in vitro bone resorption induced by Actinobacillus actinomycetemcomitans lipopolysaccharide. Journal of periodontal research 26: 155-160.
83. Angrisano T, Pero R, Peluso S, Keller S, Sacchetti S, et al. (2010) LPS-induced IL-8 activation in human intestinal epithelial cells is accompanied by specific histone H3 acetylation and methylation changes. BMC microbiology 10: 172.
84. Pugin JM, Schürer-Maly C, Leturcq D, Moriarty A, Ulevitch RJ, et al. (1993) Lipopolysaccharide activation of human endothelial and epithelial cells is mediated by lipopolysaccharide-binding protein and soluble CD14. Proceedings of the National Academy of Sciences 90: 2744-2748.
85. Cario E, Rosenberg IM, Brandwein SL, Beck PL, Reinecker H-C, et al. (2000) Lipopolysaccharide activates distinct signaling pathways in intestinal epithelial cell lines expressing Toll-like receptors. The Journal of Immunology 164: 966-972.
86. Studier FW, Daegelen P, Lenski RE, Maslov S, Kim JF (2009) Understanding the Differences between Genome Sequences of Escherichia coli B Strains REL606 and BL21(DE3) and Comparison of the E. coli B and K-12 Genomes. Journal of Molecular Biology 394: 653-680.
87. Pereira CS, de Regt AK, Brito PH, Miller ST, Xavier KB (2009) Identification of functional LsrB-like autoinducer-2 receptors. Journal of bacteriology 191: 6975-6987.
88. Li J, Wang L, Hashimoto Y, Tsao CY, Wood TK, et al. (2006) A stochastic model of Escherichia coli AI-2 quorum signal circuit reveals alternative synthesis pathways. Molecular systems biology 2.
89. Mota LJ, Cornelis GR (2005) The bacterial injection kit: type III secretion systems. Annals of medicine 37: 234-249.
90. Tateda K, Ishii Y, Horikawa M, Matsumoto T, Miyairi S, et al. (2003) The Pseudomonas aeruginosa autoinducer N-3-oxododecanoyl homoserine lactone accelerates apoptosis in macrophages and neutrophils. Infection and Immunity 71: 5785-5793.
91. Shiner E, Terentyev D, Bryan A, Sennoune S, Martinez-Zaguilan R, et al. (2006) Pseudomonas aeruginosa autoinducer modulates host cell responses through calcium signalling. Cellular microbiology 8: 1601-1610.
92. Karlin D, Mastromarino A, Jones R, Stroehlein J, Lorentz O (1985) Fecal skatole and indole and breath methane and hydrogen in patients with large bowel polyps or cancer. Journal of cancer research and clinical oncology 109: 135-141.

93. Zuccato E, Venturi M, Di Leo G, Colombo L, Bertolo C, et al. (1993) Role of bile acids and metabolic activity of colonic bacteria in increased risk of colon cancer after cholecystectomy. Digestive diseases and sciences 38: 514-519.
94. Zhu J, Pei D (2008) A LuxP-Based Fluorescent Sensor for Bacterial Autoinducer II. ACS Chemical Biology 3: 110-119.
95. Charlton TS, De Nys R, Netting A, Kumar N, Hentzer M, et al. (2000) A novel and sensitive method for the quantification of N-3-oxoacyl homoserine lactones using gas chromatography–mass spectrometry: application to a model bacterial biofilm. Environmental Microbiology 2: 530-541.
96. Zargar A, Quan DN, Emamian M, Tsao CY, Wu H-C, et al. (2015) Rational design of 'controller cells' to manipulate protein and phenotype expression. Metabolic engineering 30: 61-68.
97. Bailey JE (1991) Toward a science of metabolic engineering. Science 252: 1668-1675.
98. Stephanopoulos G, Vallino JJ (1991) Network rigidity and metabolic engineering in metabolite overproduction. Science(Washington) 252: 1675-1681.
99. Jarboe LR, Zhang X, Wang X, Moore JC, Shanmugam K, et al. (2010) Metabolic engineering for production of biorenewable fuels and chemicals: contributions of synthetic biology. BioMed Research International 2010.
100. Stephanopoulos G, Kelleher J (2001) How to make a superior cell. Science 292: 2024-2025.
101. Kramer BP, Fischer M, Fussenegger M (2005) Semi-synthetic mammalian gene regulatory networks. Metabolic engineering 7: 241-250.
102. Malphettes L, Fussenegger M (2006) Impact of RNA interference on gene networks. Metabolic engineering 8: 672-683.
103. Boyle PM, Silver PA (2012) Parts plus pipes: synthetic biology approaches to metabolic engineering. Metabolic engineering 14: 223-232.
104. Keasling JD (2012) Synthetic biology and the development of tools for metabolic engineering. Metabolic engineering 14: 189-195.
105. Weber W, Fussenegger M (2011) Molecular diversity—the toolbox for synthetic gene switches and networks. Current opinion in chemical biology 15: 414-420.
106. Purnick PE, Weiss R (2009) The second wave of synthetic biology: from modules to systems. Nature reviews Molecular cell biology 10: 410-422.
107. Nielsen J, Fussenegger M, Keasling J, Lee SY, Liao JC, et al. (2014) Engineering synergy in biotechnology. Nature chemical biology 10: 319-322.
108. Way JC, Collins JJ, Keasling JD, Silver PA (2014) Integrating Biological Redesign: Where Synthetic Biology Came From and Where It Needs to Go. Cell 157: 151-161.
109. Solomon KV, Prather KL (2011) The zero-sum game of pathway optimization: Emerging paradigms for tuning gene expression. Biotechnology journal 6: 1064-1070.
110. Farmer WR, Liao JC (2000) Improving lycopene production in Escherichia coli by engineering metabolic control. Nature biotechnology 18: 533-537.
111. Kobayashi H, Kærn M, Araki M, Chung K, Gardner TS, et al. (2004) Programmable cells: interfacing natural and engineered gene networks. Proceedings of the National Academy of Sciences of the United States of America 101: 8414-8419.
112. Tsao C-Y, Quan DN, Bentley WE (2012) Development of the quorum sensing biotechnological toolbox. Current Opinion in Chemical Engineering 1: 396-402.
113. Fuqua WC, Winans SC, Greenberg EP (1994) Quorum sensing in bacteria: the LuxR-LuxI family of cell density-responsive transcriptional regulators. Journal of bacteriology 176: 269.

114. Surette MG, Bassler BL (1998) Quorum sensing in Escherichia coli and Salmonella typhimurium. Proceedings of the National Academy of Sciences 95: 7046-7050.
115. Bentley WE, Mirjalili N, Andersen DC, Davis RH, Kompala DS (1990) Plasmid-encoded protein: the principal factor in the "metabolic burden" associated with recombinant bacteria. Biotechnology and bioengineering 35: 668-681.
116. DeLisa MP, Valdes JJ, Bentley WE (2001) Quorum signaling via AI-2 communicates the "Metabolic Burden" associated with heterologous protein production in Escherichia coli. Biotechnology and bioengineering 75: 439-450.
117. Tsao C-Y, Wang L, Hashimoto Y, Yi H, March JC, et al. (2011) LuxS Coexpression Enhances Yields of Recombinant Proteins in Escherichia coli in Part through Posttranscriptional Control of GroEL. Applied and Environmental Microbiology 77: 2141-2152.
118. Kuipers OP, de Ruyter PG, Kleerebezem M, de Vos WM (1998) Quorum sensing-controlled gene expression in lactic acid bacteria. Journal of Biotechnology 64: 15-21.
119. Tamsir A, Tabor JJ, Voigt CA (2011) Robust multicellular computing using genetically encoded NOR gates and chemical `wires'. Nature 469: 212-215.
120. Wood TK, Hong SH, Ma Q (2011) Engineering biofilm formation and dispersal. Trends in Biotechnology 29: 87-94.
121. Basu S, Mehreja R, Thiberge S, Chen M-T, Weiss R (2004) Spatiotemporal control of gene expression with pulse-generating networks. Proceedings of the National Academy of Sciences of the United States of America 101: 6355-6360.
122. Carter KK, Valdes JJ, Bentley WE (2012) Pathway engineering via quorum sensing and sRNA riboregulators—interconnected networks and controllers. Metabolic engineering 14: 281-288.
123. Sambrook J, Fritsch EF, Maniatis T (1989) Molecular cloning: Cold spring harbor laboratory press New York.
124. Gibson DG, Young L, Chuang R-Y, Venter JC, Hutchison CA, et al. (2009) Enzymatic assembly of DNA molecules up to several hundred kilobases. Nat Meth 6: 343-345.
125. Wang L, Hashimoto Y, Tsao C-Y, Valdes JJ, Bentley WE (2005) Cyclic AMP (cAMP) and cAMP receptor protein influence both synthesis and uptake of extracellular autoinducer 2 in Escherichia coli. Journal of bacteriology 187: 2066-2076.
126. Zargar A, Quan DN, Carter KK, Guo M, Sintim HO, et al. (2015) Bacterial Secretions of Nonpathogenic Escherichia coli Elicit Inflammatory Pathways: a Closer Investigation of Interkingdom Signaling. mBio 6.
127. Smith JAI, Wang J, Nguyen-Mau S-M, Lee V, Sintim HO (2009) Biological screening of a diverse set of AI-2 analogues in Vibrio harveyi suggests that receptors which are involved in synergistic agonism of AI-2 and analogues are promiscuous. Chemical Communications: 7033-7035.
128. Liu Y, Terrell JL, Tsao CY, Wu HC, Javvaji V, et al. (2012) Biofabricating Multifunctional Soft Matter with Enzymes and Stimuli-Responsive Materials. Advanced Functional Materials 22: 3004-3012.
129. Wu HC, Tsao CY, Quan DN, Cheng Y, Servinsky MD, et al. (2013) Autonomous bacterial localization and gene expression based on nearby cell receptor density. Molecular systems biology 9.
130. Hooshangi S, Bentley WE (2011) LsrR quorum sensing “switch” is revealed by a bottom-up approach. PLoS computational biology 7: e1002172.
131. Taga ME, Miller ST, Bassler BL (2003) Lsr-mediated transport and processing of AI-2 in Salmonella typhimurium. Molecular Microbiology 50: 1411-1427.

132. Xue T, Zhao L, Sun H, Zhou X, Sun B (2009) LsrR-binding site recognition and regulatory characteristics in Escherichia coli AI-2 quorum sensing. Cell Res 19: 1258-1268.
133. Xavier KB, Miller ST, Lu W, Kim JH, Rabinowitz J, et al. (2007) Phosphorylation and Processing of the Quorum-Sensing Molecule Autoinducer-2 in Enteric Bacteria. ACS Chemical Biology 2: 128-136.
134. Marques JC, Lamosa P, Russell C, Ventura R, Maycock C, et al. (2011) Processing the Interspecies Quorum-sensing Signal Autoinducer-2 (AI-2): Characterization of phospho-(S)-4,5-dyhydroxy-2,3-pentanedione isomerization by LsrG Protein Journal of Biological Chemistry 286: 18331-18343.
135. Li J, Wang L, Hashimoto Y, Tsao CY, Wood TK, et al. (2006) A stochastic model of Escherichia coli AI-2 quorum signal circuit reveals alternative synthesis pathways. Molecular systems biology 2.
136. Barrios AFG, Zuo R, Hashimoto Y, Yang L, Bentley WE, et al. (2006) Autoinducer 2 controls biofilm formation in Escherichia coli through a novel motility quorum-sensing regulator (MqsR, B3022). Journal of bacteriology 188: 305-316.
137. Hegde M, Englert DL, Schrock S, Cohn WB, Vogt C, et al. (2011) Chemotaxis to the quorum-sensing signal AI-2 requires the Tsr chemoreceptor and the periplasmic LsrB AI-2-binding protein. Journal of bacteriology 193: 768-773.
138. Lu TK, Khalil AS, Collins JJ (2009) Next-generation synthetic gene networks. Nat Biotech 27: 1139-1150.
139. Shong J, Jimenez Diaz MR, Collins CH (2012) Towards synthetic microbial consortia for bioprocessing. Current Opinion in Biotechnology 23: 798-802.
140. Marchand N, Collins CH (2013) Peptide-based communication system enables Escherichia coli to Bacillus megaterium interspecies signaling. Biotechnology and bioengineering 110: 3003-3012.
141. Hooshangi S, Bentley WE (2008) From unicellular properties to multicellular behavior: bacteria quorum sensing circuitry and applications. Current Opinion in Biotechnology 19: 550-555.
142. Aurand TC, Russell MS, March JC (2012) Synthetic signaling networks for therapeutic applications. Current Opinion in Biotechnology 23: 773-779.
143. Xavier KB, Bassler BL (2005) Regulation of Uptake and Processing of the Quorum-Sensing Autoinducer AI-2 in Escherichia coli. Journal of bacteriology 187: 238-248.
144. Herzberg M, Kaye IK, Peti W, Wood TK (2006) YdgG (TqsA) Controls Biofilm Formation in Escherichia coli K-12 through Autoinducer 2 Transport. Journal of bacteriology 188: 587-598.
145. Swinnen IAM, Bernaerts K, Dens EJJ, Geeraerd AH, Van Impe JF (2004) Predictive modelling of the microbial lag phase: a review. International Journal of Food Microbiology 94: 137-159.
146. Koseki S, Nonaka J (2012) Alternative approach to modeling bacterial lag time, using logistic regression as a function of time, temperature, pH, and sodium chloride concentration. Applied and Environmental Microbiology 78: 6103-6112.
147. Mertens L, Van Derlinden E, Van Impe JF (2012) Comparing experimental design schemes in predictive food microbiology: optimal parameter estimation of secondary models. Journal of Food Engineering 112: 119-133.
148. Cuny C, Lesbats M, Dukan S (2007) Induction of a Global Stress Response during the First Step of Escherichia coli Plate Growth. Applied and Environmental Microbiology 73: 885-889.

149. Baranyi J, Roberts TA (1994) A dynamic approach to predicting bacterial growth in food. International Journal of Food Microbiology 23: 277-294.
150. Koop AH, Hartley ME, Bourgeois S (1987) A low-copy-number vector utilizing β-galactosidase for the analysis of gene control elements. Gene 52: 245-256.
151. Servinsky MD, Terrell JL, Tsao C-Y, Wu H-C, Quan DN, et al. (2015) Directed assembly of a bacterial quorum. The ISME journal.
152. Choudhary S, Schmidt-Dannert C (2010) Applications of quorum sensing in biotechnology. Applied microbiology and biotechnology 86: 1267-1279.
153. You L, Cox RS, Weiss R, Arnold FH (2004) Programmed population control by cell-cell communication and regulated killing. Nature 428: 868-871.
154. Weber W, Daoud-El Baba M, Fussenegger M (2007) Synthetic ecosystems based on airborne inter- and intrakingdom communication. Proceedings of the National Academy of Sciences 104: 10435-10440.
155. Dong Y-H, Zhang L-H (2005) Quorum sensing and quorum-quenching enzymes. J Microbiol 43: 101-109.
156. Prindle A, Selimkhanov J, Li H, Razinkov I, Tsimring LS, et al. (2014) Rapid and tunable post-translational coupling of genetic circuits. Nature 508: 387-391.
157. Cameron DE, Collins JJ (2014) Tunable protein degradation in bacteria. Nat Biotech 32: 1276-1281.
158. Callura JM, Dwyer DJ, Isaacs FJ, Cantor CR, Collins JJ (2010) Tracking, tuning, and terminating microbial physiology using synthetic riboregulators. Proceedings of the National Academy of Sciences 107: 15898-15903.
159. Deans TL, Cantor CR, Collins JJ (2007) A tunable genetic switch based on RNAi and repressor proteins for regulating gene expression in mammalian cells. Cell 130: 363-372.
160. Basu S, Gerchman Y, Collins CH, Arnold FH, Weiss R (2005) A synthetic multicellular system for programmed pattern formation. Nature 434: 1130-1134.
161. Bentley WE, Zargar A, Payne GF (2013) Plug and Play? Interconnected multifunctional chips for enhancing efficiency of biopharmaceutical R&D. Pharmaceutical Bioprocessing 1: 225-228.
162. Gupta A, Terrell JL, Fernandes R, Dowling MB, Payne GF, et al. (2013) Encapsulated fusion protein confers “sense and respond” activity to chitosan–alginate capsules to manipulate bacterial quorum sensing. Biotechnology and bioengineering 110: 552-562.
163. Klein J, Stock J, Vorlop KD (1983) Pore size and properties of spherical Ca-alginate biocatalysts. European journal of applied microbiology and biotechnology 18: 86-91.
164. Lin J, Yu W, Liu X, Xie H, Wang W, et al. (2008) In Vitro and in Vivo characterization of alginate-chitosan-alginate artificial microcapsules for therapeutic oral delivery of live bacterial cells. Journal of Bioscience and Bioengineering 105: 660-665.
165. Park SJ, Lee YK, Cho S, Uthaman S, Park IK, et al. (2014) Effect of chitosan coating on a bacteria-based alginate microrobot. Biotechnology and bioengineering.
166. Krasaekoopt W, Bhandari B, Deeth H (2003) Evaluation of encapsulation techniques of probiotics for yoghurt. International Dairy Journal 13: 3-13.
167. Tsao C-Y, Hooshangi S, Wu H-C, Valdes JJ, Bentley WE (2010) Autonomous induction of recombinant proteins by minimally rewiring native quorum sensing regulon of< i> E. coli</i>. Metabolic engineering 12: 291-297.
168. Vendeville A, Winzer K, Heurlier K, Tang CM, Hardie KR (2005) Making'sense'of metabolism: autoinducer-2, LuxS and pathogenic bacteria. Nature Reviews Microbiology 3: 383-396.

169. Betz JF, Cheng Y, Tsao C-Y, Zargar A, Wu H-C, et al. (2013) Optically clear alginate hydrogels for spatially controlled cell entrapment and culture at microfluidic electrode surfaces. Lab on a Chip 13: 1854-1858.